AD-A179 858

VISCID/INVISCID SEPARATED FLOWS

T. Cebeci
K.C. Chang
R.W. Clark
D.P. Mack
S.M. Schimke

McDonnell Aircraft Company
McDonnell Douglas Corporation
P.O. Box 516
St. Louis. Missouri 63166

DTIC
ELECTE
S APR 2 8 1987
D

JULY 1986

Final Report for Period September 1983 – March 1986

NOTICE

When Government drawings, specifications, or other data are used for any purpose other than in connection with a definitely related Government procurement operation, the United States Government thereby incurs no responsibility nor any obligation whatsoever; and the fact that the Government may have formulated, furnished, or in any way supplied the said drawings, specifications, or other data, is not to be regarded by implication or otherwise as in any manner licensing the holder or any other person or corporation, or conveying any rights or permission to manufacture, use, or sell any patented invention that may in any way be related thereto.

This report has been reviewed by the Office of Public Affairs (ASD/PA) and is releasable to the National Technical Information Service (NTIS). At NTIS, it will be available to the general public, including foreign nations.

This technical report has been reviewed and is approved for publication.

Albert J. Murn
Project Engineer

Bohdan G. Kunciw, Maj, USAF
Chief, Aerodynamics and
   Airframe Branch
Aeromechanics Division

FOR THE COMMANDER

DONALD A. DREESBACH, Colonel, USAF
Chief, Aeromechanics Division
Flight Dynamics Laboratory

Copies of this report should not be returned unless return is required by security considerations, contractual obligations, or notice on a specific document.

REPORT DOCUMENTATION PAGE

1a. REPORT SECURITY CLASSIFICATION	1b. RESTRICTIVE MARKINGS		
Unclassified			
2a. SECURITY CLASSIFICATION AUTHORITY	3. DISTRIBUTION/AVAILABILITY OF REPORT		
	Approved for public release; distribution is unlimited.		
2b. DECLASSIFICATION/DOWNGRADING SCHEDULE			
4. PERFORMING ORGANIZATION REPORT NUMBER(S)	5. MONITORING ORGANIZATION REPORT NUMBER(S)		
MDC J3968	AFWAL-TR-86-3048		

6a. NAME OF PERFORMING ORGANIZATION	6b. OFFICE SYMBOL (If applicable)	7a. NAME OF MONITORING ORGANIZATION
McDonnell Aircraft Company		AF Wright Aeronautical Labs (AFWAL/FIMM)
6c. ADDRESS (City, State and ZIP Code)		7b. ADDRESS (City, State and ZIP Code)
P.O. Box 516 St. Louis, Missouri 63166		Wright-Patterson Air Force Base Ohio 45433-6553

8a. NAME OF FUNDING/SPONSORING ORGANIZATION	8b. OFFICE SYMBOL (If applicable)	9. PROCUREMENT INSTRUMENT IDENTIFICATION NUMBER
		F33615-83C-3026

8c. ADDRESS (City, State and ZIP Code)	10. SOURCE OF FUNDING NOS.			
	PROGRAM ELEMENT NO.	PROJECT NO.	TASK NO.	WORK UNIT NO.
	62201F	2404	10	81

11 TITLE (Include Security Classification)
Viscid/Inviscid Separated Flows

12. PERSONAL AUTHOR(S)
T. Cebeci, K.C. Chang, R.W. Clark, D.P. Mack, S.M. Schimke

13a. TYPE OF REPORT	13b. TIME COVERED	14. DATE OF REPORT (Yr., Mo., Day)	15. PAGE COUNT
Final	FROM SEP 83 TO MAR 86	July 1986	88

16. SUPPLEMENTARY NOTATION

17 COSATI CODES			18 SUBJECT TERMS (Continue on reverse if necessary and identify by block number)
FIELD	GROUP	SUB. GR	Separated Flow Wing-Body Geometry
04	02		Viscid/Inviscid Interactions Boundary Layer
01	03		Interactive Boundary Layer Theory, Subsonic Flow

19 ABSTRACT (Continue on reverse if necessary and identify by block number)

A method has been developed for calculating subsonic three-dimensional flows over fighter aircraft configurations at flow conditions including separation. The method employs a viscid inviscid interaction approach, with a panel method used for the inviscid analysis and a finite difference boundary layer method for the viscous analysis. The viscid and inviscid analyses are coupled using an interactive technique based on inverse boundary layer theory. This approach allows efficient calculation of flows with large separation regions, including both leading and trailing edge separations.

The method was validated on three fighter aircraft geometries and comparisons with test data are presented.

20 DISTRIBUTION/AVAILABILITY OF ABSTRACT	21 ABSTRACT SECURITY CLASSIFICATION	
UNCLASSIFIED/UNLIMITED ☒ SAME AS RPT ☐ DTIC USERS ☐	Unclassified	
22a NAME OF RESPONSIBLE INDIVIDUAL	22b TELEPHONE NUMBER (Include Area Code)	22c OFFICE SYMBOL
Albert J. Murn	513/255-4052	AFWAL/FIMM

DD FORM 1473, 83 APR   EDITION OF 1 JAN 73 IS OBSOLETE   UNCLASSIFIED

FOREWORD

This report was prepared for the United States Air Force by the Douglas Aircraft Company, Long Beach, California, and the McDonnell Aircraft Company, St. Louis, Missouri in partial fulfillment of Contract Number F33615-83-C-3026. This report describes a method for calculating the flowfield about fighter aircraft geometries in the presence of flow separation, and includes comparisons with test data for three fighter configurations.

The contract was under the direction of Mr. Albert J. Murn of the Air Force Flight Dynamics Laboratory, Wright-Patterson Air Force Base, Ohio. His efforts and forbearance are gratefully acknowledged.

TABLE OF CONTENTS

LIST OF ILLUSTRATIONS

SECTION I

INTRODUCTION

In past years aircraft configuration design was accomplished mainly by wind tunnel testing while flow-calculation methods contributed little because they were limited to simple geometries and restricted in the physical processes that they represented. This virtually exclusive reliance on testing had disadvantages which led to less-than-optimum designs. Each potential configuration had to be fabricated as a wind tunnel model with corresponding expense and time delay and, if the tests suggested design changes, the process should have been repeated, though on occasions this could not be done because of the time and expense involved in an iteration cycle. Moreover, tests provide incomplete information in that, for example, static-measurements may be restricted to a small number of locations. Force and moment data are seldom explained in terms of flow phenomena and the extent of separated regions is usually not determined. Finally, there is the necessary scaling from model to full-scale vehicle which can be uncertain so that, for example, separation observed on a model may be different from that encountered in full scale.

Intensive efforts have been pursued for many years to help to overcome the limitations of calculation methods and to develop them to represent accurately the flows over airplane configurations. Regardless of the specific algorithm employed, the cost and especially the elapsed time required to develop a numerical representation of a given configuration is much less than that required for an experimental test. Once such a basic numerical model has been developed, many variations on the design can be investigated computationally and only the most promising selected for wind-tunnel testing. A flow computation method is required to represent the geometry of the airplane and the essential properties of the fluid and, to achieve the objective, limitations of calculation methods have been removed in recent years by the development of new and powerful calculation tools.

There are three possible approaches which can be used for the calculation of the viscous flow over an aircraft configuration. The first approach makes use of the Reynolds-averaged Navier-Stokes equations and various reduced forms including the so-called parabolized and thin-layer Navier-Stokes equations. Significant advances have been made in this area, for example, by Shang and

Scherr [1] who made the first attempt to numerically simulate the flowfield around a complete aircraft by solving the Navier-Stokes equations. To demonstrate the feasibility of their approach, they chose the hypersonic research aircraft X24C-10D for which a detailed experimental database exists. Using a mesh system around 5×10^5 nodes, they performed impressive calculations at an angle of attack of six degrees with a nominal Mach number of 5.95, and indicated areas where future research should concentrate to make this approach more efficient and practical.

The second and third approaches both make use of solutions of inviscid and viscous flow equations coupled by special procedures. The second approach is based on the two-dimensional method developed by Gilmer and Bristow [2] in which an empirical inviscid flow model is used to represent the effects of flow separation [2,3]. A direct boundary-layer calculation is employed up to the point of separation. Downstream of this point, a free surface is introduced to model the separated flow region. The shape and the length of the separation zone are computed by satisfying a constant pressure boundary condition on the surface and very good results have been obtained for airfoils at a wide range of angles of attack including stall.

The third approach, which is referred to as the interactive boundary-layer approach, uses special coupling techniques between inviscid and viscous flows and novel numerical procedures. The particular form developed by Cebeci et al. [4] is very general and allows any inviscid flow method to be coupled with solutions of the boundary-layer equations. For example, in its application to two-dimensional subsonic flows over airfoils, it employs Halsey's inviscid procedure [5] based on the conformal mapping and Fourier analysis techniques and computes the flow over the airfoil and wake. Successive viscous sweeps are performed, after each of which the external inviscid solution is recomputed, until a converged solution is obtained. The boundary-layer method, which is an inverse finite-difference scheme developed by Cebeci [6], uses an algebraic eddy-viscosity formulation due to Cebeci and Smith [7] and is able to compute flows with large regions of separation without numerical problems. In regions of reverse flow, it uses the FLARE approximation [8] in which the streamwise convective term is set equal to zero in the recirculating region. A detailed description of the method and of its application to a range of airfoils at angles of attack up to and including stall is provided in [4]. The results

presented in Section 3.1 show that this procedure has removed a major obstacle in that flows with large regions of separation can now be computed accurately.

A comparison between the interactive procedure [4] and a method based on the thin-Navier-Stokes equation has been reported in [9] for the NACA 0012 airfoil. This study demonstrated that the Navier-Stokes approach and the interactive boundary-layer approach gave comparable results up to the stall angle. However, the interactive boundary-layer approach required much less computing time.

The purpose of the present work is to develop a general method for computing three-dimensional flows on wings with leading- and trailing-edge separation. The second and third approaches, described above, have been critically examined to determine the extent to which they can fulfill this purpose. It was considered that the second approach should be more suited to large regions of trailing-edge separation whereas the third approach should be more appropriate for leading-edge separation bubbles. Extensive tests showed that the second approach failed to converge in those situations for which it was intended and, although it was satisfactory for flows with small trailing-edge separation, considerable effort may still be required to overcome its limitations. The third approach on the other hand, has proved to be able to represent leading- and trailing-edge separation without limitations, as discussed further in Section 3.0.

The remainder of this report has been arranged in five sections. In Section 2.0, the inviscid method is briefly described prior to more extensive descriptions of interactive boundary-layer methods based on strip theory and quasi-three-dimensional approximations. The viscous-flow equations, transformations and solution procedure have been described previously in [4] for two-dimensional flows and in [10] for quasi-three-dimensional flows. Results obtained with these procedures are presented in Section 3.0 for several configurations and the relative merits of the two interactive approaches are considered. The computer program, which embodies both methods is described in Section 4.0 and sample input data for the three contract test cases are presented in Section 5.0. The report ends with a summary of the more important conclusions in Section 6.0.

SECTION II
DESCRIPTION OF THE INTERACTIVE BOUNDARY-LAYER METHODS

The method described here combines inviscid flow and inverse boundary layer procedures in an interactive manner which permits the calculation of flows with leading and trailing-edge separation. According to this method, the inviscid method of Section 2.1 is used to compute the flow over the given configuration with a zero normal velocity boundary condition. The resulting pressure distribution serves as a boundary condition for the boundary layer method of Section 2.2 which computes all relevant boundary layer parameters, including a surface blowing distribution to simulate the displacement thickness effect. While the inviscid-flow calculations (see Section 2.1) are performed for the entire configuration, viscous-flow calculations are presently restricted to the wing and make use of strip-theory and quasi three dimensional approximations discussed in Section 2.2.

The viscous effects computed by the boundary-layer method are then used to determine a distribution of normal velocity on the surface. The inviscid flow method is used for a second time with this blowing velocity distribution as a boundary condition and the procedure is repeated until convergence.

2.1 Inviscid Flow Method

The inviscid flow method, which is the first-order surface-source panel method developed by Hess, is capable of computing flow about completely arbitrary configurations. Because of its robustness and its availability, it has been acquired by several dozen facilities around the country and applied not only to aircraft but also to ships, submarines, automobiles, buildings, and topographical features. The three-dimensional body is represented by a set of plane quadrilateral panels, as shown in Fig. 1*. A three-dimensional body consists of lifting and nonlifting portions. A lifting portion, such as a wing or pylon, is characterized by having a well-defined trailing edge, from which issues a trailing vortex wake and along which the Kutta condition is applied. Nonlifting portions of the body lack such trailing edges. Every panel has a constant value of source strength σ. Panels of lifting portions have, in addition, a quadratically varying doublet strength μ. Values of source

---

*Figures begin on page   .

density on the panels are independent parameters available for satisfying the boundary condition. The chordwise dipole variation over the panels of a lifting strip (Fig. 1) is assumed in a form that leads to favorable numerics, so that the dipole strength is reduced to a single adjustable parameter – the circulation on that strip. Thus the set of independent dipole parameters equals the number of locations where the Kutta condition is enforced, i.e., at the trailing-edge segment of each strip.

The nature of the Kutta condition adopted by the many panel methods which are currently available varies greatly. The condition adopted by Hess [11] is the physically meaningful condition of equal upper and lower surface pressures at the trailing edge. All other methods make use of other derived conditions, e.g. a prescribed flow direction a short distance downstream, which do not guarantee a pressure match at the trailing edge. For instance, Margason et al. [12] showed that pressure mismatches of up to half of the freestream dynamic pressure could occur from such alternate forms of the Kutta condition. Figure 2, which is taken from [12] shows this clearly. Since we are interested in the computation of flows for which the behavior of the boundary layer at the trailing edge can have a significant effect on the overall flow solution, it is believed that the approach adopted here is more realistic.

The computational procedure is as follows. On each panel a control point is selected where the normal-velocity boundary condition is applied and where velocity and pressure are eventually calculated. Using the well-known point-source potential, the velocity induced by the source density on a panel at a point in space is

$$\vec{v}(panel) = [\iint_{panel} grad(1/r)dS]\sigma(panel) \qquad (2.1)$$

where the constant value of σ has been taken outside the integral whose value therefore depends only on geometry. Suppose N panels are used to define the body, and let σ_j denote the value of source density on the jth panel. The velocity induced by the jth panel at the control point of the ith panel is defined as $\vec{V}_{ij}\sigma_j$, where $\vec{V}_{ij}$ is an integral of the form of Eq. (2.1). The integral may be carried out analytically. Explicit formulas are contained in [11], but they are too lengthy for inclusion here. The corresponding normal velocity at the ith control point is

$$A_{ij}\sigma_j = \vec{n}_i \cdot \vec{V}_{ij}\sigma_j \qquad (2.2)$$

where $\vec{n}_i$ is the unit normal vector to the ith panel. Applying the normal velocity boundary condition at all control points then yields the following set of linear algebraic equations:

$$\sum_{j=1}^{N} A_{ij}\sigma_j = -\vec{n}_i \cdot \vec{V}_\infty \qquad (2.3)$$

This is the numerical approximation of the integral equation that expresses the zero normal-velocity boundary condition. Once the σ_j have been deter mined, the disturbance velocities at the control points due to the body are given by

$$\vec{V}_i = \sum_{j=1}^{N} \vec{V}_{ij}\sigma_j \qquad i = 1, 2, \ldots, N \qquad (2.4)$$

While the addition of lift in two dimensions causes no significant increase in the complexity of the problem, the problem of three dimensional lifting flow is not only considerably more complicated than nonlifting flow but requires assumptions that are somewhat arbitrary [11]. The main features are illustrated in Fig. 1. As mentioned above, wings or other lifting portions of the configuration are characterized by having trailing edges from which issue trailing vortex wakes. So-called bound circulation is hypothesized to lie on or within the wing surface, with strength varying in both the chordwise direction and in the direction parallel to the trailing edge ("spanwise" in aerodynamic jargon). The variation of the bound circulation in the chordwise direction is predetermined, while the spanwise variation is adjusted to satisfy a condition of smooth flow off the entire trailing edge, and the trailing vor ticity has constant strength in the stream direction and an initial strength at the trailing edge equal to the local "spanwise" derivative of bound circula tion strength. The location of the wake once it leaves the trailing edge is initially unknown, which introduces a nonlinearity into the problem. It is customary simply to assume a wake location, because in most problems the calcu lated results are not sensitive to the details of the wake shape. However, the location can be determined by iterating the calculation if necessary.

With regard to computing effort and cost, the two principal tasks associ ated with this method are calculation of the N^2 velocities $\vec{V}_{ij}$ and the

solution of the set of linear equations, Eq. (2.3). Other portions of the calculation require comparatively negligible computing efforts. In three dimensional applications rather large numbers of panels are employed. Panel numbers over 3000 are common. These are the number of unknowns actually solved for after all symmetries, etc., have been utilized. Accordingly, it is economically important that all possible efficiencies be employed in carrying out the two principal tasks. For the first task this is accomplished by using simple approximate expressions for $\vec{V}_{ij}$ when computing the influence of distant panels [13]. The second task is speeded up by the use of block iterative matrix solutions, as developed by Clark [14]. The source method lends itself particularly well to these efficiencies, without which no three dimensional method is practical.

In updating the external inviscid velocity to account for the boundary layer displacement effects, two approaches can be considered. The first, known as the displacement surface approach, involves modifying the geometry to account for the boundary layer displacement thickness. The second approach is to introduce a blowing velocity on the surface of the original body so that the dividing stream surface of the inviscid flow approximates the displacement thickness computed by the boundary-layer procedure. While both approaches have been applied in our studies, the first approach has been found to be less suitable because it involves the computation of the inviscid flow past a body with a finite opening at the trailing edge. For separated flow, the size of this open trailing edge can become significant and the computation of the inviscid flow past such a body is nonunique unless some additional conditions are imposed along this trailing-edge opening. By adopting the surface blowing approach, the equivalent trailing edge thickness of the dividing stream surface is controlled by the blowing velocity introduced on the wing surface in a physically realistic way without resorting to additional boundary conditions.

The blowing velocity computed by the boundary-layer procedure is applied on the wing surface. However, as pointed out above, the aim is to model the flow past the displacement surface. For flows involving large trailing-edge separation, it has been shown in [4] that it is important to both evaluate the external inviscid pressure distribution and apply the Kutta condition on the displacement surface. In the present method this is achieved by introducing additional off body points corresponding to each control point for which the

boundary layer distribution has been computed. These off body points are used both to compute the final pressure distribution and to apply the Kutta condition.

2.2 Interactive Viscous-Flow Method

An accurate prediction of the flowfield over a wing requires the calculation of flow on the surface and in the wake. The airfoil studies conducted in [4] indicate that the wake influence is negligible for airfoils at low angles of attack and that it is sufficient to calculate the flow on the airfoil only. In the case of the NACA 0012 airfoil, for example, the wake effect begins to become important for angles of incidence, α, greater than $10°$, and is important at angles of incidence approaching stall, which for this airfoil is around $16°$ as shown in Fig. 3. The inclusion of the wake effect, which is not considered here, reduces the flow separation on the surface and allows the numerical calculations to be performed with less difficulty. In the present study, we investigate the ability of the interactive boundary-layer scheme to calculate flows with massive separation and perform calculations for configurations at high angles of attack, as discussed in Section 3.0.

2.2.1 Boundary-Layer Equations

The full three-dimensional boundary-layer equations and their boundary conditions may be written as the following nonorthogonal curvilinear coordinate system [10]:

Continuity Equation

$$\frac{\partial}{\partial x} (u h_2 \sin\theta) + \frac{\partial}{\partial z} (w h_1 \sin\theta) + \frac{\partial}{\partial y} (v h_1 h_2 \sin\theta) = 0 \qquad (2.5a)$$

x-Momentum Equation

$$\frac{u}{h_1} \frac{\partial u}{\partial x} + \frac{w}{h_2} \frac{\partial u}{\partial z} + v \frac{\partial u}{\partial y} - \cot\theta \, K_1 u^2 + \csc\theta \, K_2 w^2 + K_{12} uw$$

$$= - \frac{\csc^2\theta}{\rho h_1} \frac{\partial p}{\partial x} + \frac{\cot\theta \, \csc\theta}{\rho h_2} \frac{\partial p}{\partial z} + \frac{\partial}{\partial y} (v \frac{\partial u}{\partial y} - \overline{u'v'}) \qquad (2.5b)$$

z-Momentum Equation

$$\frac{u}{h_1} \frac{\partial w}{\partial x} + \frac{w}{h_2} \frac{\partial w}{\partial z} + v \frac{\partial w}{\partial y} + \csc\theta \, K_1 u^2 - \cot\theta \, K_2 w^2 + K_{21} uw$$

$$= \frac{\cot\theta \, \csc\theta}{\rho h_1} \frac{\partial p}{\partial x} - \frac{\csc^2\theta}{\rho h_2} \frac{\partial p}{\partial z} + \frac{\partial}{\partial y} \left(\nu \frac{\partial w}{\partial y} - \overline{v'w'} \right) \tag{2.5c}$$

$$y = 0: \qquad u, \, v, \, w = 0 \tag{2.6a}$$

$$y = \delta: \qquad u = u_e(x,z), \qquad w = w_e(x,z) \tag{2.6b}$$

Here x,z denote the coordinate system on the surface of the body and y is the actual distance measured normal to the surface. The boundary-layer equations and boundary conditions for this system according to first-order boundary-layer theory are based on the assumption that the pressure is constant across the shear layer and stress gradients in directions parallel to the surface are negligible compared with those normal to the surface. In the above equations h_1 and h_2 denote the metric coefficients and θ denotes the angle between the coordinate lines and, as a result of first-order boundary-layer theory, they are functions of the surface coordinates x and z only. They can be obtained from the relations which define the three-dimensional body in the Cartesian coordinate system $\bar{x}, \bar{y}, \bar{z}$ by

$$F(\bar{x}, \bar{y}, \bar{z}) = 0 \tag{2.7}$$

and those that define the curvilinear coordinate system. Thus the metric coefficients and the angle between θ are given by

$$h_1^2 = \left(\frac{\partial \bar{x}}{\partial x}\right)^2 + \left(\frac{\partial \bar{y}}{\partial x}\right)^2 + \left(\frac{\partial \bar{z}}{\partial x}\right)^2 \tag{2.8a}$$

$$h_2^2 = \left(\frac{\partial \bar{x}}{\partial z}\right)^2 + \left(\frac{\partial \bar{y}}{\partial z}\right)^2 + \left(\frac{\partial \bar{z}}{\partial z}\right)^2 \tag{2.8b}$$

$$\cos\theta = \frac{(\partial \bar{x}/\partial x)(\partial \bar{x}/\partial z) + (\partial \bar{y}/\partial x)(\partial \bar{y}/\partial z) + (\partial \bar{z}/\partial x)(\partial \bar{z}/\partial z)}{h_1 h_2} \tag{2.9}$$

The parameters K_1 and K_2 are known as the geodesic curvatures of the curves z = constant and x = constant, respectively, see Fig. 4, and are given by

$$K_1 = \frac{1}{h_1 h_2 \sin\theta} \left[\frac{\partial}{\partial x}(h_2 \cos\theta) - \frac{\partial h_1}{\partial z}\right] \qquad (2.10a)$$

$$K_2 = \frac{1}{h_1 h_2 \sin\theta} \left[\frac{\partial}{\partial z}(h_1 \cos\theta) - \frac{\partial h_2}{\partial x}\right] \qquad (2.10b)$$

The parameters K_{12} and K_{21} are defined by

$$K_{12} = \frac{1}{\sin\theta}\left[- K_1 - \frac{1}{h_1}\frac{\partial\theta}{\partial x} + \cos\theta\left(K_2 + \frac{1}{h_2}\frac{\partial\theta}{\partial z}\right)\right] \qquad (2.11a)$$

$$K_{21} = \frac{1}{\sin\theta}\left[- K_2 - \frac{1}{h_2}\frac{\partial\theta}{\partial z} + \cos\theta\left(K_1 + \frac{1}{h_1}\frac{\partial\theta}{\partial x}\right)\right] \qquad (2.11b)$$

The magnitude of the velocity vector u_t in the boundary layer is given by

$$u_t = (u^2 + w^2 + 2uw \cos\theta)^{1/2} \qquad (2.12)$$

In the present study we use two reduced forms of the above boundary-layer equations. The first is referred to as the quasi-three-dimensional boundary-layer equations in which the flow variations with respect to z are neglected so that the equations become

$$\frac{\partial}{\partial x}(uh_2 \sin\theta) + \frac{\partial}{\partial y}(vh_1 h_2 \sin\theta) = 0 \qquad (2.13a)$$

$$\frac{u}{h_1}\frac{\partial u}{\partial x} + v\frac{\partial u}{\partial y} - K_1 u^2 \cot\theta + K_2 w^2 \csc\theta + K_{12}uw = -\frac{\csc^2\theta}{h_1 \rho}\frac{\partial p}{\partial x} + \frac{\partial}{\partial y}\left(\nu\frac{\partial u}{\partial y} - \overline{u'v'}\right)$$
$$(2.13b)$$

$$\frac{u}{h_1}\frac{\partial w}{\partial x} + v\frac{\partial w}{\partial y} + K_1 u^2 \csc\theta - K_2 w^2 \cot\theta + K_{21}uw = \frac{\csc\theta \cot\theta}{h_1 \rho}\frac{\partial p}{\partial x} + \frac{\partial}{\partial y}\left(\nu\frac{\partial w}{\partial y} - \overline{u'w'}\right)$$
$$(2.13c)$$

The second is referred to as the strip-theory approximation which essentially solves the well-known two-dimensional boundary-layer equations,

$$\frac{\partial u}{\partial x} + \frac{\partial v}{\partial y} = 0 \qquad (2.14)$$

$$u\frac{\partial u}{\partial x} + v\frac{\partial u}{\partial y} = u_e \frac{du_e}{dx} + \frac{\partial}{\partial y}\left(\nu\frac{\partial u}{\partial y} - \overline{u'v'}\right) \qquad (2.15)$$

In this approach, the streamwise external velocity u_e is replaced by the total velocity V defined by

$$V = (u_e^2 + w_e^2 + 2u_e w_e \cos\theta)^{1/2} \qquad (2.16)$$

and is assigned to each spanwise strip.

2.2.2 Interactive Scheme

It is well known that the boundary-layer equations are singular at separation when solved for a prescribed external velocity distribution. They are not singular at separation, however, when the external velocity is computed as part of the solution by, for example, prescribing a displacement thickness: this is known as the <u>inverse problem</u> and leads to solution of the boundary-layer equations with separation.

For flows with separation, the presence of the upstream velocity component introduces a numerical instability into the solution of the boundary-layer equations. Over the years, several approaches have been proposed to overcome this problem. One popular approach, known as the FLARE approximation after the originators, Flugge-Lotz and Reynher [8], neglects the longitudinal convection terms $u(\partial u/\partial x)$ and $u(\partial w/\partial x)$ in the momentum equations (2.5). This approximation is satisfactory provided that the size of the separated region remains small. However, as the size of the recirculation region increases, this approximation becomes less accurate and requires the development of additional procedures to account for the neglected convective terms. One successful scheme, which has been applied to two-dimensional flows, is referred to as the DUIT procedure [15, 16] (Downstream, Upstream Iteration) and requires several sweeps through the recirculation region. With this scheme, the FLARE approach is used to compute a solution within the recirculation region, and then in successive sweeps the $u(\partial u/\partial x)$ term is progressively introduced until it is fully represented. Another successful approach developed by Cebeci [17] makes use of the unsteady boundary-layer equations in which the convective term is introduced into the equations progressively as a function of time. The present method uses only the FLARE approach for both 2-D and quasi-3-D flows, and does not consider the effect of the terms neglected due to this approximation.

In an interactive boundary-layer scheme, a link between a displacement thickness and external flow is provided, and two types of procedures have been developed for this purpose for two-dimensional flows. In the first approach

[18-22], the solutions of the boundary-layer equations are computed initially for a prescribed external velocity to obtain an estimate of the displacement thickness $\delta^*(x)$ distribution, and then in an inverse mode for a specified displacement-thickness distribution $\delta^*(x)$. If this initial calculation encounters separation, $\delta^*(x)$ is extrapolated to the trailing edge. The subsequent boundary-layer calculations are then performed in an inverse mode to compute the blowing velocity needed in the inviscid flow method. In general, this procedure leads to two external velocity distributions, $u_{ev}(x)$ derived from the inverse boundary-layer solution and $u_{e1}(x)$ derived from the updated approximation to the inviscid velocity past the body with viscous effects. A relaxation formula in the form

$$\delta^{*\,\nu+1}(x) = \delta^{*\,\nu}(x) \left[1 + \omega \left(\frac{u_{ev}(x)}{u_{e1}(x)} - 1\right)\right], \quad \nu = 0, 1, 2, \ldots \tag{2.17}$$

where ω denotes a relaxation parameter, is then introduced to define an updated displacement thickness distribution and to obtain new solutions of the boundary-layer equations and the inviscid flow equations so that the inter-active procedure between inviscid and viscous flow solutions can be iterated until convergence is achieved.

The second approach [23], which is recommended on the grounds of general-ity and physical basis, treats the external velocity $u_e(x)$ and the displace-ment thickness $\delta^*(x)$ as unknown quantities. The boundary-layer equations are solved simultaneously in an inverse mode and with successive sweeps over the body surface. For each sweep, the external boundary condition is written as the sum of the inviscid velocity $u_e^o(x)$ over the body, and a perturba-tion velocity $\delta u_e(x)$, that is,

$$y = \delta, \quad u_e(x) = u_e^o(x) + \delta u_e(x) \tag{2.18}$$

The perturbation velocity δu_e is computed from a local approximation based on a thin airfoil theory in terms of the local blowing velocity, $d/d\sigma$ $(u_e \delta^*)$, required to simulate the boundary layer thickness. The perturbation velocity is written as

$$\delta u_e(x) = \frac{1}{\pi} \int_{x_a}^{x_b} \frac{d}{d\sigma} (u_e \delta^*) \frac{d\sigma}{x - \sigma} \tag{2.19}$$

where the interaction region is confined to $[x_a, x_b]$. Introducing a discrete approximation for this integral enables the perturbation velocity to be expressed in terms of the geometric coefficients of the airfoil, as discussed in [4].

This two-dimensional interactive procedure has recently been extended under an AFOSR contract [10] to the quasi-three-dimensional equations referred previously. The relationship between displacement thickness and external velocity needed in the interactive calculations was obtained by generalizing the formulation used for two-dimensional flows. The irrotationality condition, which for an orthogonal system is

$$\frac{\partial}{\partial x} [h_2(w_e^o + \delta w_e)] = [\frac{\partial}{\partial z} h_1(u_e^o + \delta u_e)] \tag{2.20}$$

was used to provide a relationship between the two velocity components u_e and w_e and shows that the choice of computing the perturbation velocities due to viscous effects is not arbitrary. The assumption that $\delta u_e(x)$ is a function of x alone requires that

$$\frac{\partial}{\partial x} (\delta w_e) = 0$$

and that

$$w_e = w_e^o \tag{2.21}$$

In this way the edge boundary conditions for a quasi-three-dimensional boundary-layer flow with interaction are given by Eqs. (2.6) and (2.18).

2.2.3 Turbulence Model

The presence of Reynolds shear stress terms in the boundary-layer equations requires a turbulence model. The algebraic eddy-viscosity ϵ_m formulation of Cebeci and Smith [7] is used here. According to this formulation for two-dimensional wall boundary-layer flows, ϵ_m is defined by two separate formulas, given by

$$\epsilon_m = \begin{cases} \{0.4y[1 - \exp(-y/A)]\}^2 \left|\frac{\partial u}{\partial y}\right| \gamma_{tr} & 0 \leq y \leq y_c \tag{2.22a} \\ \\ \alpha \left|\int_0^\infty (u_e - u)dy\right| \gamma_{tr}\gamma & y_c \leq y \leq \delta \tag{2.22b} \end{cases}$$

where

$$A = 26\nu u_\tau^{-1}, \qquad u_\tau = (\frac{\tau_\ell}{\rho})^{1/2}_{max},$$

$$\tau_\ell = \mu \frac{\partial u}{\partial y}, \qquad \gamma = \frac{1}{1 + 5.5(y/\delta)^6} \qquad (2.23)$$

The condition used to define y_c is the continuity of the eddy viscosity; from the wall outward Eq. (2.22a) is applied until its value is equal to the one given by Eq. (2.22b).

In Eq. (2.22), γ_{tr} is an intermittency factor which accounts for the transitional region that exists between a laminar and turbulent flow. It is given by

$$\gamma_{tr} = 1 - \exp[-G(x - x_{tr}) \int_{x_{tr}}^{x} \frac{dx}{u_e}] \qquad (2.24a)$$

Here x_{tr} is the location of the start of transition. The empirical factor G is

$$G = \frac{1}{1200} \frac{u_e^3}{\nu^2} R_{x_{tr}}^{-1.34} \qquad (2.24b)$$

where the transition Reynolds number $R_{x_{tr}} = (u_e x/\nu)_{tr}$ and the transition location x_{tr} is either specified or calculated from the empirical formula of Michel [29]

$$R_{\theta_{tr}} = 1.174 R_{x_{tr}}^{0.46} (1 + \frac{22,400}{R_{x_{tr}}}) \qquad (2.24c)$$

According to the Cebeci Smith model, the parameter α in Eq. (2.22b) is equal to 0.0168 for values of R_θ greater than 5000, and is given by the expression in [24] for R_θ less than 5000. Studies conducted by Head and his associates [25,26] the recent experimental data of Nakayama [27] and Simpson et al. [28] and the numerical studies of Carter [20] indicate that in flows with strong pressure gradient, the value of α should also be changed when R_θ 5000. Head and his associates recommend that α in Eq. (2.22b) be given by

$$\alpha = \alpha_{eq} F(r) \qquad (2.25a)$$

where

$$\alpha_{eq} = 0.002094 + 0.02672[1 - \exp(-0.1163G)] \qquad (2.25b)$$

$$G = 4.8285 \; (\Pi + 1.0717)^{1/2} + 1.8438 \qquad (2.25c)$$

$$\Pi = \frac{\delta^*}{\tau_w} \frac{dp}{dx} \qquad (2.25d)$$

$$F = \begin{cases} (5 - 4r)/(3 - 2r) & r < 1 \qquad (2.25e) \\[2mm] \dfrac{1}{2r - 1} & r \geq 1 \qquad (2.25f) \end{cases}$$

In Eqs. (2.25e) and (2.25f), r represents the ratio of the local rate of growth of the boundary layer to the rate of growth of the corresponding equilibrium layer.

They also suggested that γ in Eq. (2.23) be replaced by

$$\gamma = \frac{2.0}{1 - \text{erf}[1/2(y/\delta - \beta)]} \qquad (2.25g)$$

where β is a function of shape factor H.

Simpson et al. [28] suggest that

$$\alpha = 0.0168/F^{2.5} \qquad (2.26a)$$

Here F denotes the ratio of the product of the turbulent energy by normal stresses to that by shear stress evaluated at the location where shear stress is maximum, that is,

$$F = \{\frac{(\overline{u'^2} - \overline{v'^2}) \; \partial u/\partial x}{-\overline{u'v'} \; (\partial u/\partial y)}\} \; (-\overline{u'v'})_{max} \qquad (2.26b)$$

Before Eq. (2.26a) can be used in Eq. (2.26b), an additional relationship between $(\overline{u'^2} - \overline{v'^2})$ and $(-\overline{u'v'})$ at $(-\overline{u'v'})_{max}$ is needed. Here we assume that the ratio in Eq. (2.26b),

$$\beta = \{\frac{\overline{u'^2} - \overline{v'^2}}{-\overline{u'v'}}\} \; (-\overline{u'v'})_{max} \qquad (2.26c)$$

is a function of $R_T = \tau_w/(-\overline{u'v'})_{max}$ which, according to the data of Nakayama [27], can be represented by

$$\beta = \frac{6}{1 + 2R_T(2 - R_T)} \tag{2.26d}$$

for $R_T < 1.0$. For $R_T \geq 1.0$, we take β to be

$$\beta \cong \frac{2R_T}{1 + R_T} \tag{2.26e}$$

Introducing the above relationships into the definition of F, we have the following expression for α, according to Eq. (2.26a),

$$\alpha = \frac{0.0168}{[1 - \beta(\partial u/\partial x)/(\partial u/\partial y)]^{2.5}} \tag{2.27}$$

where β is given by Eqs. (2.26d) and (2.26e). This expression is used here although further studies are clearly required to evaluate its range of validity. Work of this nature is in progress.

For three-dimensional flows, the above formulation was generalized as discussed in [16] and in the inner region ε_m is defined by

$$(\varepsilon_m)_i = L^2[(\frac{\partial u}{\partial y})^2 + (\frac{\partial w}{\partial y})^2 + 2(\frac{\partial u}{\partial y})(\frac{\partial w}{\partial y})\cos\theta]^{1/2} \tag{2.28}$$

where

$$L = 0.4y[1 - \exp(-y/A)], \quad A = 26\frac{\nu}{u_\tau}, \quad u_\tau = (\frac{\tau_{tw}}{\rho})^{1/2}$$

$$\tau_{tw} = \mu[(\frac{\partial u}{\partial y})^2_w + (\frac{\partial w}{\partial y})^2_w + 2(\frac{\partial u}{\partial y})_w(\frac{\partial w}{\partial y})_w\cos\theta]^{1/2} \tag{2.29}$$

In the outer region ε_m is defined by

$$(\varepsilon_m)_o = \alpha \left| \int_0^\infty (u_{te} - u_t)dy \right| \tag{2.30}$$

and α is given by Eq. (2.27).

2.2.4 Transformed Equations

The equations of Section 2.2.1 may be solved in the forms presented or expressed in other forms which are more convenient for accurate solution. For two-dimensional flows, as in [4], we use the Falkner-Skan transformation in the early stages of the flow

$$\eta = \sqrt{u_e/\nu x}\ y, \quad \psi = \sqrt{u_e \nu x}\ f(x,\eta) \tag{2.31}$$

With primes denoting differentiation with respect to η and $b = 1 + \epsilon_m/\nu$, Eqs. (2.14) and (2.15) and their boundary conditions can be written in the form:

$$(bf'')' + \frac{m+1}{2}\ ff'' + m[1 - (f')^2] = x(f'\ \frac{\partial f'}{\partial x} - f''\ \frac{\partial f}{\partial x}) \tag{2.32}$$

$$\eta = 0, \qquad f = f' = 0 \tag{2.33a}$$

$$\eta = \eta_e, \qquad f' = 1 \tag{2.33b}$$

Here ψ is the usual definition of the stream function that satisfies the continuity equation,

$$u = \frac{\partial \psi}{\partial y}, \qquad v = -\frac{\partial \psi}{\partial x} \tag{2.34}$$

and m is a dimensionless pressure-gradient parameter,

$$m = \frac{x}{u_e}\ \frac{du_e}{dx} \tag{2.35}$$

This transformation provides the generation of initial conditions at the stagnation point of the airfoil and allows the calculations to be performed economically and accurately around the leading edge, where the governing equations are being solved for the prescribed external velocity distribution. For interactive boundary-layer calculations, where $u_e(x)$ is not known, a constant reference velocity u_o is used in the transformation

$$Y = \sqrt{u_o/\nu x}\ y, \qquad \psi = \sqrt{u_o \nu x}\ F(x,Y) \tag{2.36}$$

In terms of these new variables, Eqs. (2.14) and (2.15) and their boundary conditions can be written in the form:

$$(bF'')' + \frac{1}{2}\ FF'' + xe\ \frac{de}{dx} = x(F'\ \frac{\partial F'}{\partial x} - F''\ \frac{\partial F}{\partial x}) \tag{2.37}$$

$$Y = 0, \qquad F = F' = 0 \tag{2.38a}$$

$$Y = Y_e, \qquad F' = e, \qquad e - \dot{c}_{11}\ (Y_e e - F) = g_1 \tag{2.38b}$$

where

$$\dot{c}_{11} = c_{11}\ \sqrt{\nu x/u_o}, \qquad e = \frac{u_e}{u_o}$$

Here the parameter g_i, which results from the discrete approximation to Eq. (2.19) is given by

$$g_i = \bar{u}_e^\kappa + \sum_{j=1}^{i-1} c_{ij}(D_j - D_j^\kappa) - c_{ii}D_i^\kappa \qquad (2.39)$$

where

$$D = \sqrt{\nu x/u_o} \ (Y_e e - F_e)$$

For quasi-three-dimensional flows, we define

$$x = x, \qquad d\eta = \left(\frac{u_o}{\nu s_1}\right)^{1/2} dy \qquad (2.40)$$

Here u_o is a reference velocity and s_1 denotes the length in the longitudinal direction measured from the initial line $x = x^*$. We again introduce the definition of stream function $\psi(x,y)$

$$uh_2 \sin\theta = \frac{\partial\psi}{\partial y}, \qquad vh_1h_2\sin\theta = -\frac{\partial\psi}{\partial x} \qquad (2.41))$$

so that with the definition of eddy viscosity, the quasi-three-dimensional boundary-layer equations given by Eq. (2.13) can be written as [10]

$$(bf'')' + m_1 ff'' + m_3[(f')^2 - e^2] + m_5(f'g' - \bar{w}_e e) + m_4[(g')^2 - (\bar{w}_e)^2]$$

$$= m_9\left(f'\frac{\partial f'}{\partial x} - e\frac{\partial e}{\partial x} - f''\frac{\partial f}{\partial x}\right) \qquad (2.42)$$

$$(bg'')' + m_1 fg'' + m_6[(g')^2 - \bar{w}_e^2] + m_7[(f')^2 - e^2)] + m_8(f'g' - \bar{w}_e e)$$

$$= m_9\left(f'\frac{\partial g'}{\partial x} - e\frac{\partial \bar{w}_e}{\partial x} - g''\frac{\partial f}{\partial x}\right) \qquad (2.43)$$

where, with $f' = u/u_o$, $g' = w/u_o$, $\bar{w}_e = w_e/u_o$

$$m_1 = \frac{\sqrt{s_1}}{h_1h_2 \sin\theta}\frac{\partial}{\partial x}(\sqrt{s_1}\ h_2 \sin\theta), \qquad m_3 = K_1 s_1 \cot\theta$$

$$m_4 = -K_2 s_1 \csc\theta, \qquad m_5 = -K_{12}s_1, \qquad m_6 = s_1 K_2 \cot\theta \qquad (2.44)$$

$$m_7 = -m_3, \qquad m_8 = -K_{21}s_1, \qquad m_9 = s_1/h_1$$

The boundary conditions become

$$\eta = 0, \qquad\qquad f = f' = 0, \qquad\qquad g = g' = 0 \qquad\qquad (2.45a)$$

$$\eta = \eta_e, \qquad\qquad f' = e(x), \qquad\qquad g' = \bar{w}_e(x) = \bar{w}_e^o \qquad\qquad (2.45b)$$

$$e(x) = \bar{u}_e^o + \frac{1}{\pi} \int_{x_a}^{x_b} \frac{d\Delta}{d\sigma} \frac{d\sigma}{x - \sigma}$$

where

$$\Delta = \frac{s_1}{\sqrt{R}} (\eta_e e - f_e), \qquad\qquad R = \frac{u_o s_1}{\nu} \qquad\qquad (2.46)$$

2.2.5 Solution Procedure

The numerical solution of the system of equations given in the previous section is obtained with Keller's box method for the standard and interactive methods. This is an efficient, second-order finite-difference method extensively used by Cebeci and his associates for a wide range of flows, as discussed in Bradshaw et al. [16]. The description of the standard method is given in that reference as well as in Cebeci and Bradshaw [29]. The general features of the inverse method which makes use of the Mechul-function formulation are also described for two-dimensional flows in Bradshaw et al. [16] and in [10] for quasi-three-dimensional flows. As in previous two-dimensional studies the FLARE approximation in which the convective term $\partial F'/\partial x$ is set equal to zero in the recirculating region is employed, and no attempt was made to improve the accuracy of the solutions resulting from this approximation.

As in the solution of two-dimensional flows by Keller's method, we write Eq. (2.37) as a first-order system. For this purpose we let

$$F' = u \qquad\qquad (2.47a)$$
$$u' = v \qquad\qquad (2.47b)$$

and write Eq. (2.37) as

$$(bv)' + \frac{1}{2} Fv + xe \frac{de}{dx} = x(u \frac{\partial u}{\partial x} - v \frac{\partial F}{\partial x}) \qquad\qquad (2.47c)$$

Since e is a function of x, only, we write

$$e' = 0 \qquad\qquad (2.47d)$$

The boundary conditions for the system given by Eqs. (2.47) now can be written as

$$Y = 0, \qquad F = 0, \qquad u = 0 \qquad\qquad (2.48a)$$

$$Y = Y_e, \qquad u = e, \qquad e - \dot{c}_{11} (Y_e e - F) = g_1 \qquad\qquad (2.48b)$$

After the finite-difference approximations to Eqs. (2.47) and (2.48) are written, the resulting nonlinear algebraic system is linearized by Newton's method and the linear system is then solved by the block elimination method. For further details, see [29].

SECTION III
RESULTS AND DISCUSSIONS

The interactive boundary-layer procedure described in the previous section has been applied to a number of test cases and the results will be presented here.

Section 3.1 presents the results obtained from the application of the two-dimensional strip theory approach to two wing alone configurations to verify the soundness of the interactive boundary layer technique. Section 3.2 will present the results obtained from the two-dimensional and the quasi-three dimensional methods for three wing-body fighter configurations.

3.1 Wing Alone Configurations

The first configuration considered is an RAE clean wing with a 28° sweep angle for which experimental data has been obtained by Lovell [30]. Figure 5 shows the computed lift curve up to 18° angle of attack. It can be seen that there is good agreement up to about 12°, beyond which the discrepancy increases. This disagreement at the higher angles of attack is due to the three-dimensional nature of the flow, and due to the sensitivity of the flow to the transition location. This sensitivity is illustrated by Fig. 6 which shows the variation of the flow solution to the transition location at an angle of attack of 17.5°. Moving the transition location leads to a significant change in the lift separation location and displacement thickness, particularly near the wing tip. Figure 7 shows the results for α = 18.5° with the computed transition location. As can be seen the separation location at this angle of attack occurs at about the midchord location. The size of the leading and trailing edge separation regions at α = 17.5° can be seen from Fig. 8 in which the local skin friction is plotted.

Near the wing tip it can be seen that there is a small leading edge separation, shown by the region of negative skin friction, and that the trailing edge separation is occurring at about 65% local chord.

Figures 9-11 illustrate the results obtained for a NACA 0012 swept wing for which data was obtained by Yip and Shubert [31] for a range of angles of attack. Figure 9 shows the viscous and inviscid lift up to 21-18° from which the effects of the increasing flow separation at higher angles of attack can

clearly be seen. Figure 10 shows the computed and experimental pressure distributions for $\alpha = 19.35°$ at two sections, 50% and 85% of semispan, both of which agree very well.

The importance of the transition location is illustrated by Figure 11 which shows the computed separation location, trailing-edge displacement thickness and lift distribution for $\alpha = 21.12°$. Two curves are shown, the solid line was obtained with a computed transition location at about 3% chord on the upper surface. The dashed line was obtained by specifying a transition location closer to the leading edge attachment line on the lower surface. It can be seen that this small movement in the transition location moves the separation location forward from 60% chord to about 30% chord.

3.2 Application to Wing/Body Test Cases

Three wing/body test cases were identified for which there was experimental data available to evaluate the current procedure. The three cases are, an F-15 with a modified wing designed to investigate the role of a leading-edge laminar separation, an Advanced Navy Fighter configuration, and an unmodified F-15. The geometry and input data associated with these test cases is discussed in detail in Section 5 (Figs. 26-30).

The F-15 laminar bubble configuration has been run at a range of angles of attack using both the 2-D and the quasi 3-D boundary-layer procedures. Figure 12 shows the computed lift compared with the experimental data [32]. It can be seen that at lower angles of attack the 2-D and quasi 3-D approaches agree closely, while at higher angles of attack the quasi 3-D boundary-layer procedure agrees better with the experimental data. At lower angles of attack both approaches over-predict the lift, possibly due to an inadequate modelling of the flow over the body.

Figure 13 shows an example of the computed and experimental pressure distributions for $\alpha = 10.75°$ angle of attack at three stations across the span from close to the wing tip to close to the wing root. It can be seen that for this angle of attack there is very little difference between the 2-D and the quasi three dimensional boundary layer methods, and that both give a reasonable approximation to the measured pressures except close to the leading edge.

One further aspect of the present method which has been investigated concerns the use of a panel method for the calculation of compressible flow. A panel method is an incompressible solution procedure and so Mach number effects must be accounted for by means of a compressibility correction. In this case a Goethert correction is applied using the following procedure: the solution to the linearized potential flow equation

$$(1 - M_\infty^2) \frac{\partial^2 \phi}{\partial x^2} + \frac{\partial^2 \phi}{\partial y^2} + \frac{\partial^2 \phi}{\partial z^2} = 0 \qquad (3.1)$$

is obtained, where ϕ is the perturbation in the potential due to the body. Provided that this perturbation velocity is small compared with the freestream velocity equation (3.1) provides a good approximation to the flow. This is true for the flow over thin wings. However, around the leading edge, or on any forward facing surface, this basic assumption is violated.

The compressibility correction for the initial velocity calculation is implemented here by first scaling the y and z coordinates by $\beta = \sqrt{(1 - M_\infty^2)}$. The incompressible flow is then computed about this equivalent body and the computed velocity components are divided by β^2 in the x-direction and β in the y- and z-directions.

For the subsequent updates to the inviscid velocity to account for the viscous effects the same procedure is adopted. However, this calculation involves two additional features over the initial inviscid calculation. The first is the introduction of the blowing velocity required to simulate the displacement thickness and the second is the introduction of off-body points at which the Kutta condition is to be applied and the final velocity computed. In applying the Mach number correction two additional assumptions are therefore necessary. The first is that the blowing velocity is predominantly in the y,z direction so that the blowing velocity applied on the "equivalent incompressible body" can be scaled by β. The second assumption is that the displacement effect of the boundary layer is also predominantly in the y,z direction. Therefore in defining the off-body point location in the transformed plane the displacement thickness is first scaled by β. Since both the displacement thickness and the blowing velocity are most significant near the trailing edge both of these assumptions are valid.

It should be pointed out that the interactive viscous calculation is performed entirely in the physical plane. The Mach number correction outlined above is used to provide the compressible external velocity distribution.

While the compressibility correction will provide a good approximation at lower angles of attack, it becomes less accurate at higher angles of attack when the flow can become supercritical and shock waves can form through the leading edge region. Figure 14 shows the inviscid computed pressure distribution at the mid-semispan location computed by the present panel method and by the transonic full-potential wing/body code developed by Chen et al. [33] at $\alpha = 6.84°$, $10.75°$ and $12.95°$ for $M = 0.6$. At the lower angle of attack the two procedures agree well except close to the leading edge where the transonic code predicts a higher suction peak. However, at $\alpha = 12.95°$ the transonic method predicts a shock wave and a larger difference in the pressure distribution through this region is predicted.

The second wing/body test case which has been considered is the Advanced Navy Fighter (ANF) for which experimental data is available [34]. This configuration was tested experimentally both with and without a canard. Figure 15 shows the computed and experimental lift distribution for this configuration without the canard and Figure 16 shows the viscous and inviscid pressure distribution compared with experimental data at $\alpha = 7.7°$ across the span. It can be seen that there is good agreement. The only other pressure data for this particular configuration is for $\alpha = 22°$ at which angle the data shows the presence of a shock wave near the leading edge suction peak. Due to the limitations of the compressibility correction outlined above this case has not been pursued. The effect of the canard is shown in Figure 17, in which the computed viscous lift distribution is shown with and without the canard. This case was run with the canard at zero deflection angle for which there was no experimental data, and the viscous effects were computed only on the main wing.

The final configuration which has been investigated is an unmodified F-15 wing/body for which experimental data was obtained by Anderson [35]. Figure 18 shows the computed and experimental lift curves from which it can be seen that there is good agreement up to $8.66°$ angle of attack. Figure 19 shows the computed pressure distribution for $8.66°$ which is in good agreement with the experimental data.

SECTION IV
PROGRAM DESCRIPTION

The method developed here calculates the viscous flow over a lifting body through the use of an interactive boundary layer technique in which a three dimensional panel method is coupled with a finite-difference boundary layer method. Two distinct boundary-layer procedures have been adopted, the first of which uses a two-dimensional strip theory approach while the second is a quasi-three-dimensional boundary-layer method.

The structure of the code is illustrated in Figure 20, which gives a schematic flow chart of the code. There are three major computational modules required, namely the inviscid panel method, the two-dimensional boundary-layer routines and the quasi-three-dimensional boundary-layer routines. The communication between the potential flow code and the boundary-layer routines is handled through the use of external disk storage.

For a given flow condition the inviscid solution is first computed and the pressure distribution over the wing is saved. If the 2-D boundary-layer mode is selected, this data is separated into strips, and an interactive boundary-layer calculation is performed independently for the upper and lower parts of each lifting strip using the method outlined in Section 2.2.5. Each of these boundary-layer calculations require a number of iterative sweeps over each surface in order to match the current external velocity distribution, given by Eqs. (2.18) and (2.19), with that computed by the boundary-layer equations, (2.47) and (2.48). Once these inner iterations have been completed and the corresponding displacement thickness and blowing velocity has been computed these data are transferred back to the inviscid flow code and the external velocity distribution is updated to incorporate the viscous effects. One complete iteration between the viscous and inviscid codes is referred to as a cycle. Several such cycles are usually performed in order to obtain a fully converged solution in which the computed viscous and inviscid solutions match one another. The precise number of cycles performed is governed either by an input parameter which specifies the maximum number of cycles, or else by a convergence check which is based on the maximum change in a displacement thickness parameter form one cycle to the next. Typically up to 5 cycles may be required for a fully converged solution.

A similar procedure is employed for the quasi three-dimensional boundary layer method with interface routines handling the transfer of the data between the viscous and the inviscid codes. In this case the data required is more extensive than that required for the two-dimensional boundary layer calculation since surface coordinates and curvatures are required for the complete surface. Therefore, the interface program accesses the velocity data produced by the inviscid calculations, and computes a dividing line separating the upper and lower portions of the wing flowfield. For each surface, a boundary-layer grid is now defined and the geometric surface curvatures and the velocity components are interpolated onto the boundary-layer grid. The quasi three-dimensional boundary-layer procedure now iterates over each surface in a similar fashion to the two-dimensional approach in which the perturbed inviscid velocity is matched with that computed by the boundary-layer equations, (2.42) - (2.46). The computed displacement thickness and blowing velocity is then transferred back to the potential flow code for the next viscous/inviscid cycle.

After a converged solution has been obtained for the first specified angle of attack, the process is repeated for the next angle of attack. However, rather than start the calculation using the purely inviscid potential flow solution, the blowing velocity and displacement thickness computed for the previous angle of attack are used for boundary conditions in the first inviscid flow solution. Therefore, when running multiple angles of attack, the angles should be specified in increasing order. In this way the number of cycles required for a converged solution is reduced, particularly at higher angles of attack when boundary-layer separation can lead to fairly large displacement thicknesses. To take further advantage of this fact, the program may be exe cuted in a restart mode in which data stored by a previous run may be input as a starting solution for the next angle of attack to be computed. After each run, the following two datasets may therefore be saved for use in a subsequent run:

Unit #33   This stores the blowing velocity and the displacement
           thickness data.

and

Unit #47   This unit stores the geometric coefficients of the airfoil
           appearing in the interaction formula used in the quasi
           three-dimensional boundary layer methoa.

or

> Unit #51 - This unit stores the geometric coefficients of the air-
> foil appearing in the interaction formula used in the
> two-dimensional boundary-layer method.

The user can therefore run a range of angles of attack either by specify-
ing all of the angles of attack in one single run, or else as a series of
separate runs which make use of the restart capability.

4.1   Input Data Description

4.1.1   Body Geometry

The input to this program consists of the coordinates of a number of
points that define the surface of a three-dimensional configuration on which
the flow is to be computed. For the purpose of organizing these points for
computation, each point is assigned a pair of integers, m and n.   These
integers need not be input, but their use must be understood to insure the
correctness of the input and to facilitate the interpretation of the output.

For each point, n identifies the "column" of points to which it belongs,
while m identifies its position in the "column," i.e, the "row." The first
point of a "column" always has m = 1.   To insure that the program will compute
outward normal vectors, the following condition must be satisfied by the input
points.   If an observer is located in the flow and is oriented so that locally
he sees points on the surface with m values increasing upward, he must also see
n values increasing toward the right.   Examples of correct and incorrect input
are shown in Figure 21.   In this figure the flowfield lies above the paper,
while the interior of the body lies below the paper.   Occasionally, it happens
that despite all care a body is input incorrectly.   If the entire body is input
incorrectly - not some sections correctly and some incorrectly - the difficulty
can be remedied by changing the sign of one coordinate of all the input points.
This trick will give an input body of the proper shape at perhaps a peculiar
location.   Otherwise, the input will have to be done over.

The body surface is divided into sections, which may be actual physical
divisions or may be selected for convenience.   A section is defined as con-
sisting of a group of at least two n-lines.   Within each section the n-lines

are input in order of increasing n. On each n-line the points are input in order of increasing m. All n-lines in a section must have the same number of points, but this may vary from section to section. The first n-line of the first section is n = 1. From then on the n-lines may be thought of as numbered consecutively through all sections, i.e., the numbering is not begun over at the beginning of each section. Panels will be formed that are associated with points on every n-line except those that are last in their respective sections. Points on these latter n-lines are used only to form panels associated with points on the next lowest n-lines.

To illustrate this procedure, consider the plan view of a body shown in Figure 22. This body has been divided into four sections, as shown in the figure. The first section contains four n-lines, n = 1, 2, 3, 4; the second, five n-lines, n = 5, 6, 7, 8, 9; the third three n-lines, n = 10, 11, 12; and the fourth three n-lines; n = 13, 14, 15. The number of points on each n-line are:

$$\text{Section} = 1\ 2\ 3\ 4$$
$$M = 4\ 7\ 4\ 2$$

Notice that the line n = 4 has only four points, the points m = 1, 2, 3, 4 and the m-grid of Section 1, which is listed in the figure along the n = 1 line. The lines n = 4 and n = 5 are physically identical. Some of the points on the two lines are physically identical but correspond to different values of m. This is of no consequence. In this scheme sections are completely independent. No elements are computed corresponding to points on lines n = 4, 9, 12, 15.

There is no restriction that the m and n lines of different sections have to be roughly parallel. The arrangement shown in Figure 23 is permissible.

As discussed in Section 2.1, the body is divided into lifting and nonlifting sections. The arrangement of the input requires that all lifting sections precede nonlifting sections with a one-point-per-card format of (3F10.5,2I1) with a maximum of 2000 panels and 100 strips defining the configuration. This data is input to the program through Unit #29. Also, since the boundary-layer calculations can be made for only one lifting section, this section must precede any other lifting sections. The two integers that follow each set of coordinates are the status flag and label flag, respectively, that is

STATUS FLAG	LABEL FLAG
2 - new section	1 - lifting body, or 0 - nonlifting body
1 - new N-line	(these flags are needed only when STATUS FLAG = 2)
0 - same N-line	
3 - end of input for the whole body	

4.1.2 Namelist Block Input

There are two namelist blocks that contain two groups of input data.

Namelist Name A:

This namelist block consists of all the control flags and flow conditions
required to control the interactive viscous calculation.

Variables	Remarks
LIFT3D	Control flag for the execution of the potential-flow program. = 0 Skip the initial potential flow and execution will start with the boundary-layer code. = 1 Use the potential flow program for every cycle. (default is 1)
IBL3D	Control flag for executing a boundary-layer program. = 0 Use the two-dimensional boundary-layer program. = 1 Use the quasi-three-dimensional boundary-layer program. (default is 0)
KINKNO	Total number of "kink" stations input ("kink" station means a discontinuity in the planform of the first lifting section). (default is 0, maximum is 5)
MS	Station numbers where "kink" occurs in the planform. The order of these "kink" stations should be in the same order as the spanwise stations input to the Neumann program. They are also part of the input spanwise stations. (default is 0)
MLINE(i)	Number of defining chordwise points on each N-line of the i-th lifting section.
NLINE(i)	Number of defining spanwise points on each M-line of the i-th lifting section.
MAXCYC	Maximum number of interaction cycles. (default is 0)

Variables	Remarks
MAXANG	Number of angles of attack to be calculated. (default is 1, maximum is 10)
IPNTGM	Optional (debug) print flag for the interfacing program. = 0 No intermediate print. = 1 With intermediate print. (default is 0)
IPNTNU	Optional (debug) print flag for the potential flow program. = 0 No intermediate print. = 1 With intermediate print. (default is 0)
IPNTB3	Optional (debug) print flag for the quasi-three-dimensional boundary layer program. = 0 No intermediate print. = 1 With intermediate print. (default is 0)
DBMAX	Maximum difference in circulation values generated from potential flow solution for convergence. (default is 0.01)
ALPHAI	Input angles of attack values. Total number input = MAXANG. (default is 0.0)
AMACH	Input Mach number. (default is 0.0)

Namelist Name B:

Namelist B contains the geometric variables and control flags which pertain to the potential flow calculation.

Variables	Remarks
BOV2	The semi-span value of the lifting body. (default is 1.0)
IAUTOW	Automatic wake generation flag: = 1 Program generates bisector wake. = 2 Program generates flat wake, i.e. wake panel is parallel to the x-axis. = 0 User input wake panels. (default is 1)
IPCV	Chordwise vorticity flag. = 0 Constant vorticity used. = 1 Parabolic vorticity used. (default is 0)

Variables	Remarks

NOTE: This flag controls the form of the predetermined chordwise bound-vorticity variation discussed in Section 2.1. For wings with cusped or thin trailing edges, the constant variation may lead to unrealistic variations in the pressure close to the trailing edge. In such cases, the parabolic variation should be used. Otherwise the constant chordwise option should be used.

ITERAT   Matrix Solution flag.
= 0   (direct solution for 350 panels or less, otherwise use iterative solution).
= 1   Iterative solution.
= 2   Direct solution.
(default is 1)
Note: Iterative solution must be used when viscous calculations are made.

IVNSP   Nonuniform Flow/Specified Normal Velocity flag.
= 0   No nonuniform flow or blowing velocity.
= 1   Nonuniform Flow Specified. In the case onset flow velocity components at every control point must be input on Unit 33 in 3F10.6 card image format. Otherwise velocity components are computed from freestream flow direction.
= 2   Nonzero normal velocity condition is specified on some section or sections. If this option is used, then Unit 33 must contain the following data:
    1st record: "SECTION k"
    Subsequent records: required normal velocity (FORMAT 1F10.6) with 1 record for each control point in the k-th section. These cards are repeated for each section for which nonzero boundary condition is satisfied.
NOTE: These options are only available for a purely inviscid calculation.

LIFSEC   Number of lifting sections input.
NOTE: Boundary-layer calculations can be made for the first lifting body only.

LINEAR   Spanwise vorticity flag.
= 0   Constant vorticity used.
= 1   Linear vorticity used. If selected, the variables, NLINE1 and NLINEN must be input.
(default is 0)
NOTE: This flag controls the variation of spanwise vorticity across a given lifting strip. The level on each strip is determined by the Kutta condition as discussed in Section 2.1.

Variables	Remarks
NLINE1(i)	Condition for the first N-line of the i-th lifting section. = 1 The first N-line is the wing tip. = 4 The first N-line belongs to an extra strip or is next to a symmetry plane.
NLINEN(i)	Condition for the last N-line of the i-th lifting section. = 1 The last N-line is the wing tip. = 4 The last N-line belongs to an extra strip or next to a symmetry plane.
LIST	Geometry formation flag. = 0 Complete potential flow calculation modes. = 1 Calculation stop after geometry formation (default is 0)
NOFF	Off-body point flag. = 0 No off-body point input. = 1 Off-body point input. (default is 0) NOTE: Off-body points are points in the flow at which the velocity and pressure are to be computed. If this option is used, the off-body coordinates must be supplied on Unit 32 using 3F10.6 card image format.
NSYM1	First plane of symmetry flag. = 0 No symmetry. = 1 One plane of symmetry (about the x-z plane). (default is 1)
NSYM2	Second plane of symmetry flag. = 0 No second plane of symmetry used. = 1 Symmetry about the y-z plane (NSYM1 must also be = 1). (default is 0)
ORIGNX ORIGNY ORIGNZ	The x,y,z coordinates of the input moment origin (default is 0, 0, 0).
NSORCE(i)	Number of on-body panels per strip for the i-th lifting section.
NWAKE(i)	Total number of wake panels input for the i-th lifting section. (If IAUTOW $\neq$ 0, NWAKE $\equiv$ 1)
NSTRIP(i)	Total number of strips in the i-th lifting section.
IXFLAG(i)	Extra strip option input for the i-th lifting section. = 0 No extra strip. = 1 First strip is an extra strip. = 2 First and last strips are extra strips. = 3 Last strip is an extra strip.

Variables	Remarks

NOTE: An extra strip is a strip of panels on a lifting section which carries a vorticity distribution but on which no boundary conditions are satisfied. Such a strip is used for instance at an intersection between a wing and a fuselage in order to provide a more accurate carry-over of the wing lift across the fuselage. In this case the extra strip is internal to the fuselage, and it extends from the wing root to the fuselage centerline. Further details of the use of extra strips is discussed by Hess [36].

REFCHD — Reference chord value. (This is needed for the calculation of the lift coefficient.) (default is 1.0)

RFAREA — Reference area value. (This is needed for the calculation of the lift coefficient.) (default is 1.0)

4.1.3 Boundary-Layer Calculation Data Input

(a) Card number 1
Format (6F10.0)

Card Column	Variables	Remarks
1-10	$RC \times 10^{-6}$	Reynolds number based on CREF.
11-20	CREF	Reference length. In the same physical units that are used for the input geometry.

NOTE: This need not be the same value as REFCHD used above. CREF is only used to calculate the local Reynolds number in terms of the input coordinates. e.g. If the geometry is specified in inches, and the Reynolds number/ft is input, then CREF would be 12.

31-40	FRSTAT	= 1.0	Option for using a previous angle of attack solution as an initial estimate for the current angle of attack calculation.
		= 0.0	Option not used (or the initial run).
41-50	FPRNT	= 1.0	Detailed boundary-layer print.
		= 0.0	No boundary-layer print.

(b) Card Number 2
   Format (6F10.0)

Card Column	Variables	Remarks
1-10	FNBLU	Number of boundary layer stations at which calculations are made on the upper surface of the first lifting body (max = 100).
11-20	FTRIU	Transition input flag = 0 Transition location specified across the span. See Cards 3 and 4. = 1 Transition calculated by the program at pressure peak. = 2 Transition calculated by the program using Michel's criteria.
21-30	FSWPU	Number of iteration sweeps to be made for the upper surface. (FSWPU = 10.0 is recommended)
31-40	FNTRU	Number of transition locations to be specified. (if FTRIU = 0)

(c) Card number 3 (needed only if FTRIU = 0).
   Format (6F10.0)

Card Column	Variables	Remarks
1-10	YTRN	Spanwise location, in the input geometry system, where transition will be specified (this location does not have to correspond to the coordinates used to define the geometry).
11-20	YTRN+1	
	.	
	.	
	.	
51-60	YTRN+5	

(Repeat this card if necessary until i = FNTRU.)

(d) Card number 4 (needed only if FTRIUF 0).
   Format (6F10.0)

Card Column	Variables	Remarks
1-10	XCTRN	x/c chordwise location of specified transition.

5227H   44

11-20   XCTRN+1
                                  .
                                  .
          51-60   XCTRN+5

            (Repeat this card if necessary until i = FNTRU.)

     The following cards, numbers 5, 6 and 7, have the same format as cards
2, 3 and 4 and the variables have the same meaning but correspond to the lower
surface.

     (e)   Card number 5
           Format (6F10.0)

           Variables   FNBLL, FTRIL, FSWPL, FNTRL

                FSWPL = 5.0 is recommended.

     (f)   Card number 6
           Format (6F10.0)

           Variable   YTRN

     (g)   Card number 7
           Format (6F10.0)

           Variable   XCTRN

     Note that the chordwise location of specified transition must be preceded
by a minus sign when it is being input on the airfoil lower surface.

     The cards in this section, (a) through (g), are to be repeated for each
angle of attack calculated.

4.2 Output Data Description

4.2.1 Summary
Potential Flow

     The following data are printed for the potential flow calculation:

     1.   Input flags.

II. Panel formation.

III. Matrix solution (by iteration method).

IV. Solution summary. This includes:

lift coefficient, drag coefficient, pitch, roll, yaw and η values for each lifting and nonlifting section, plus the same set of data for the whole configuration.

V. Final cycle. For every panel, the following data are printed:
. panel number
. control point coordinates - x_o, y_o, z_o
. inviscid velocities - v_x, v_y, v_z
. inviscid total velocity V_T and viscous corrected pressure coefficient Cp
. displacement thickness - DELS
. shape factor - H
. skin friction - CF.

4.2.2 Format

A test case consisting of one lifting and four nonlifting sections with a total of 221 panels, Figure 24, was created to present a sample of the program output, and a listing of this geometry (input through Unit #29) is presented in Table 1. Two angles of attack were calculated with the transition locations on the lifting section computed by the program. The namelist block input for this case is:

```
     REPORT TEST CASE,TRANS. CALC., 2DSTRIP BL, M=0.6, ALPHAS
  &A   LIFT3D=1,IBL3D=0,
   MAXCYC=2,NLINE=5,MLINE=21,
   MAXANG=2,ALPHAI(1)=1.3,ALPHAI(2)=3.4,
   AMACH=0.6,&END
  &B  BOV2=12.955,IAUTOW=2,NSYM1=1,LIFSEC=1,REFCHD=8.2912,
   LINEAR=0,IXFLAG(1)=3,IPCV=1,
   RFAREA=95.904,NSORCE=20,NSTRIP=4,NWAKE=1,&END
   7.0         12.0        0.0         0.0
   70.0        2.0         10.0
   51.0        2.0         5.0
   7.0         12.0        0.0         0.0
   70.0        2.0         10.0
   51.0        2.0         5.0
```

For conciseness, the output presented here will be the pertinent information for the first angle of attack only and is shown in Figure 25.

Table 1. Input geometry data for the sample test case.

x	y	z	x	y	z	x	y	z
20.320007	12.950000	5.899997221	22.049906	5.8999998	5.479327200	25.103775	0.0000000	8.985786300
20.246164	12.950000	5.659627600	21.466964	5.8999998	5.458943400	26.737654	0.0000000	8.692972200
20.039001	12.950000	5.642726900	21.294366	5.8999998	5.502729400	28.032578	0.0000000	8.436945900
20.712478	12.950000	5.627047600	21.491623	5.8999998	5.590655600	28.658848	0.0000000	8.247252500
20.301103	12.950000	5.604248100	22.046367	5.8999998	5.692218800	29.130996	0.0000000	8.169997200
20.040039	12.950000	5.580801300	22.921061	5.8999998	5.774380700	1.4399998	0.0084315	8.159999920
27.390901	12.950000	5.529635300	24.025009	5.8999998	5.855646100	1.4399996	0.0096637	8.161227200
27.079998	12.950000	5.503608700	25.251343	5.8999998	5.891611400	1.4399998	0.0104338	8.160467200
28.653732	12.950000	5.482165600	26.476624	5.8999998	5.850277900	1.4399998	0.0103374	8.157036000
28.444412	12.950000	5.467030400	27.582291	5.8999998	5.778900300	1.4399998	0.0085511	8.151741000
28.371002	12.950000	5.412908200	28.461606	5.8999998	5.720014000	1.4399998	0.0027379	8.149518000
28.441605	12.950000	5.511903600	29.026606	5.8999998	5.690284300	1.4399998	0.0001827	8.150368700
28.650253	12.950000	5.537014000	29.220001	5.8999998	5.899997200	1.4399998	-0.0004819	8.149361800
28.975100	12.950000	5.572729600	29.161774	1.6310434	5.889997210	1.4399998	-0.0004818	8.145678600
27.385144	12.950000	5.614417200	28.907547	1.8265334	5.863852200	1.4399998	0.0000000	8.139994400
27.640240	12.950000	5.660013200	28.172606	1.6335669	6.000514400	3.0000000	0.1926538	8.099999610
28.296280	12.950000	5.661705600	27.029626	1.6679520	5.521410000	3.0000000	0.3631787	8.060020300
28.700923	12.950000	5.631177000	25.508023	1.7761669	5.490619700	3.0000000	0.4918574	7.767053600
28.036098	12.950000	5.675670900	23.966262	1.8357840	5.536683900	3.0000000	0.5807862	8.616421700
28.247543	12.950000	5.694785600	22.388857	1.9419851	5.619744300	3.0000000	0.4959082	8.435597400
28.320007	12.950000	5.689997200	20.949631	2.0539112	5.699937600	3.0000000	0.3800985	8.237468700
29.270004	9.3299999	5.522551600	19.806320	2.1326818	5.759287600	3.0000000	0.1880037	8.053067200
29.137955	9.3299999	5.489905900	18.071396	2.1760240	5.786211000	3.0000000	0.0000000	5.914361000
28.750611	9.3299999	5.443327900	18.846486	2.2000370	5.877244000	6.0000004	0.3767620	5.818710300
28.162079	9.3299999	5.426945700	18.097867	2.1932545	5.896942500	6.0000004	0.6720765	5.759999300
27.409607	9.3299999	5.395072800	19.618451	2.1306517	6.138426900	6.0000004	0.9096854	8.000000010
28.576279	9.3299999	5.436118900	20.959732	2.0326290	6.215392100	6.0000004	1.0701628	7.875558900
25.743439	9.3299999	5.507829700	22.402405	1.9267807	6.247961100	6.0000004	1.1407099	7.807360800
24.891823	9.3299999	5.547428100	24.003601	1.8385239	6.225801200	6.0000004	1.0307589	7.261573300
24.394516	9.3299999	5.696475000	25.601136	1.7746687	6.115730300	6.0000004	0.7527732	8.911097600
24.012182	9.3299999	5.660374100	27.036620	1.6863613	5.901447700	8.0000004	0.3936298	8.517292000
23.880367	9.3299999	5.699997210	28.160146	1.6216841	5.824655500	8.0000004	0.0000000	8.135311100
24.009415	9.3299999	5.669997210	28.911484	1.6256928	5.714833300	8.0000004	0.3798224	8.645423700
24.391281	9.3299999	5.651124000	29.161774	1.6310434	5.869997200	8.0000004	0.8868429	8.806372800
24.980047	9.3299999	5.587138200	28.139996	0.0000000	6.189997210	8.0000004	0.9008196	8.278782800
25.734804	9.3299999	5.509122800	28.846022	0.0000000	6.186208100	8.0000004	1.0639114	8.909449600
26.586064	6.8999996	5.478988800	28.003937	0.0000000	6.146660800	8.0000004	1.1430740	8.518009200
27.400864	6.8999998	5.480446800	28.888950	0.0000000	6.150129300	8.0000004	1.0284891	8.137653400
28.154190	6.8999998	5.478463300	25.034119	0.0000000	6.235987600	8.0000004	0.7542807	5.843463900
28.753342	6.8999998	5.478735500	23.206055	0.0000000	6.412736900	8.0000004	0.3924263	5.672342300
29.138046	6.8999998		21.384949	0.0000000	6.657525100	8.0000004	0.0000000	5.799999900
29.270004	6.8999998		19.750641	0.0000000	6.928585100	9.0400000	0.5151825	9.399999610
29.220001	6.8999996		18.454025	0.0000000	7.150182700	9.0400000	0.7953402	9.148937200
29.026016	6.8999998		17.620010	0.0000000	7.282521200	9.0400000	0.7559274	9.648261200
28.466064	6.8999998		17.362259	0.0000000	7.422036200	9.0400000		8.067444800
27.581843	6.8999998		17.644577	0.0000000	7.553010000	9.0400000	1.1865821	7.672409100
26.486252	6.8999998		18.488068	0.0000000	7.802229100			
24.033788	6.8999998		19.803375	0.0000000	7.556008300			
22.927994	6.8999998		21.457535	0.0000000	7.437680200			
			23.288806	0.0000000	7.253735500			

Table 1. Continued

x	y	z	x	y	z	x	y	z
9.0400000	1.3772736	7.1422977000	16.826364	2.2364789	6.4821363000	35.999969	1.1518841	8.3654528000
9.0400000	1.3486974	6.5717669900	16.826660	2.1972888	5.8584911100	35.999989	1.4077408	8.0171423000
9.0400000	1.0454197	6.0654399700	20.896666	0.0000000	6.9289703100	35.999989	1.5362034	7.8066999900
9.0400000	0.5897094	5.7634668800	20.905899	0.5430155	6.8945010100	35.999989	1.5333587	7.1736472000
9.0400000	0.0000000	5.6599969900	20.905563	1.0725905	6.7725143000	35.999985	1.4977627	8.7433760600
11.470000	0.0000000	9.4399999610	20.903854	1.6052437	6.6773920000	35.999989	1.3128396	8.3533230000
11.470000	0.5272306	9.1727278200	20.906996	2.0392651	6.3914681000	35.999998	2.4956245	8.0893668820
11.470000	0.7217981	8.6267798800	20.896912	2.0496791	7.8465309000	13.239998	1.6660210	5.9955902000
11.470000	1.1584234	8.2870378800	20.887116	2.0407467	7.3022671000	13.239998	1.2355471	5.9532220400
11.470000	1.4464529	7.7632658800	20.864354	2.0329008	6.7577740000	13.239998	0.8313735	5.7581118700
11.470000	1.4618241	7.1560811100	20.692029	2.0360592	6.2136876000	13.240000	0.0000000	5.6999979900
11.470000	1.4360714	6.5510311400	23.896637	0.0000000	9.0014973100	18.428421	2.3336849	5.9365378610
11.470000	1.1643350	6.0307217600	23.902847	0.5091249	8.9858610500	18.429657	1.7531338	5.8315001000
11.470000	0.8007650	5.7631112600	23.901586	1.0143394	8.8693740000	18.428345	1.1574640	5.7804999500
11.470000	0.0000000	5.6999969900	23.901718	1.4788288	8.6671462000	18.428558	0.5921336	5.6120800600
13.240000	0.0000000	9.1599999610	23.892563	1.7295752	8.2544269000	18.428741	0.0000000	5.5310584000
13.240000	0.4588438	8.8608024400	23.894185	1.8317699	7.7552862000	18.626680	2.1972666	5.6564900110
13.240000	0.9617893	8.5989238600	23.865254	1.8213902	7.2454644000	18.832536	1.7481203	5.8121264000
13.240000	1.4046888	8.2144146000	23.865834	1.8420534	6.7356701000	18.829605	1.1604424	5.5781710700
13.240000	1.5412828	7.6338644400	23.893600	1.8425722	6.2256775000	18.831253	0.5821130	5.4660666000
13.240000	1.5678000	7.0369557700	23.970082	0.0000000	8.9509439100	18.831085	0.0000000	5.4083719000
13.240000	1.4770479	6.4517138800	28.974182	0.4979566	8.9059105000	20.868703	2.0584173	5.6982275610
13.240000	1.1558962	5.9570923300	28.972397	0.9851420	8.7283631000	20.879913	1.7316999	5.3964062000
13.240000	0.5905445	5.7697886800	28.965439	1.3427353	8.4039043000	20.876480	1.1529741	5.3717511800
13.240000	0.0000000	5.6799994400	28.957245	1.5826340	7.9859643000	20.876432	0.5750989	5.3348083000
13.240000	0.0000000	9.1800000320	28.959717	1.6736930	7.4734249000	20.881332	0.0000000	5.2802442900
13.239998	0.5253173	8.8546889900	28.957230	1.8788139	6.9734344000	23.872177	1.8409662	5.5432899210
13.239998	1.0979891	8.5714035500	28.959368	1.8910200	6.4728639000	23.855942	1.4630432	5.4351044000
13.239998	1.5787401	8.1857996800	28.969768	1.6907854	5.9717769000	23.855820	0.9678683	5.4457235000
13.239998	2.2372141	8.1921468600	28.432963	0.0000000	8.9234610000	23.850540	0.4829558	5.5521120600
13.239998	2.7671642	7.9364222300	28.435518	0.6035288	8.8393784000	23.849945	0.0000000	5.4801903000
13.239998	2.8483087	7.2823963300	28.433823	0.9718443	8.6406097000	28.953282	1.8929741	5.5201960910
13.239998	2.8114061	6.6344268000	28.426285	1.3321495	8.2824440000	28.940323	1.4043455	5.5585980600
13.239998	2.4954042	6.0893086700	28.420990	1.5627708	7.8270880000	28.936279	0.9289543	5.6686654400
16.429108	0.6114895	8.9390507010	28.423891	1.6278817	7.3215275000	28.933533	0.4748038	5.6715554600
16.428986	1.1782858	8.8954228000	28.423798	1.6208820	6.6105440000	28.933487	0.0000000	5.8061697000
16.427963	1.5787401	8.6825688000	28.426085	1.6278219	6.2996111000	28.438095	1.6290388	5.8236719000
16.434341	1.6870451	8.3610077700	28.442827	1.6184026	5.7896165000	28.421432	1.3282881	5.8392117110
16.426437	2.2952358	8.2904339800	30.761002	0.0000000	8.9183664100	28.416946	0.8805089	5.7757072000
16.432297	2.4785501	7.7308064000	30.761002	0.4970595	8.8279037000	28.416856	0.4509697	5.7309816800
16.426482	2.4764688	7.1183176000	30.761002	0.9552400	8.6228654000	28.417343	0.0000000	5.6573811100
16.425522	2.4915514	6.5059808500	30.761017	1.3085413	8.2855277000	30.773056	1.6295404	5.8240805100
16.426421	2.3335943	6.9384727000	30.761002	1.5700121	7.8346109000	30.773056	1.2827339	5.8008223300
16.830948	0.0000000	6.9938472700	30.761017	1.6472712	7.3846363000	30.773056	0.8504359	5.8972166800
16.830780	0.6015922	8.9930892100	30.761002	1.6413708	6.8332748000	30.773071	0.4332541	5.7818661000
16.829712	1.1878748	8.8574457000	30.761002	1.8388779	6.3279839000	30.773056	0.0000000	5.7166666100
16.835739	1.7537479	8.7018239900	30.761002	1.6295509	5.8229733000	35.999989	1.3129187	5.3529081000
16.825607	2.2591143	8.5244086400	38.000000	0.0000000	8.8900000310	35.999989	1.0792589	6.0374623000
16.832809	2.2711515	8.2849255500	35.999989	0.4266687	8.8216467000	35.999969	0.7593449	5.8101749000
16.830536	2.2706423	7.8751204000	35.999969	0.8200570	8.6423454000	35.999969	0.3885908	5.8811399300
						38.000000	0.0000000	5.8199996000

4.3 External Units

There are a total of 50 external units required although they are not simultaneously used. A list of the unit numbers and types follows:

1. Direct access data sets:

    Unit #20 - 400 records, each 200 words long - potential flow velocity

    Unit #61 - 3280 records, each 990 words long - used for quasi-3-D boundary-layer program

    Unit #62 - 41 records, each 990 words long - used for quasi-3-D boundary-layer program

2. Sequential data sets: This includes units 3, 4, 5, 8, 9, 10, 11, 12, 13, 14, 15, 16, 17, 18, 19, 22, 23, 24, 25, 26, 27, 28, 29, 30, 31, 32, 33, 34, 35, 36, 38, 39, 40, 41, 42, 43, 44, 45, 56, 47, 51, 63, 64, 65, 66, 67.

    Unit #29 is the geometry data set for the input body. These datasets are used both for the inviscid velocity calculation and for the communication between the viscous and the inviscid parts of the calculation.

3. Datasets required to be saved:

    Unit #34 - This unit contains the inviscid velocities and control points.

    Unit #33 - This unit contains the blowing velocities and the displacement thickness values for viscous/inviscid interactive runs.

    Unit #51 - This unit contains some input data to the 2-D boundary-layer program.

    Unit #47 - This unit contains the blowing velocities from the 3-D boundary-layer program.

4.4 CRAY JCL

An example of the JCL required for the execution of the program on CRAY using the two-dimensional strip theory boundary-layer procedure, follows. Example 1 is for an initial calculation with the appropriate data saved for

subsequent runs and example 2 shows how the previously saved data is used to make additional calculations.

Example 1

```
JOB,JN=xxxxx  ,T=900,MFL=2000000.
ACCOUNT,US=xxxxxx  ,UPW= xxxxx ,AC=xxxxxxxx  .
*.
COPYF,I=$IN,O=INPUT. COPY INPUT FILE
REWIND,DN=INPUT.
*.
COPYF,I=$IN,O=GEOM.  COPY INPUT FILE
REWIND,DN=GEOM.
*.
ACCESS,DN=KCMCAIR,PDN=KCMCAIRCRAY,ID=OBJLIB.
STATIC,LEVEL=NEW.
BUILD,I=0,L=0,OBL=KCMCAIR,B=0,NBL=MCARBIN,NODIR.    CREATE SEQUENTIAL BIN
*.
ASSIGN,DN=INPUT,A=FT05.    ALLOCATE APPROPRIATE FILES
ASSIGN,DN=$OUT,A=FT06.
ASSIGN,DN=GEOM,A=FT29.
ASSIGN,DN=FILE34,A=FT34.
ASSIGN,DN=FILE33,A=FT33.
ASSIGN,DN=FILE51,A=FT51.
*.
MODE,FI=DISABLE.
*.
SEGLDR,CMD='BIN=MCARBIN'.    LINK BINARIES
SABD.    EXECUTE LOAD MODULE
*.
SAVE,DN=FILE34,PDN=INVELNEW.    SAVE OUTPUT DATASET FOR THE NEXT CAL.   ⎫ saved for
SAVE,DN=FILE33,PDN=BLOW2DNEW.                                            ⎬ future
SAVE,DN=FILE51,PDN=BL2DINPNEW.                                           ⎭ runs
*.
EXIT.
/EOF
F15 WITH LAMINAR BUBBLE WING, MULTIPLE ALPHAS, M=0.6       ⎫
 &A LIFT3D=1,IBL3D=0,MAXCYC=2,MLINE=51,NLINE=14,           ⎪
  MAXANG=2,ALPHAI(1)=6.95,ALPHAI(2)=8.95,AMACH(1)=0.60,    ⎪
  AMACH(2)=0.6,&END                                        ⎪
 &B BOV2=13.008,IAUTOW=2,NSYM1=1,LIFSEC=1,NSTRIP=13,       ⎬ input
  IXFLAG(1)=3,NSORCE=50,NWAKE=1,RFAREA=96.7,REFCHD=8.325,&END ⎪ data set
 6 022        8.325        0.0          0.0                ⎪
 61.0         2.0          10.0         0.0                ⎪
 51.0         2.0          5.0          0.0                ⎪
 6.022        8.325        1.0          0.0                ⎪
 61.0         2.0          10.0         0.0                ⎪
 51.0         2.0          5.0          0.0                ⎭
/EOF
 32.966003 13.008000 5.949856821                           ⎫
 32.924698 13.008000 5.950995400                           ⎪
 32.863266 13.008000 5.952991500                           ⎪
 32.782425 13.008000 5.956209200                           ⎪
 32.683380 13.008000 5.959699600                           ⎪
 32.567581 13.008000 5.961723300                           ⎪
      :         :         :                                ⎬ geometry
      :         :         :                                ⎪ data set
      :         :         :                                ⎪
 43.000000 1.3186102 5.600000400                           ⎪
 43.000000 0.5522600 5.600000400                           ⎪
 43.000000 0.1862400 5.600000400                           ⎪
 43.000000 0.0000000 5.600000400                           ⎭
/EOF
```

Example 2

```
JOB,JN=xxxxxx ,T=1200,MFL=2400000.
ACCOUNT,US=xxxxxxx ,UPW=xxxxxxx,AC=xxxxxxxxx .
*.
COPYF,I=$IN,O=INPUT. COPY INPUT FILE
REWIND,DN=INPUT.
*.
COPYF,I=$IN,O=GEOM.  COPY INPUT FILE
REWIND,DN=GEOM.
*.  ACCESS PERMANENT DATASETS
ACCESS,DN=KCMCAIR,PDN=KCMCAIRCRAY,ID=OBJLIB.
ACCESS,DN=DUMMY34,PDN=INVELNEW.
ACCESS,DN=DUMMY33,PDN=BLOW2DNEW.
ACCESS,DN=DUMMY51,PDN=BL2DINPNEW.
*.                    COPY DATASETS
*.                    COPY FILE34
REWIND,DN=DUMMY34.
COPYR,I=DUMMY34,O=FILE34,NR.
REWIND,DN=FILE34.
*.                    COPY FILE33
REWIND,DN=DUMMY33.
COPYR,I=DUMMY33,O=FILE33,NR.
REWIND,DN=FILE33.
*.                    COPY FILE51
REWIND,DN=DUMMY51.
COPYR,I=DUMMY51,O=FILE51,NR.
REWIND,DN=FILE51.
*.
STATIC,LEVEL=NEW.
BUILD,I=0,L=0,OBL=KCMCAIR,B=0,NBL=MCARBIN,NODIR.    CREATE SEQUENTIAL BIN
*.
ASSIGN,DN=INPUT,A=FT05.    ALLOCATE APPROPRIATE FILES
ASSIGN,DN=$OUT,A=FT06.
ASSIGN,DN=GEOM,A=FT29.
ASSIGN,DN=FILE34,A=FT34.
ASSIGN,DN=FILE33,A=FT33.
ASSIGN,DN=FILE51,A=FT51.
*.
MODE,FI=DISABLE.
*.
SEGLDR,CMD='BIN=MCARBIN'.    LINK BINARIES
$ABD.    EXECUTE LOAD MODULE
*.
SAVE,DN=FILE34,PDN=INVELNEW.    SAVE OUTPUT DATASET FOR THE NEXT CAL.
SAVE,DN=FILE33,PDN=BLOW2DNEW.
SAVE,DN=FILE51,PDN=BL2DINPNEW.
*.
EXIT.
/EOF
F15 WITH LAMINAR BUBBLE WING, MULTIPLE ALPHAS, M=0.6
 &A LIFT3D=1,IBL3D=0,MAXCYC=2,MLINE=51,NLINE=14,
   MAXANG=2,ALPHAI(1)=7.95,ALPHAI(2)=8.95,AMACH(1)=0.60,
   AMACH(2)=0.6,&END
 &B BOV2=13.008,IAUTOW=2,NSYM1=1,LIFSEC=1,NSTRIP=13,
   IXFLAG(1)=3,NSORCE=50,NWAKE=1,RFAREA=96.7,REFCHD=8.325,&END
6.022      8.325      1.0       0.0
61.0       2.0        10.0      0.0
51.0       2.0        5.0       0.0
6.022      8.325      1.0       0.0
61.0       2.0        10.0      0.0
51.0       2.0        5.0       0.0
/EOF
 32.966003 13.008000 5.949856821
 32.924698 13.008000 5.950995400
 32.863266 13.008000 5.952991500
 32.782425 13.008000 5.956209200
     .         .          .
     .         .          .
     .         .          .
 43.000000 0.5522600 5.600000400
 43.000000 0.1862400 5.600000400
 43.000000 0.0000000 5.600000400
/EOF
```

Annotations:
- data from previous run (brace: ACCESS lines)
- saved for future runs (brace: SAVE lines)
- input data set (brace: F15 ... /EOF)
- geometry data set (brace: 32.966003 ... /EOF)

SECTION V
TEST CASES

Three test cases were investigated: (1) F-15 with laminar bubble wing, (2) Advanced Navy Fighter (ANF), and (3) unmodified F-15.

5.1 Test Case 1 - F-15 with Laminar Bubble Wing

The coordinates of the geometry for test case 1 are given in model scale (4.7%) in inches. 1084 panels defined this configuration with 600 of them describing the wing, as shown in Figure 26. All of the calculations use the symmetry option of the program so that the given number of panels are for only half the configuration.

Inviscid and viscous calculations for Case 1 were made to compare with test data [32] at a Mach number ≈ 0.6, Rc $\approx 8.5 \times 10^6$/ft and a range of angle of attack from 6.84° through 15.83°. Viscous solutions were calculated by both the two-dimensional strip theory boundary layer and the quasi-three-dimensional boundary-layer procedures, and the location of transition was calculated by the program using Michel's criterion.

The input required to execute the two-dimensional strip theory boundary-layer procedure for case 1 was:

1. A data set, Unit 29, Format (3F10.0, 2I1), containing the x,y,z coordinates of the geometry, and

2. A data set, Unit 5, containing the flags, geometry and flow parameters, and boundary-layer parameters.

```
F15 - LAMINAR BUBBLE WING, A=6.84, M=0.6, TRANS. CALC.
&A LIFT3D=1,IBL3D=0,MAXCYC=2,MLINE=51,NLINE=14,
 MAXANG=1,ALPHAI(1)=6.84,AMACH=0.60,&END
&B BOV2=13.008,IAUTOW=2,NSYM1=1,LIFSEC=1,NSTRIP=13,
 NSORCE=50,NWAKE=1, RFAREA=96.7,REFCHD=8.325,&END
6.022     8.325      0.0        0.0
81.0      2.0        10.0
51.0      2.0        5.0
```

If more calculations are desired for additional, higher angles of attack, the results of the calculations of a lower angle of attack may be used for the initial guess for these calculations. The data saved on units 33 and 51 from

the first calculation is now used as input for the additional calculations and
the namelist block input will appear as:

```
F15 WITH LAMINAR BUBBLE WING, MULTIPLE ALPHAS, M=0.6
 &A LIFT3D=1,IBL3D=0,MAXCYC=2,MLINE=51,NLINE=14,
  MAXANG=2,ALPHAI(1)=10.75,ALPHAI(2)=12.95,
  AMACH=0.6,&END
 &B BOV2=13.008,IAUTOW=2,NSYM1=1,LIFSEC=1,NSTRIP=13,
  NSORCE=50,NWAKE=1, RFAREA=96.7,REFCHD=8.325,&END
 8.022      8.325      1.0        0.0
 61.0       2.0        10.0
 51.0       2.0        5.0
 6.022      8.325      1.0        0.0
 61.0       2.0        10.0
 51.0       2.0        5.0
```

To execute the program using the quasi-three-dimensional boundary-layer
procedure, the input is identical to that of the two-dimensional strip theory
boundary-layer procedure with the exception of the following flags in
Namelist A: IBL3D = 1, INTF = 1.

5.2 Test Case 2 - Advanced Navy Fighter (ANF)

Geometry data for the Advanced Navy Fighter consisted of 6% model scale
coordinates given in inches. The configuration (Figure 27) was defined by
approximately 1200 panels which provided for 360 panels to describe the wing
and 192 panels to describe the canard. Since the boundary-layer effects can
be calculated on only one lifting section, this configuration was first run
without the canard (Figure 27a) and the results were compared with experiment
(Figures 15 and 16). Calculations with the canard on (Figure 27b) were then
made and the effect was compared with the canard off case (Figure 17).

Because the wing is mounted so low on the fuselage the wing extra strip
would protrude through the fuselage if it were defined as a continuation of
the wing to the centerline as is usually done. Therefore the extra strip was
tilted "up" so that it fell completely inside the fuselage so as not to change
the fuselage geometry, See Figure 28.

Calculations for test case 2 were made for $M = 0.5988$, $R_L = 7.0 \times 10^6/ft$,
$C_L = 0.45$ and $\alpha = 7.7182°$ to compare pressure data given in Reference 34.
Viscous solutions were obtained with the strip theory boundary-layer procedure
being used to calculate the viscous effects. As in test case 1, the

transition location was calculated by the program using Michel's criterion. The namelist block input for this case was:

```
      ANF. NO CANARD.,TRANS. CALC., 2DSTRIP BL, M=0.6
      &A  LIFT3D=0,IBL3D=0,
      MAXCYC=2,NLINE=8,MLINE=51,
      MAXANG=1,ALPHAI(1)=7.7182,AMACH=0.6,&END
      &B BOV2=12.955,IAUTOW=2,NSYM1=1,LIFSEC=1,REFCHD=8.2912,
      LINEAR=0,IXFLAG(1)=3,IPCV=1,
      RFAREA=95.904,NSORCE=50,NSTRIP=7,NWAKE=1,&END
      7.0         12.0        0.0         0.0
      70.0        2.0         10.0
      51.0        2.0         5.0
```

A series of calculations at various angles of attack were made to compare the calculated and experimental lift coefficients for the canard-off case. These calculations were repeated for the configuration with the canard to compare the calculated effect of the canard. The namelist block input for the configuration with canard for multiple angles of attack was:

```
      ANF. CANARD.,TRANS. CALC., 2DSTRIP BL, M=0.6, MULT. ALPHAS
      &A  LIFT3D=1,IBL3D=0,
      MAXCYC=2,NLINE=8,MLINE=51,
      MAXANG=6,ALPHAI(1)=1.3,ALPHAI(2)=3.4,ALPHAI(3)=4.7,
      ALPHAI(4)=6.0,ALPHAI(5)=7.7182,ALPHAI(6)=9.2,AMACH=0.6,&END
      &B BOV2=12.955,IAUTOW=2,NSYM1=1,LIFSEC=2,REFCHD=8.2912,
      LINEAR=0,IXFLAG(1)=3,IXFLAG(2)=3,IPCV=1,RFAREA=95.904,
      NSORCE(1)=50,NSORCE(2)=48,NSTRIP(1)=7,NSTRIP(2)=5,NWAKE(1)=1,
      NWAKE(2)=1,&END
      7.0         12.0        0.0         0.0
      70.0        2.0         10.0
      51.0        2.0         5.0
      7.0         12.0        0.0         0.0
      70.0        2.0         10.0
      51.0        2.0         5.0
      7.0         12.0        0.0         0.0
      70.0        2.0         10.0
      51.0        2.0         5.0
      7.0         12.0        0.0         0.0
      70.0        2.0         10.0
      51.0        2.0         5.0
      7.0         12.0        0.0         0.0
      70.0        2.0         10.0
      51.0        2.0         5.0
      7.0         12.0        0.0         0.0
      70.0        2.0         10.0
      51.0        2.0         5.0
```

5.3   Test Case 3 - Unmodified F-15

The unmodified F-15 geometry coordinates were full scale in inches. This configuration [35] was defined by 981 panels, 450 of which described the wing (F ig. 29). The wing is mounted high on the fuselage and as in the case of the Advanced Navy fighter configuration, the extra strip had to be tilted, in this case "down", so as not to protrude through the top of the nacelle. Figure 30 shows the arrangement of the panels on the wing used in the calculations of

test case 3. The measured data was obtained with a sting-mounted fuselage/wing configuration which included the vertical tail. The computed results, however, were for a configuration without the vertical tail.

Viscous and inviscid calculations were made for this configuration to compare with experiment [35] at $M = 0.6$, $R_L/ft = 5.78 \times 10^6$ for a range of angle of attack, $2.21° \leq \alpha \leq 8.66°$. The two-dimensional strip theory boundary-layer procedure was used in the interaction calculation to compute the viscous results. The namelist block input for test case 3 follows:

```
NEW F15 CONFIGURATION, M=0.6, STRIP2D BL, TRANSITION INPUT
&A LIFT3D=1,IBL3D=0,
 MAXCYC=2,NLINE=11,MLINE=61,
 MAXANG=2,ALPHAI(1)=4.36,ALPHAI(2)=6.51,
 AMACH=0.6,KINKNO=1,MS=6,&END
&B BOV2=256.20,IAUTOW=2,NSYM1=1,LIFSEC=1,
 IXFLAG(1)=3,IPCV=1,REFCHD=191.23,RFAREA=43776.,NSORCE=60,
 NSTRIP=10,NWAKE=1,&END
4.33       191.23      0.0        0.0
71.0       0.0         10.0       6.0
254.0      220.0       185.0      150.0      115.0      80.0
0.05       0.05        0.05       0.05       0.05       0.05
61.0       0.0         5.0        6.0
254.0      220.0       185.0      150.0      115.0      80.0
-0.05      -0.05       -0.05      -0.05      -0.05      -0.05
4.33       191.23      1.0        0.0
71.0       0.0         10.0       6.0
254.0      220.0       185.0      150.0      115.0      80.0
0.05       0.05        0.05       0.05       0.05       0.05
61.0       0.0         5.0        6.0
254.0      220.0       185.0      150.0      115.0      80.0
-0.05      -0.05       -0.05      -0.05      -0.05      -0.05
```

SECTION VI
CONCLUSIONS AND RECOMMENDATIONS

An interactive viscous/inviscid procedure has been developed for the computation of viscous flow over 3-D wing/body configurations. The method developed makes use of a three-dimensional surface-source panel method developed by Hess [11] and an inverse finite-difference boundary-layer procedure of [6].

Two alternative boundary-layer formulations have been considered, the first is a two-dimensional strip theory implementation [4] and the second [10] is a quasi-three-dimensional boundary-layer method. These procedures have been coupled with the external potential flow calculation via an interface routine which handles the necessary interpolation and transfer of data between the viscous and the inviscid parts of the calculation.

The present method is able to compute flows with both leading- and trailing-edge separations. In most of the cases considered here, the calcu- lations were performed by computing transition by an empirical formula, which, at higher angles of attack, resulted in a separated region as much as 35% upstream of the trailing edge. However, at the conditions approaching stall, a small change in transition location led to regions of massive flow separa- tion on the wing, which the present method handled without any numerical difficulties.

The studies conducted here indicate that at lower angles of attack there is very little difference between the results computed by either of the two boundary-layer procedures. However, at higher angles of attack, for which there are significant regions of flow separation, the quasi-three-dimensional boundary-layer procedure has been found to provide a useful improvement in the results when compared with the experimental data.

The inviscid method used here is general and can be applied to complex aircraft configurations. The viscous effects, however, are limited to the wing alone with some approximations. For example, the use of either two- dimensional strip theory or the quasi-three-dimensional boundary-layer approx- imation is satisfactory at low to medium angles of attack. At higher angles

of attack, the flow becomes "more" three dimensional and the calculations should use the complete equations. Furthermore, the effect of the viscous wakes neglected in the solution procedure also becomes important at higher angles of attack and needs to be included in the solution procedure.

The viscous capabilities of the present computer code can also be extended to the other components of the airplane configurations to include, for example, multiple lifting sections, as well as the fuselage and other nonlifting components.

SECTION VII
REFERENCES

1. J. S. Shang, and S. J. Scherr, Navier-Stokes Solution of the Flow Field Around a Complete Aircraft. AIAA Paper 85 1509, 1985.

2. B. R. Gilmer, and D. R. Bristow, "Analysis of Stalled Airfoils by Simultaneous Perturbations to Viscous and Inviscid Equations." AIAA J. 20, 1982, pp. 1160-1166.

3. G. Maskew, and F. A. Dvorak, "Investigation of Separation Models for the Prediction of $C_{L\ max}$." J. Am. Helicopter Soc. 23, 1978, pp. H.

4. T. Cebeci, R. W. Clark, K. C. Chang, N. D. Halsey, and K. Lee, "Airfoils with Separation and the Resulting Wakes," J. Fluid Mechanics, 163, 1986, pp. 323-347.

5. N. D. Halsey, "Potential Flow Analysis of Multielement Airfoils Using Conformal Mapping," AIAA J. 17, 1979, pp. 1281 1288.

6. T. Cebeci, Separated Flows and Their Representation by Boundary Layer Equations, Mech. Engg. Dept. Rept. ONR CR215 234 2, California State University, Long Beach, 1976.

7. T. Cebeci, and A.M.O. Smith, Analysis of Turbulent Boundary Layers, Academic Press, N.Y., 1974.

8. T. A. Reyhner, and I. Flugge Lotz, "The Interaction of a Shock wave with a Laminar Boundary Layer," Int. J. on Nonlinear Mech. 3, 1968, pp. 173-199.

9. U. Mehta, K. C. Chang, and T. Cebeci, "Relative Advantages of Interactive and Thin Navier Stokes Procedures." In Numerical and Physical Aspects of Aerodynamic Flows III (Ed. T. Cebeci, Springer Verlag, 1986 and NASA TM 86778.)

10. T. Cebeci, K. Kaups, and A. A. Khattab, Studies of Interactive Procedures for Three-Dimensional Flows. Pt. I, Separation and Reattachment Near the Leading Edge of a Thin Wing. Douglas Aircraft Co. Rept. MDC J3835, 1985.

11. J. L. Hess, "The Problem of Three Dimensional Lifting Flow and Its Solution by Means of Surface Singularity Distribution," Comp. Meth. in Appl. Mech. and Engg. 4, 1974.

12. R. J. Margason, S. O. Kjelgaard, W. L. Sellers, III, C. E. K. Morris, Jr., K. B. Walkley, and E. W. Shields, Subsonic Panel Methods - A Comparison of Several Production Codes. AIAA Paper No. 85-280, 1985.

13. J. L. Hess, and A. M. O. Smith, "Calculation of Nonlifting Potential Flow About Arbitrary Three Dimensional Bodies," J. Ship Research, Vol. 8, No. 2, 1964. (An expanded version is given in Douglas Aircraft Company Report No. ES 40622, 1962.)

14. R. W. Clark, A New Iterative Matrix Solution Procedure for Three-Dimenisonal Panel Methods, AIAA Paper No. 85-0176, 1985.

15. P. G. William, "A Reverse Flow Computation in the Theory of Self-Induced Separation," Proc. 4th Int. Conf. Numer. Meth. Fluid Mech., Lecture Notes in Phys. 35, 1975, p. 445.

16. P. Bradshaw, T. Cebeci, and J. H. Whitelaw, Engineering Calculation Methods for Turbulent Flow, Academic Press, London, 1981.

17. T. Cebeci, "Calculation of Unsteady Two-Dimensional Laminar and Turbulent Boundary Layers with Fluctuations in External Velocity," Proc. Royal Soc. London, Series A 355, 1977, pp. 225 238.

18. J. C. LeBalleur, "Couplage Visqueux Non Visquex: Methode Numerique et Applications Aux Ecoulements Bidimensionnels Transsonique Set Supersoniques," Le Recherche Aerospatiale, No. 1978 2, 1978, pp. 65 76.

19. J. E. Carter, A New Boundary Layer Inviscid Iteration Technique for Separated Flow, AIAA Paper 79 1450, 1979.

20. J. E. Carter, <u>Viscous-Inviscid Interaction Technique for Separated Flow</u>, AIAA Paper 81-1241, 1981.

21. J. E. Carter, and V. N. Vasta, <u>Analysis of Airfoil Leading-Edge Separation Bubbles</u>, NASA Contractor Rept. 165935, Contract NAS1-16585, 1982.

22. J. C. LeBalleur, "Numerical Viscid-Inviscid Interaction in Steady and Unsteady Flows," In <u>Numerical and Physical Aspects of Aerodynamic Flows II</u> (Ed. T. Cebeci), Springer-Verlag, N.Y., 1984.

23. A. E. P. Veldman, "New Quasi-Simultaneous Method to Calculate Interacting Boundary Layers," AIAA J. <u>19</u>, 1981, p. 769.

24. T. Cebeci, and P. Bradshaw, <u>Momentum Transfer in Boundary Layers</u>, McGraw-Hill/Hemisphere, 1977.

25. M. J. Nituch, S. Sjolander, and M. R. Head, "An Improved Version of the Cebeci-Smith Eddy-Viscosity Model," Aero. Quarterly <u>XXIX</u>, 1978.

26. M. R. Head, "Eddy Viscosity in Turbulent Boundary Layers," Aero. Quarterly <u>XXVII</u>, 1976.

27. A. Nakayama, <u>Measurements in the Boundary Layer and Wake of Two Airfoil Models</u>, Douglas Aircraft Co. Rept. MDC J2403, 1982.

28. R. L. Simpson, Y. T. Chew, and B. G. Shivaprasad, "The Structure of a Separating Turbulent Boundary Layer. Pt. 1, Mean Flow and Reynolds Stresses," J. Fluid Mech. <u>113</u>, 1981, p. 23.

29. T. Cebeci, and P. Bradshaw, <u>Physical and Computational Aspects of Convective Heat and Momentum Transfer</u>, Springer-Verlag, New York, 1984.

30. D. A. Lovell, <u>A Wind Tunnel Investigation of the Effects of Flap Span and Deflection Angle, Wing Planform and a Body on the High Lift Performance of a 28° Swept Wing</u>, RAE CP 1372, 1977.

31. L. P. Yip, and G. L. Shubert, <u>Pressure Distributions on a 1- by 3-Meter Semispan Wing at Sweep Angles from 0° to 40° in Subsonic Flow</u>, NASA TN D-8307, 1976.

32. K. E. Tatum, and J. Pavelka, <u>Wind Tunnel Pressure Distribution Test Results of Short Laminar Separation Bubble Wing Design</u>, PSWT Test 409, Rept. No. MDC A5983, 1979.

33. L. T. Chen, J. C. Vassberg, and C. C. Peavey, <u>A Transonic Wing-Body Flowfield Calculation with Improved Grid Topology and Shock Point Operators</u>, AIAA Paper 84-2155, 1984.

34. J. S. Althuis, <u>Close Coupled Canard-Wing Interactions on Panel Loads Series I</u>, McDonnell Douglas Corp. Preliminary Report MDC IR0184, 1985.

35. R. M. Anderson, <u>Wind Tunnel Test on the 4.7 Percent Scale F-15 Model in the McDonnell Douglas Polysonic Wind Tunnel, Tests PSWT 281 and 286</u>, Vol. I and II. McDonnell Douglas Corp. Report MDC A0974, 1971.

36. J. L. Hess, <u>Calculation of Potential Flow about Arbitrary Three-Dimensional Lifting Bodies</u>, McDonnell Douglas Corp. Report No. MDC J5679-01, 1972.
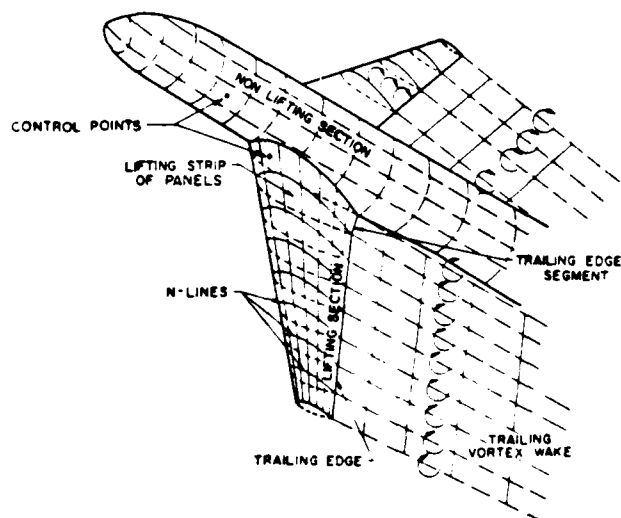
Figure 1. Wing/body configuration.
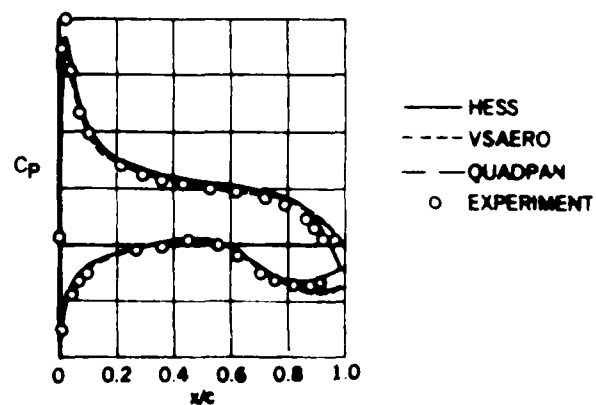
Figure 2. Effect of alternate Kutta conditions.
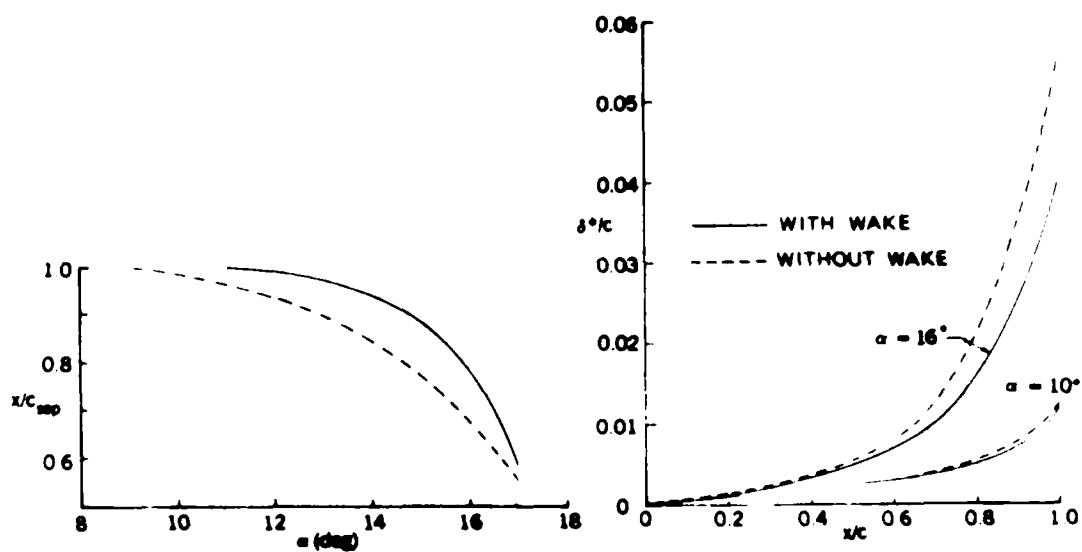
Figure 3. Effect of wake on the separation region and displacement thickness for the NACA 0012 airfoil, $R_c = 6.0 \times 10^6$.
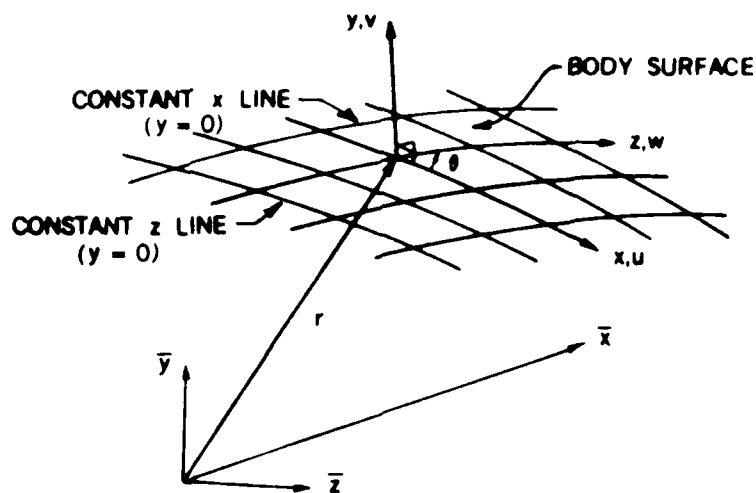
Figure 4.   Notation for nonorthogonal curvilinear coordinate system on the body surface. Note that x and z are not orthogonal to each other but y is to x and z.
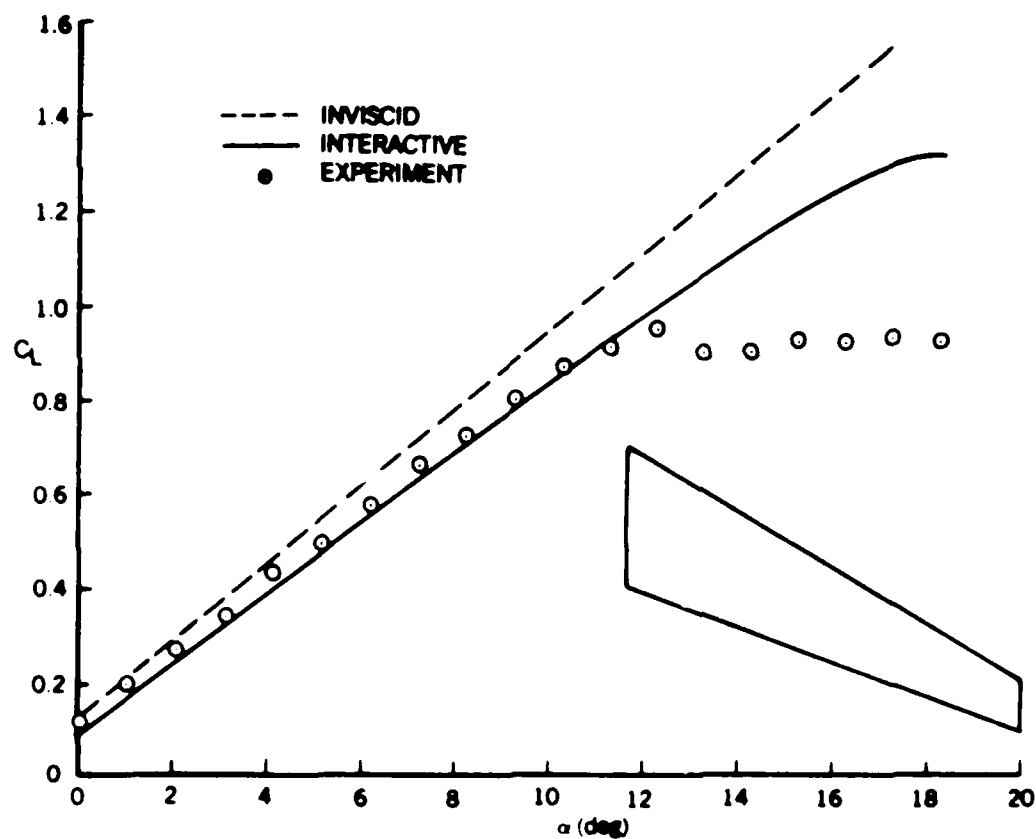
Figure 5. Comparison of computed and experimental lift curves for the RAE wing.
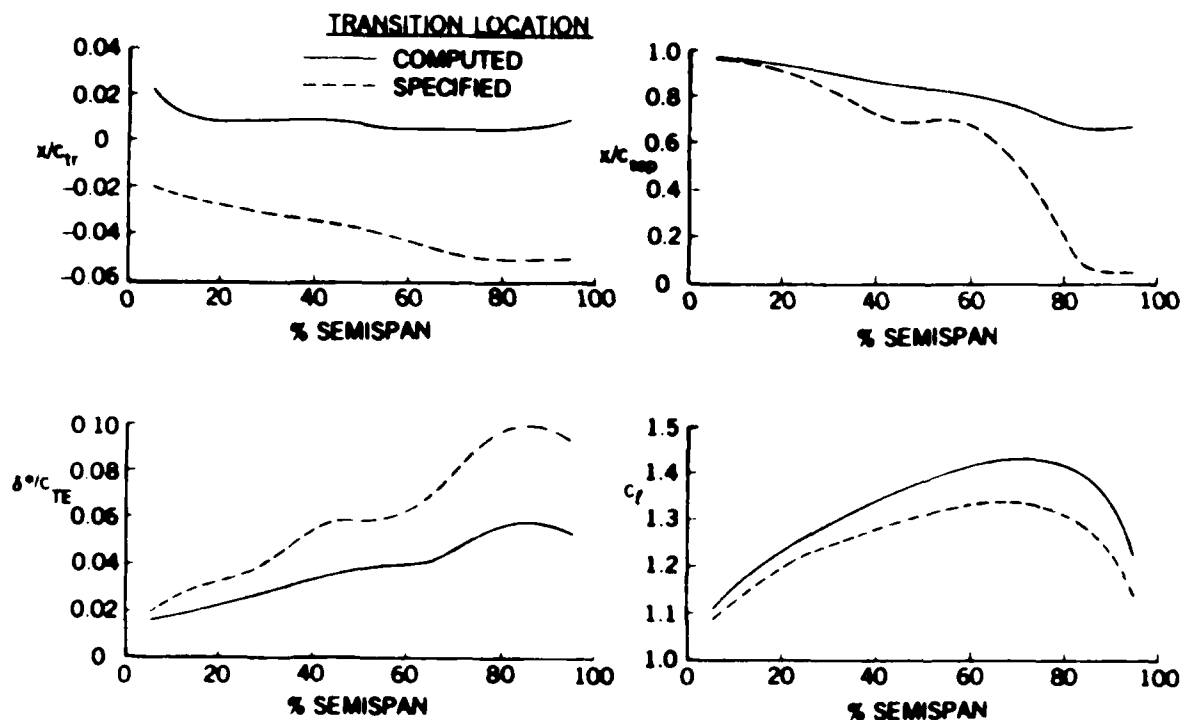
Figure 6. Effect of transition location on flow separation, displacement thickness and lift distribution for the RAE wing, $\alpha = 17.5°$.
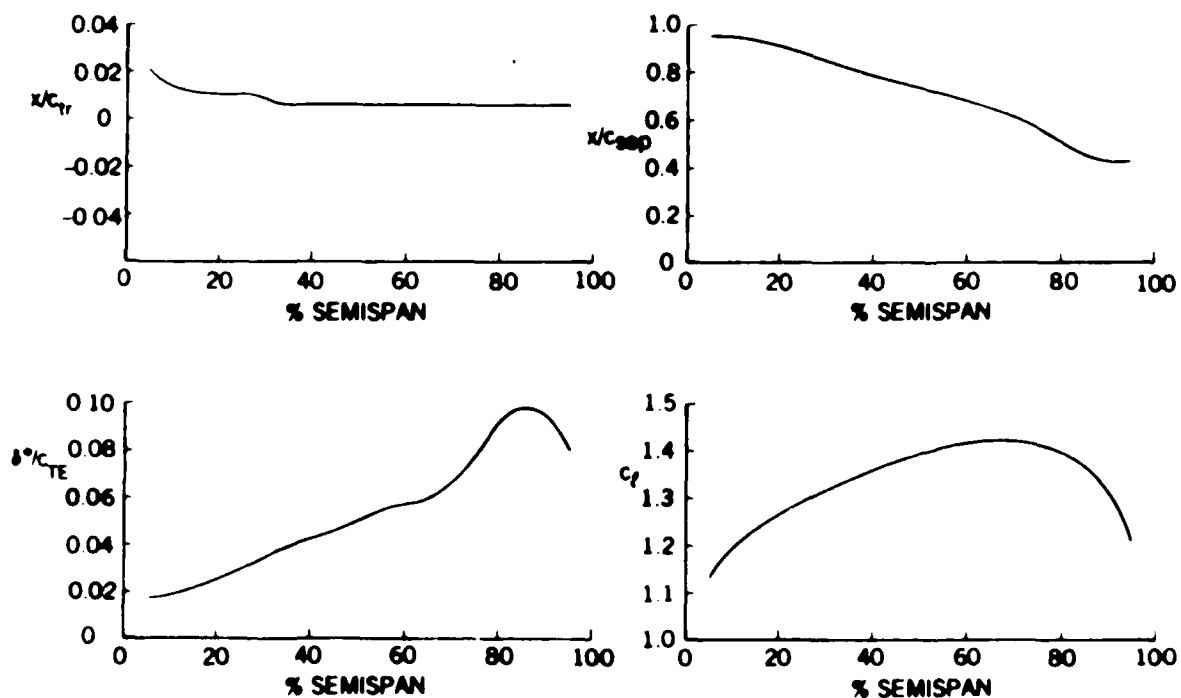
Figure 7. Computed transition location, flow separation, displacement thickness and lift distribution for the RAE wing, $\alpha = 18.5°$.
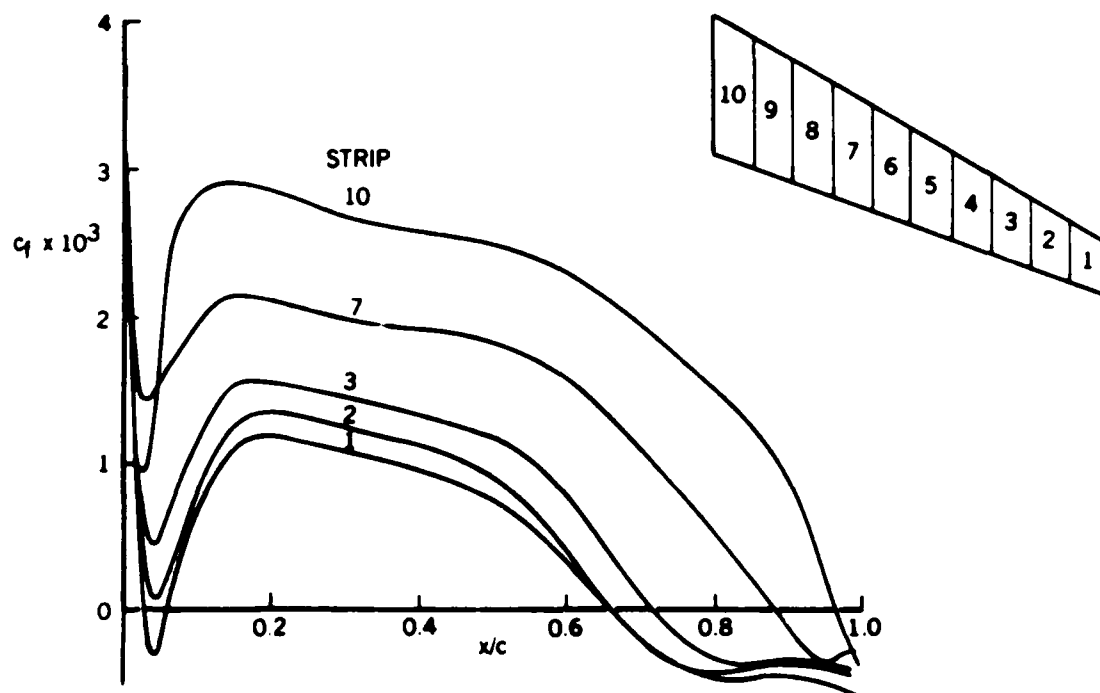
Figure 8. Leading and trailing edge separation location for the RAE wing, $\alpha = 17.5°$.
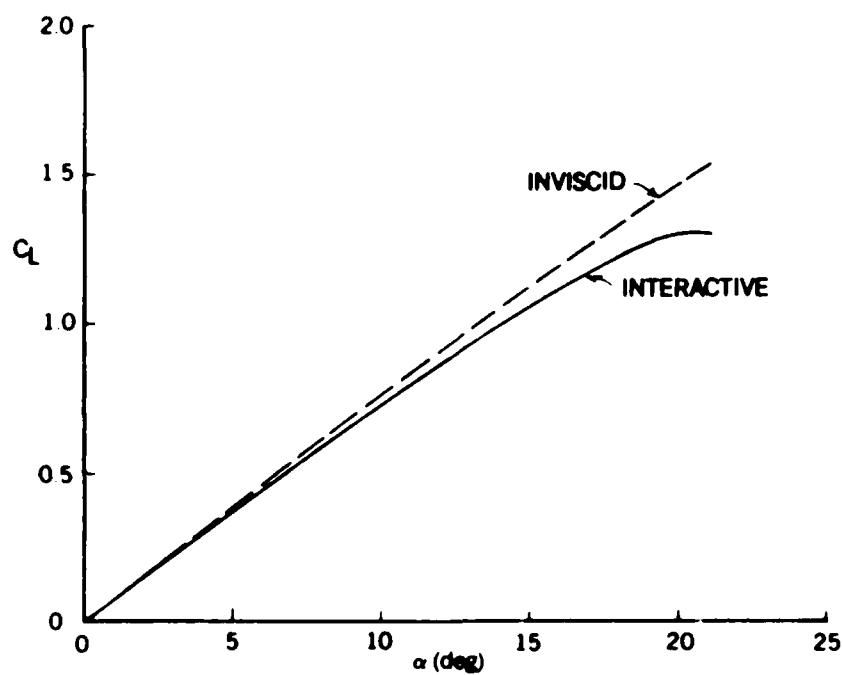
Figure 9. Computed viscous and inviscid lift curve for the NACA 0012 swept wing.
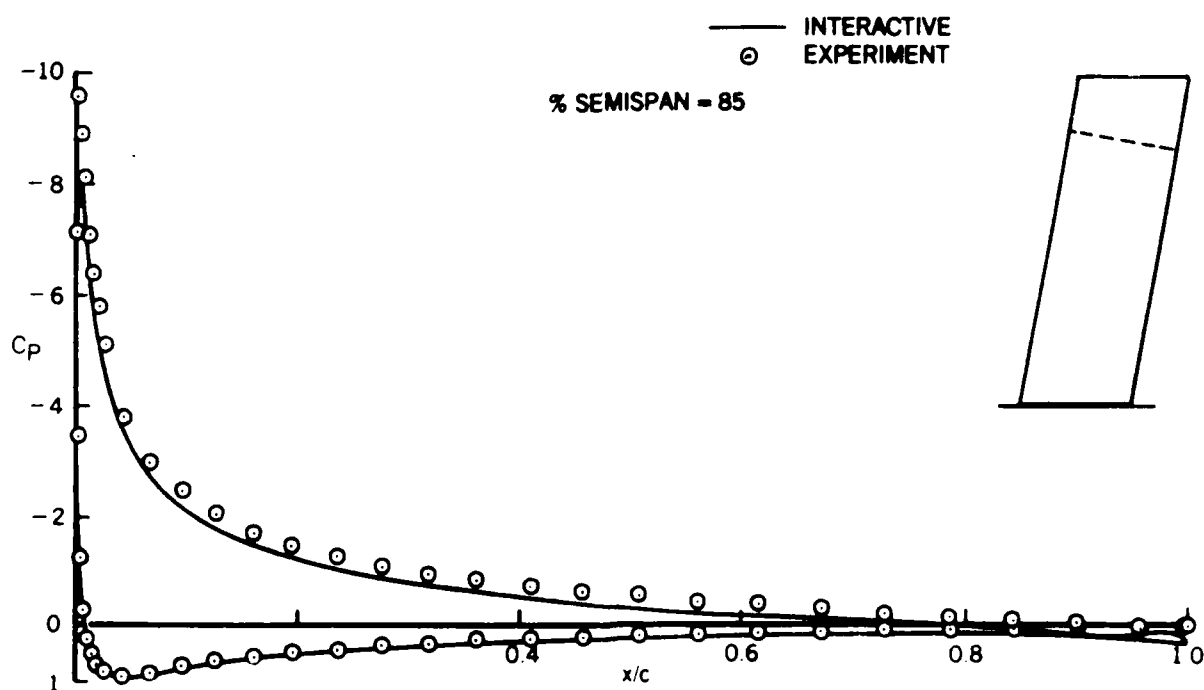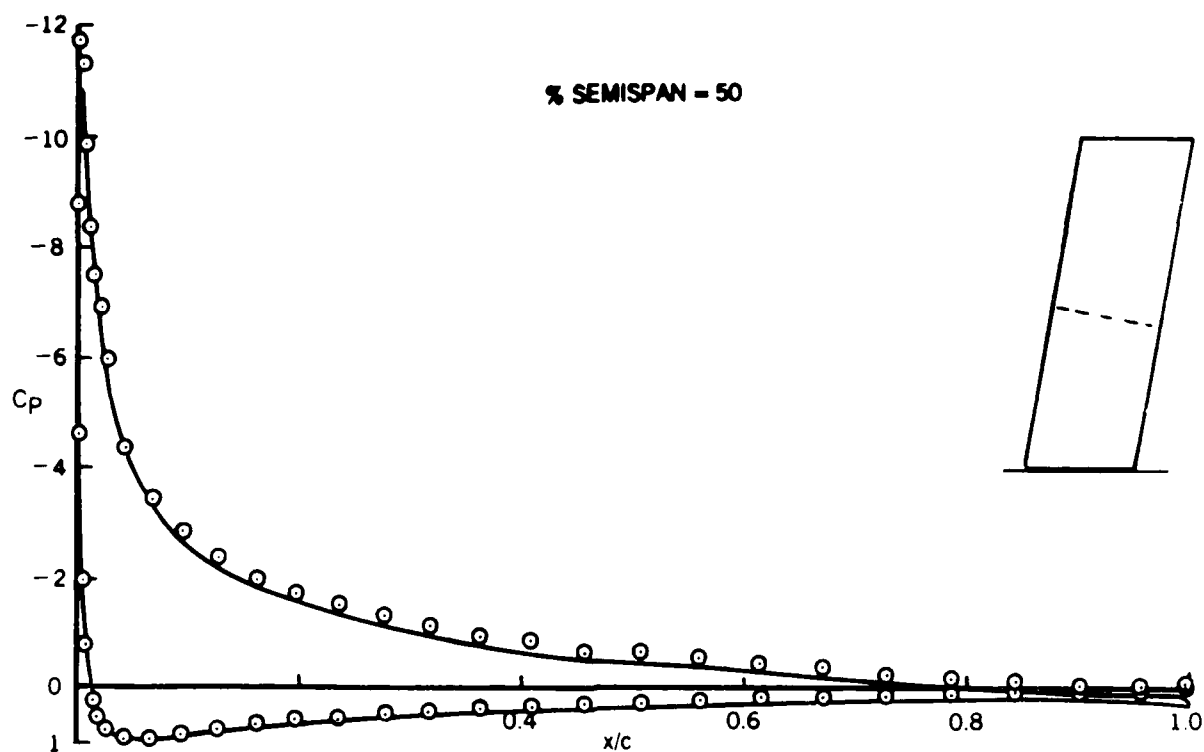
Figure10. Comparison of calculated and experimental pressure distribution on the NACA 0012 swept wing, $\alpha = 19.35°$.
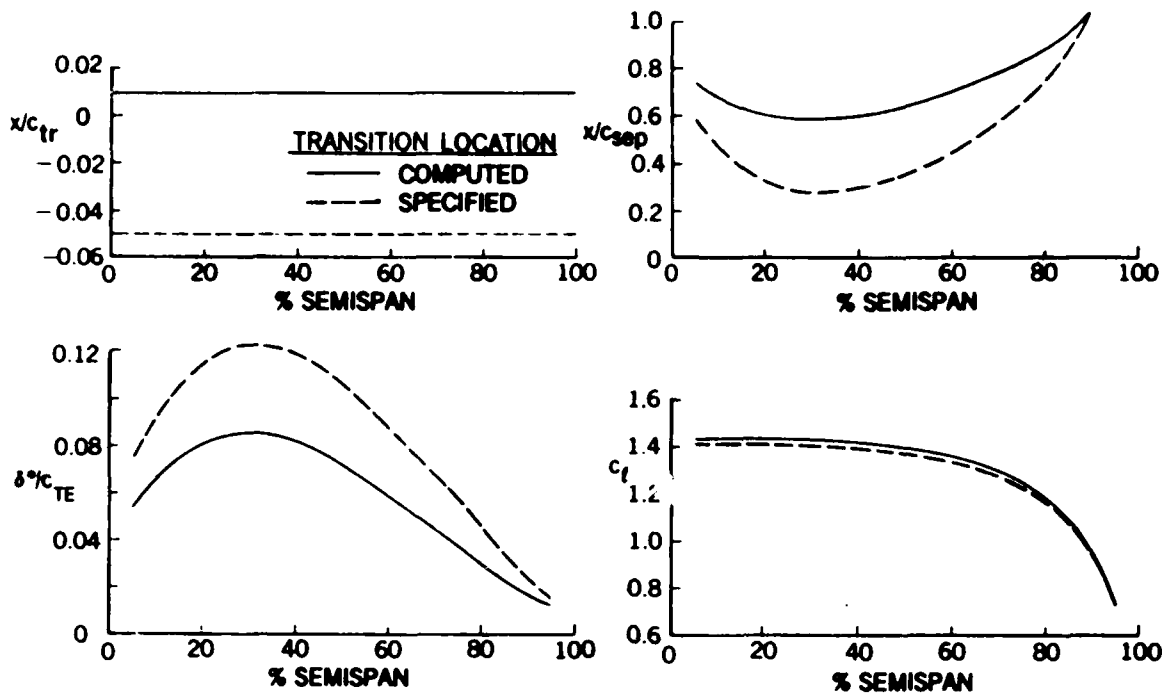
Figure 11. Effect of transition location on flow separation, displacement thickness and lift distribution for the NACA 0012 swept wing, $\alpha = 21.12°$.
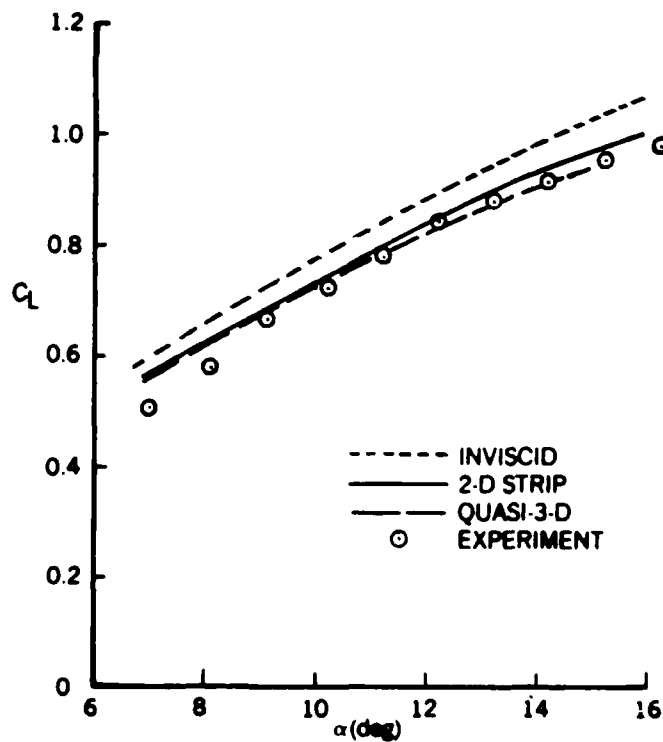
Figure 12. Comparison of 2-D strip theory and quasi-3-D methods for the F-15 fighter with laminar bubble wing.
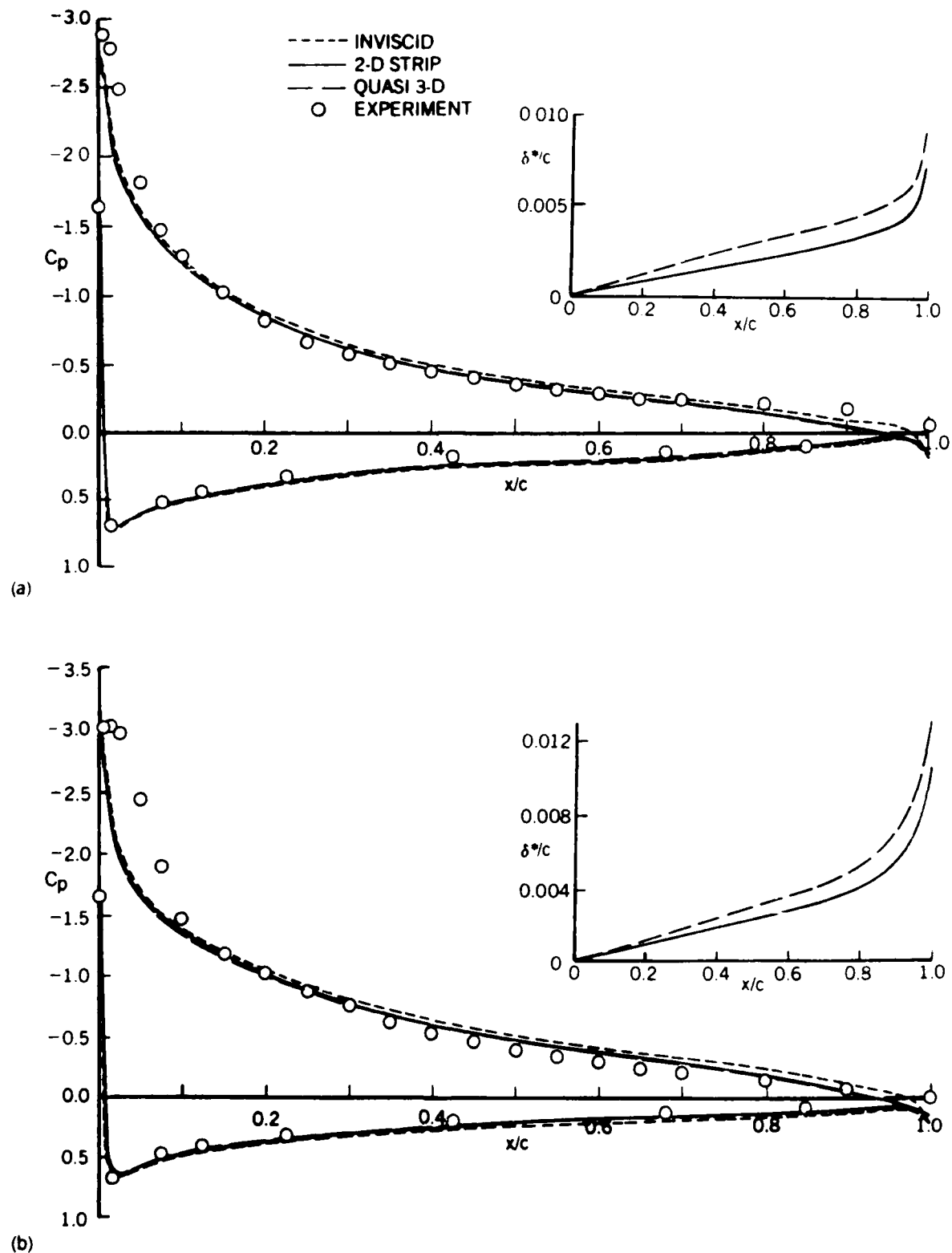
Figure 13. Comparison of the calculated and experimental pressure distribution for the F-15 with laminar bubble wing, $\alpha = 10.75°$. Insert shows the chordwise variation of displacement thickness as calculated by the 2-D strip theory and the quasi-three-dimensional boundary-layer methods. (a) 38% semispan. (b) 58% semispan.

58
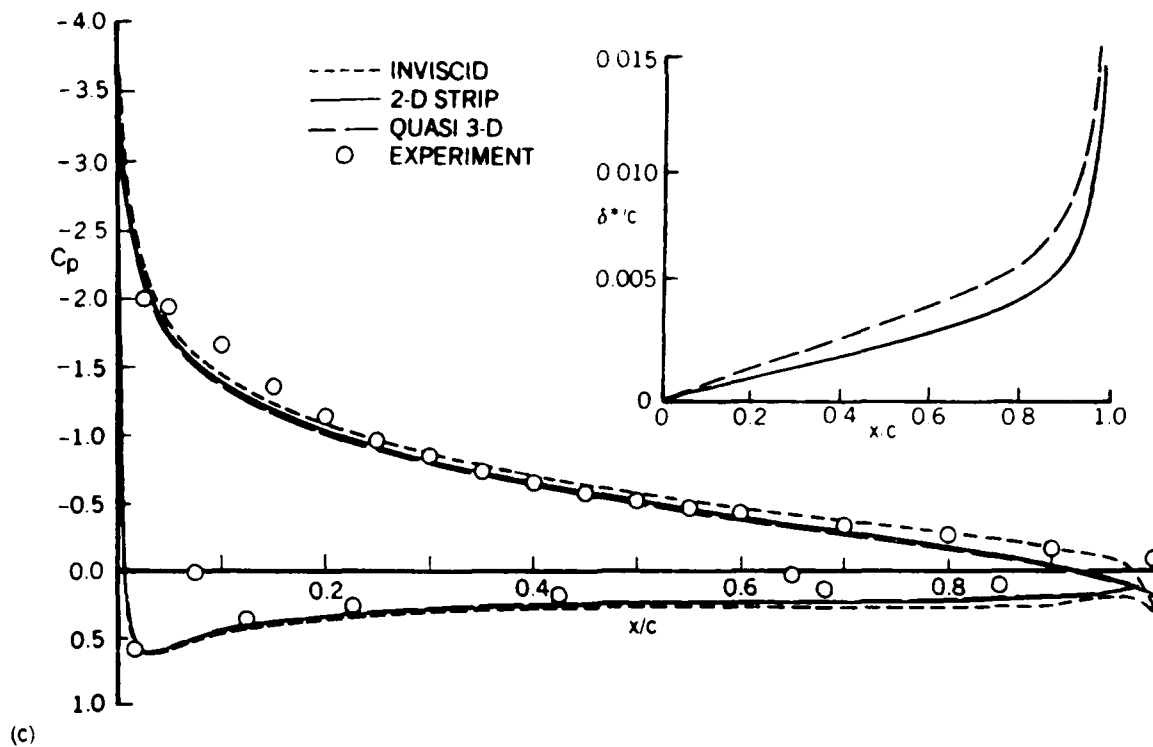
Figure 13. (Continued) (c) 88% semispan.
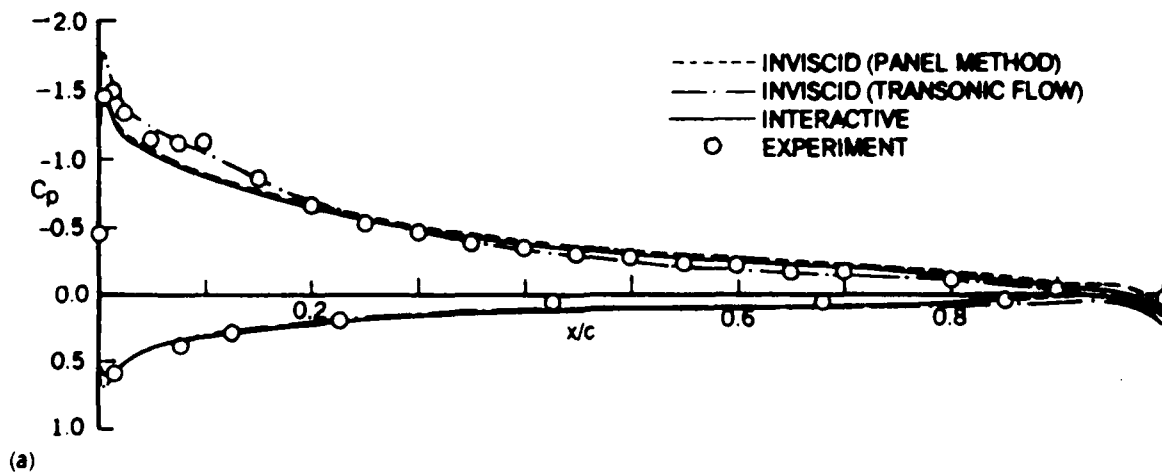
Figure 14. Comparison of the mid-semispan pressure distribution obtained by the panel method and the transonic flow method for the F-15 with laminar bubble wing, M = 0.6. (a) α = 6.84°.
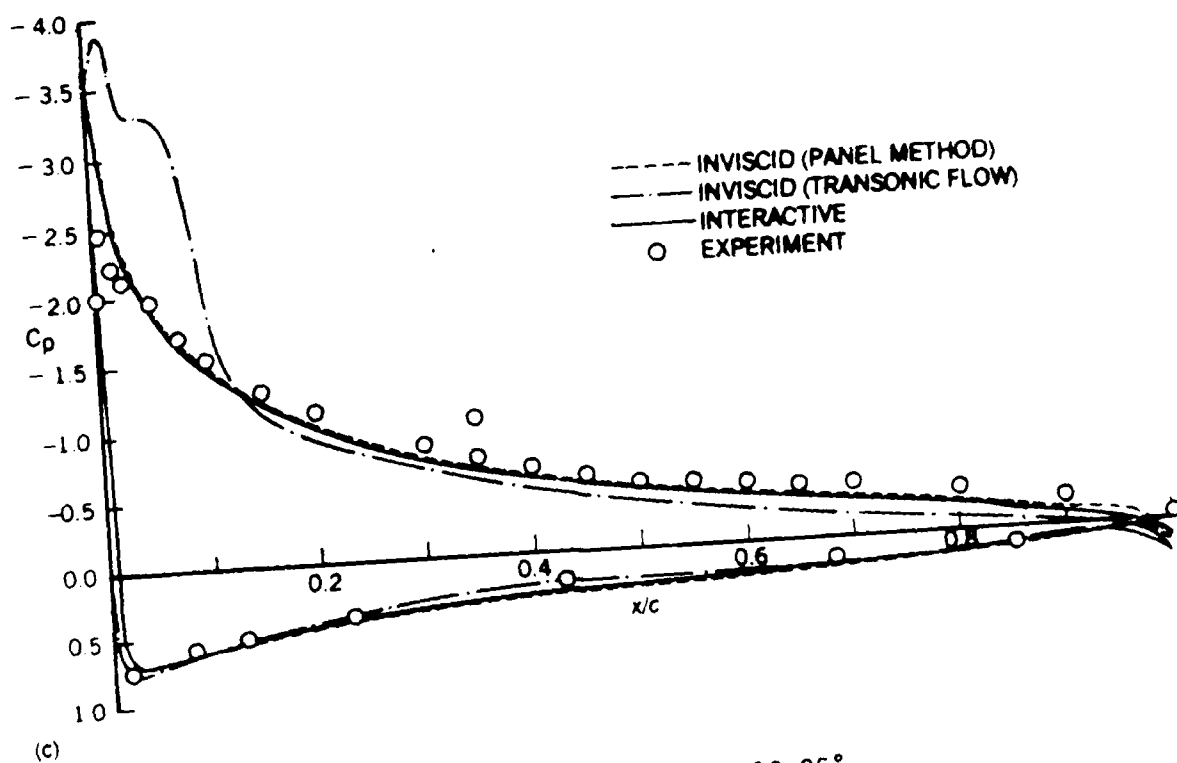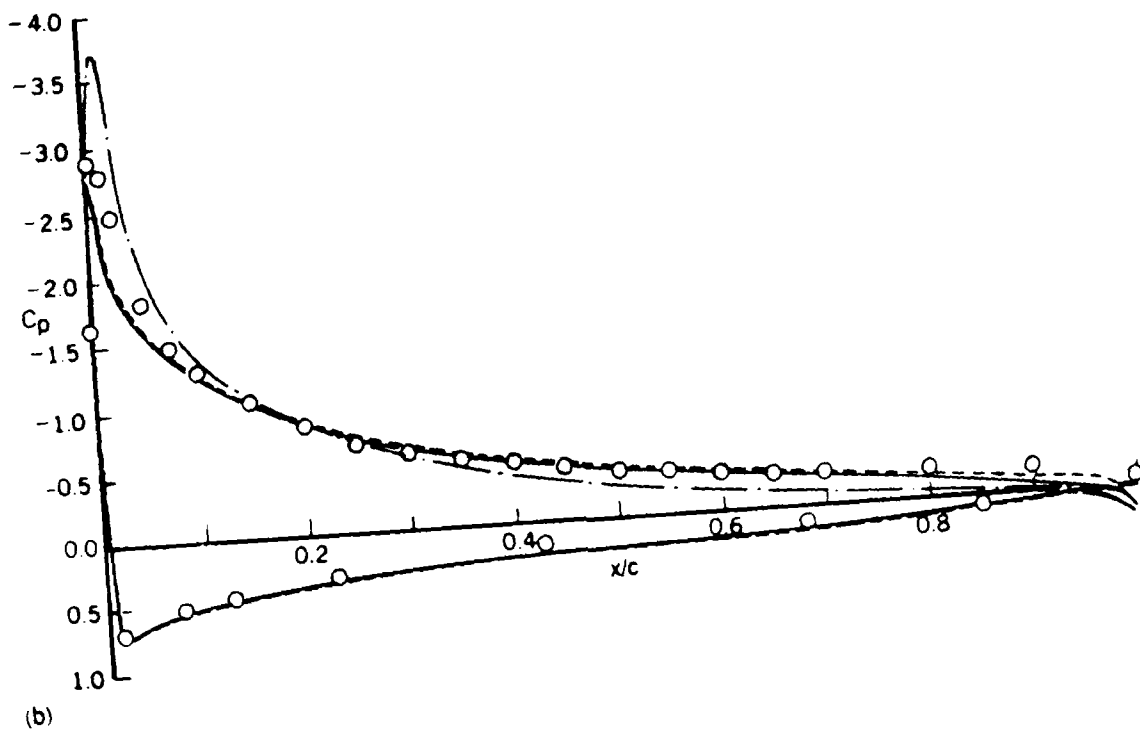
Figure 14. (Continued) (b) $\alpha = 10.75°$. (c) $\alpha = 12.95°$.
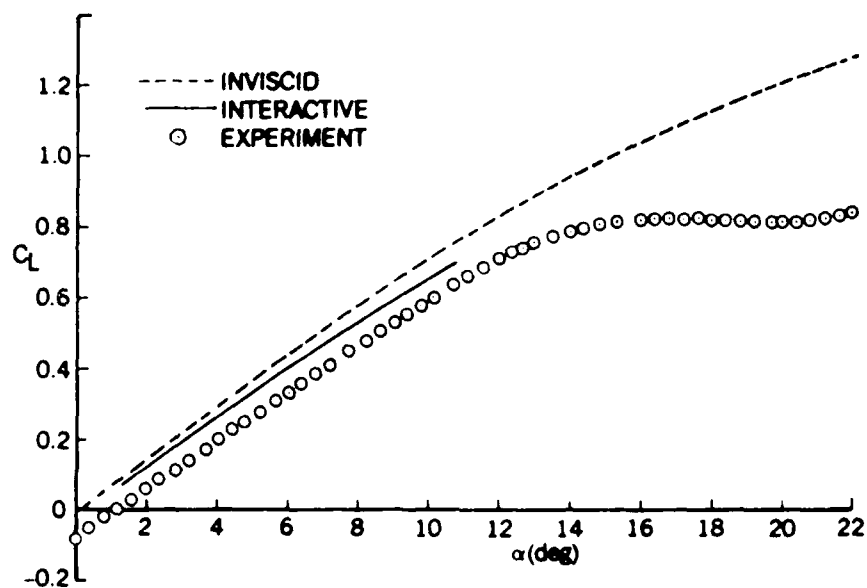
Figure 15. Comparison of computed and experimental lift curves for the ANF wing/body configuration.
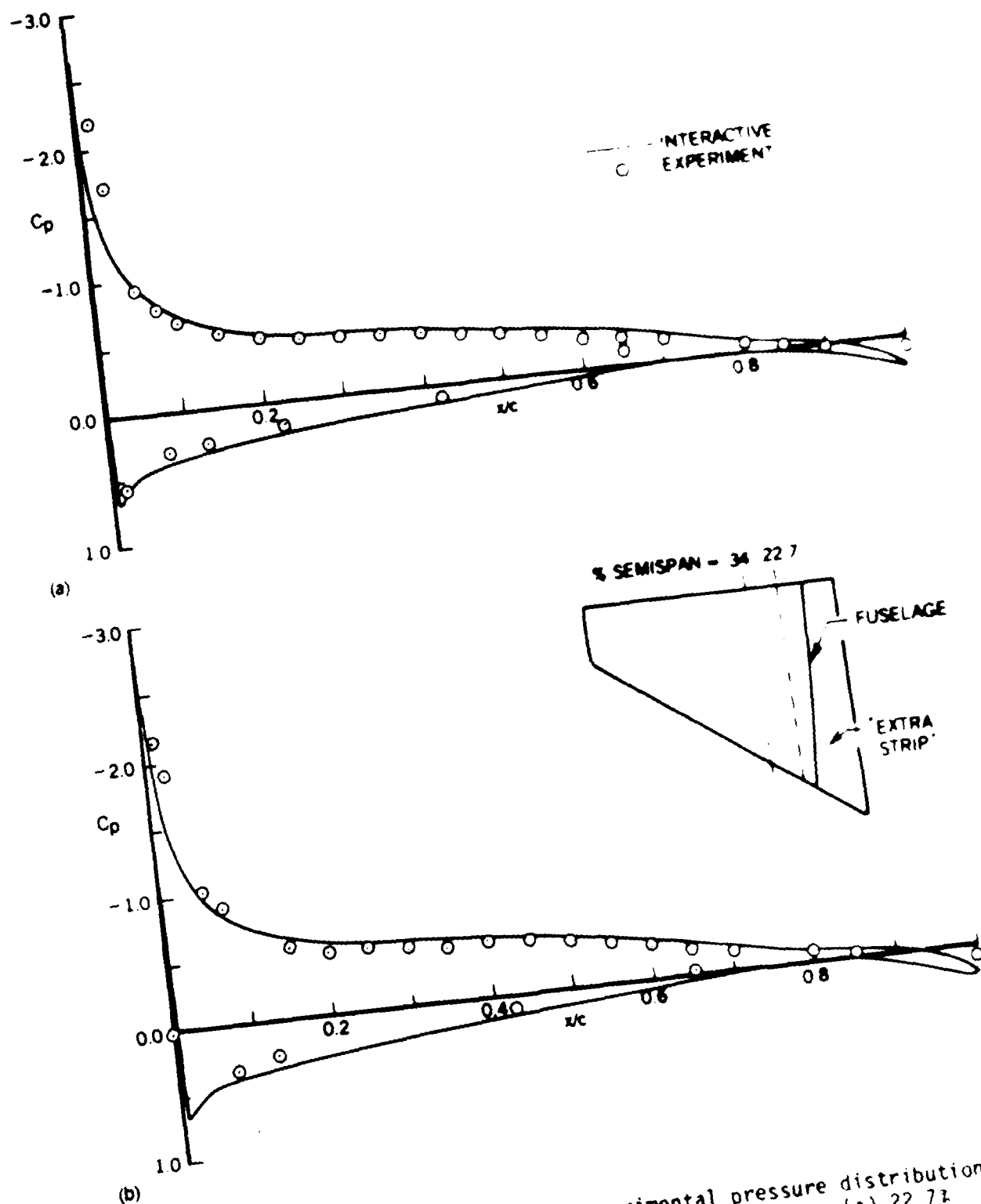
Figure 16. Comparison of computed and experimental pressure distribution for ANF wing/body configuration, $\alpha = 7.7°$, M = 0.6. (a) 22.7% semispan. (b) 34.5% semispan.
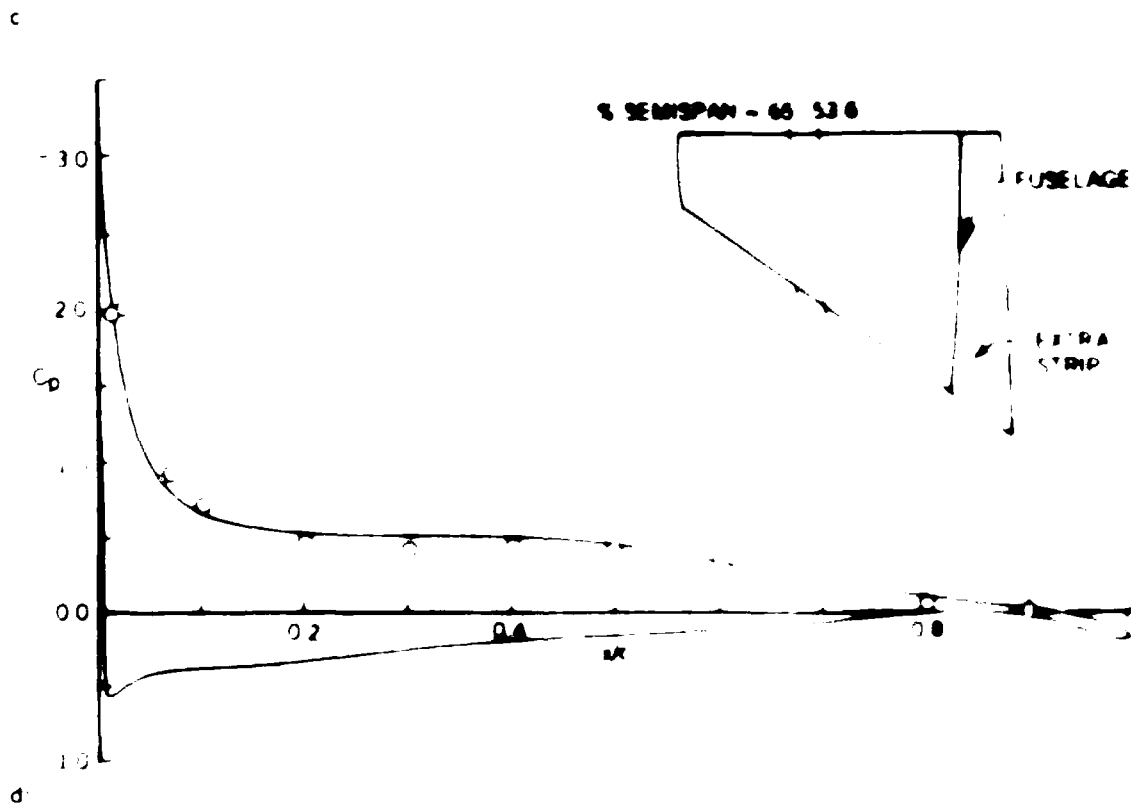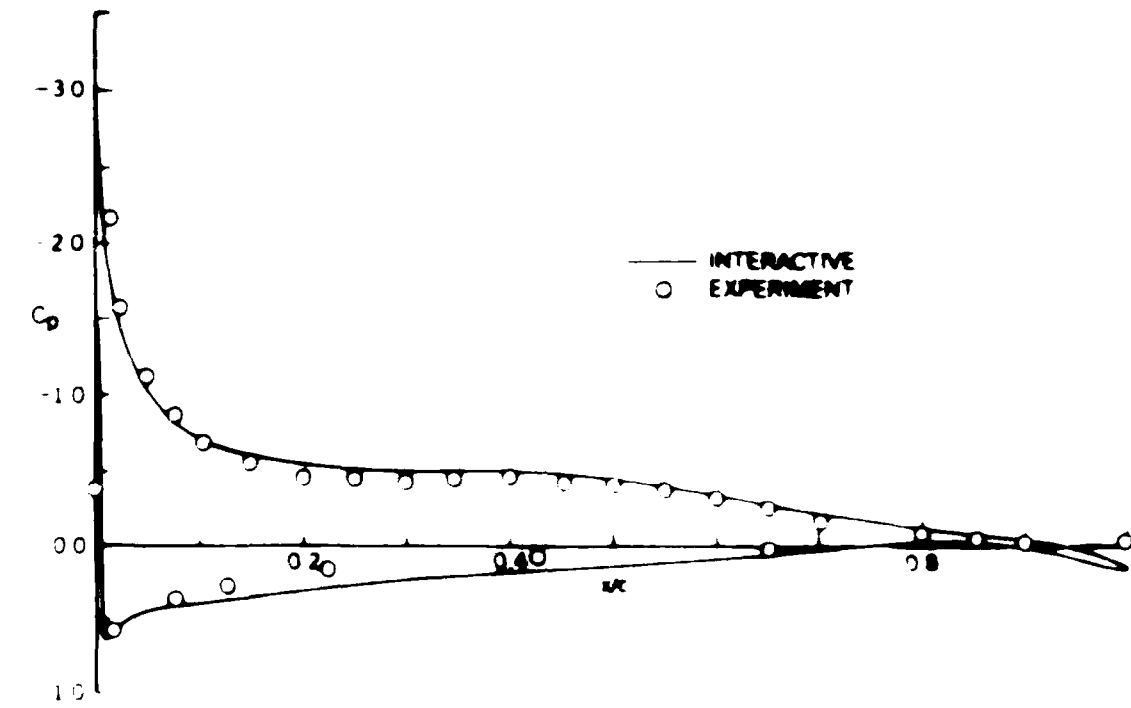
Figure ... ...
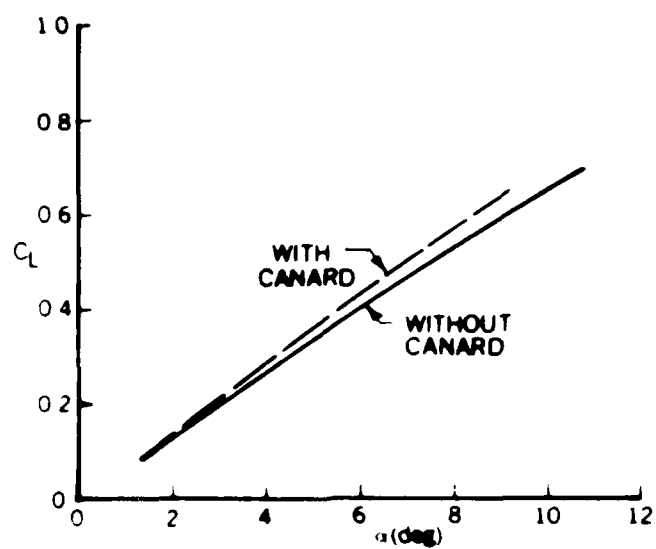
Figure . Effect of canard on the calculated lift curve of the ANF wing/body configuration, M = 0.6.
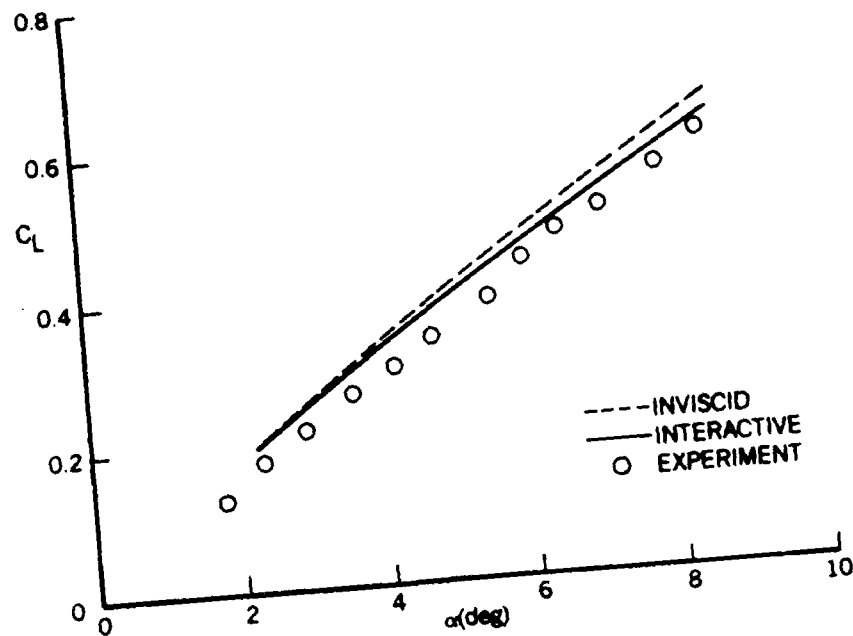
Figure 18. Comparison of computed and experimental lift curves for the unmodified F-15.
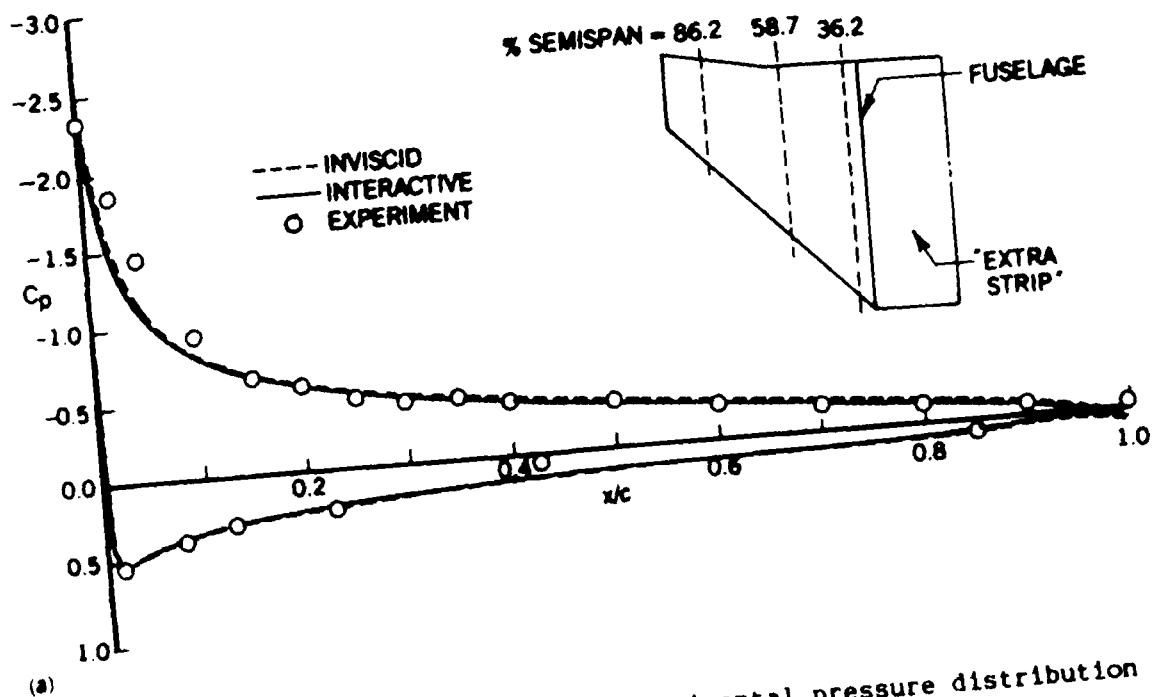
Figure 19. Comparison of computed and experimental pressure distribution for the unmodified F-15, $\alpha = 8.66°$, (a) 36.2% semispan.
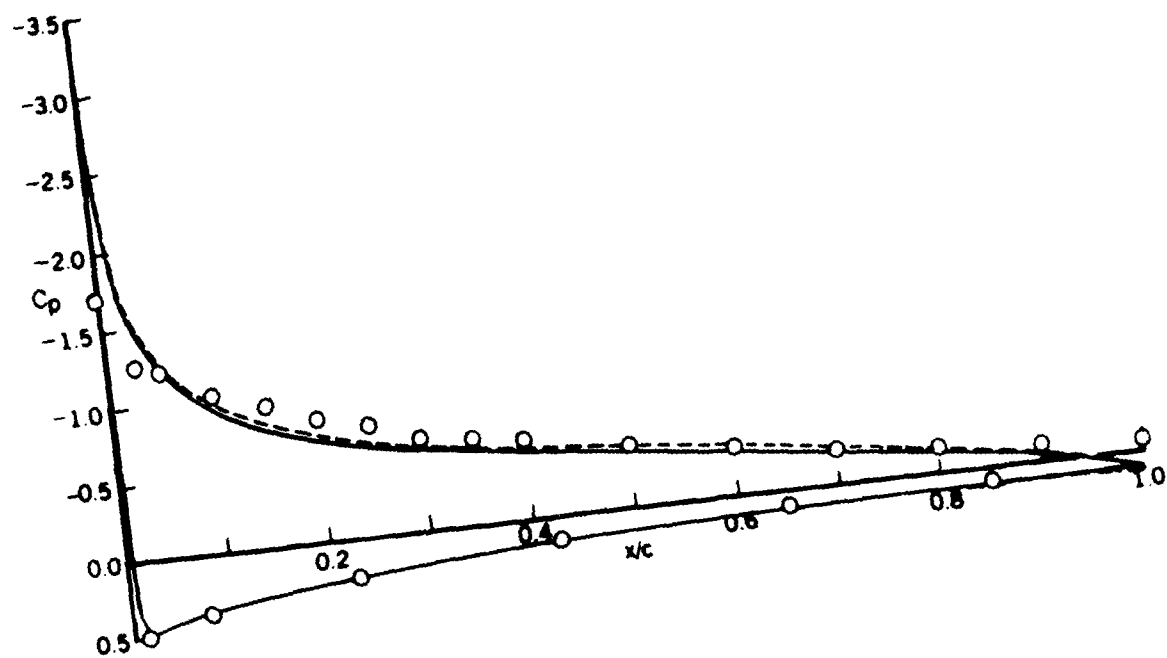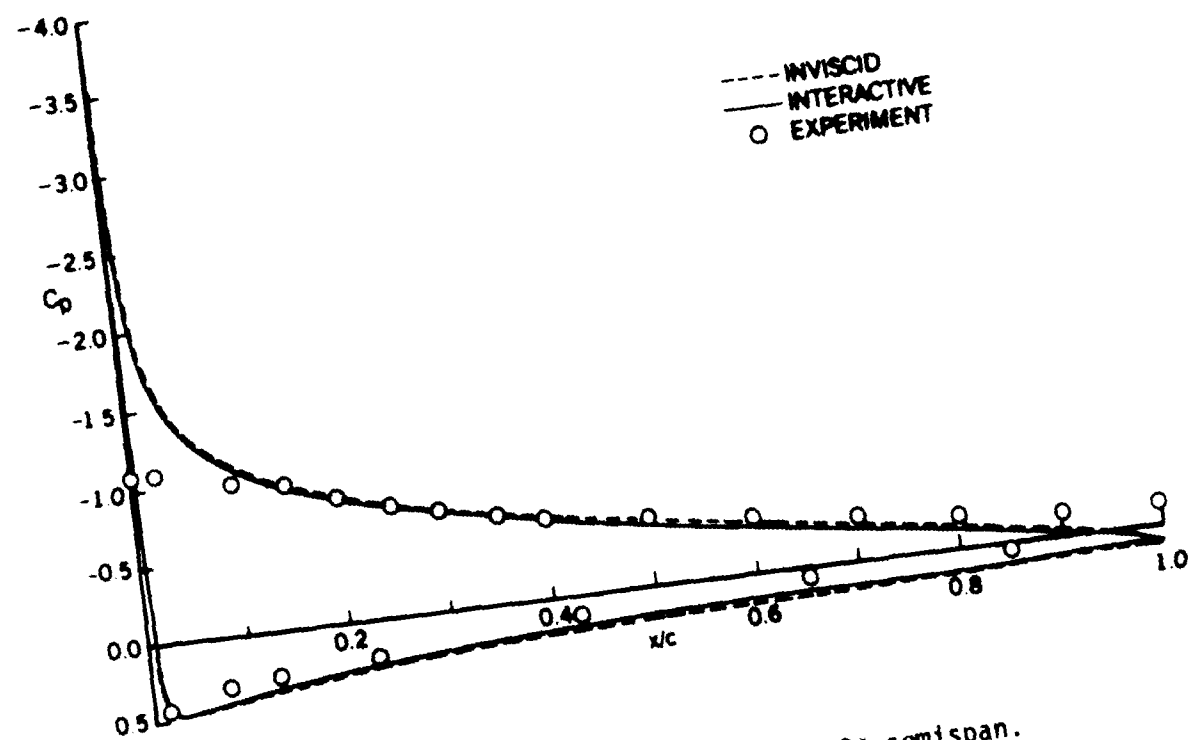
Figure 19. (Continued) (b) 58.7% semispan. (c) 86.2% semispan.
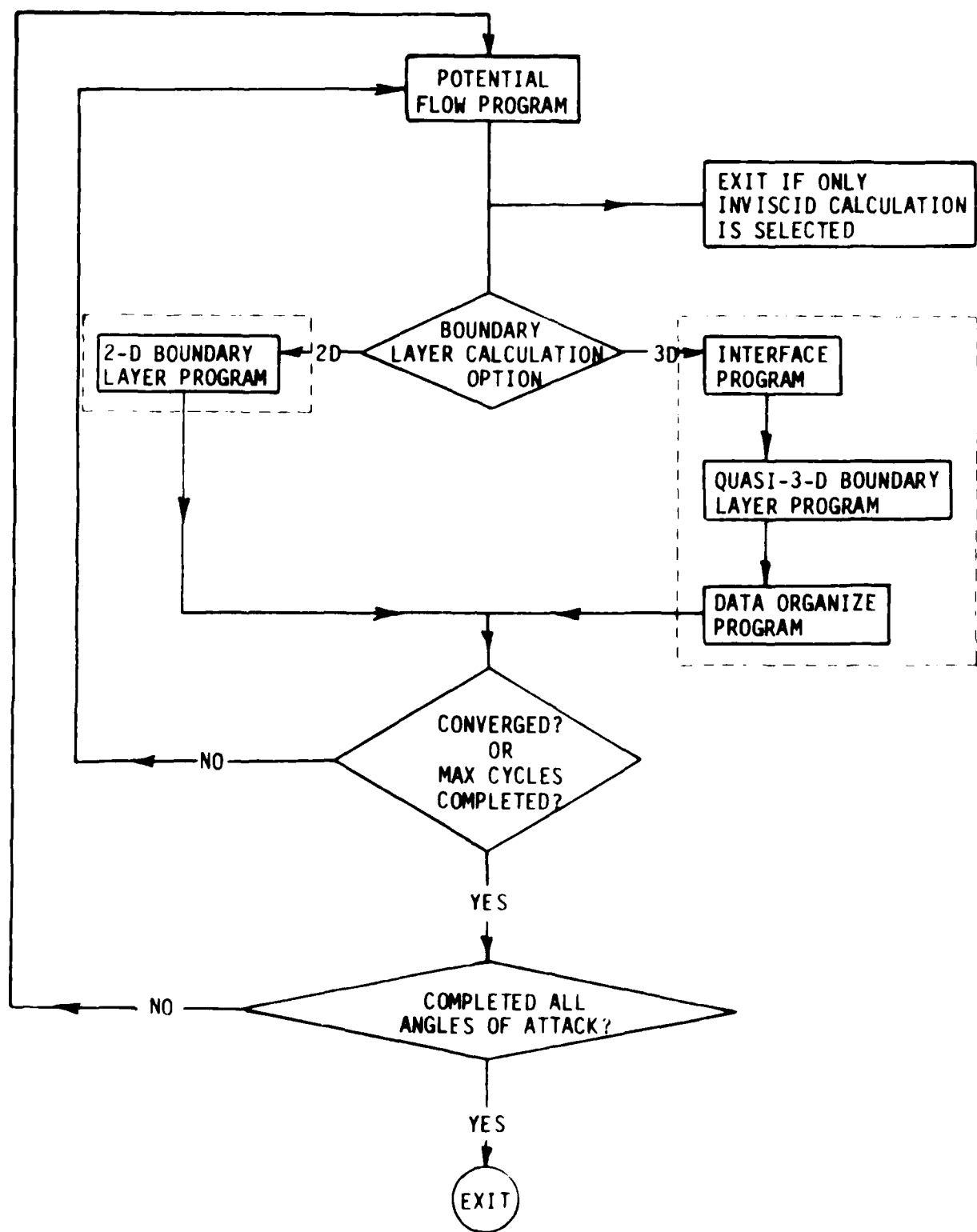
Figure 20. Flow structure of three-dimensional viscous/inviscid interaction program.
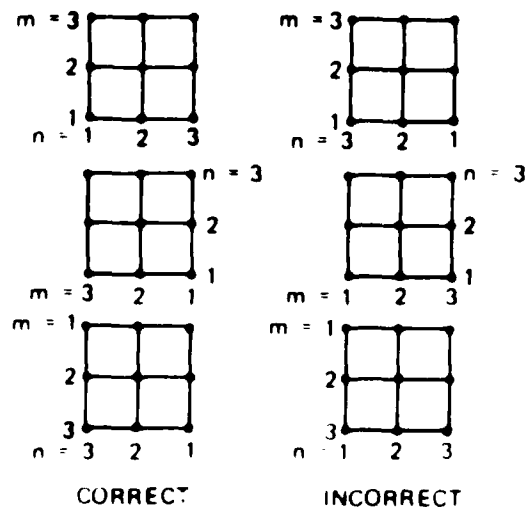
Figure 21. Examples of correct and incorrect input.
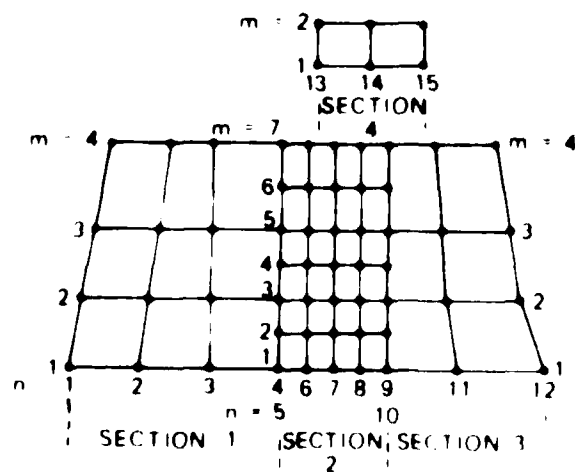
Figure 22. Plan view of the input points on a body divided into sections.
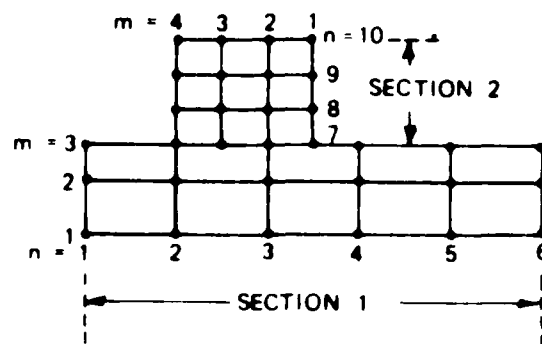
Figure 23. Another possible division into sections.
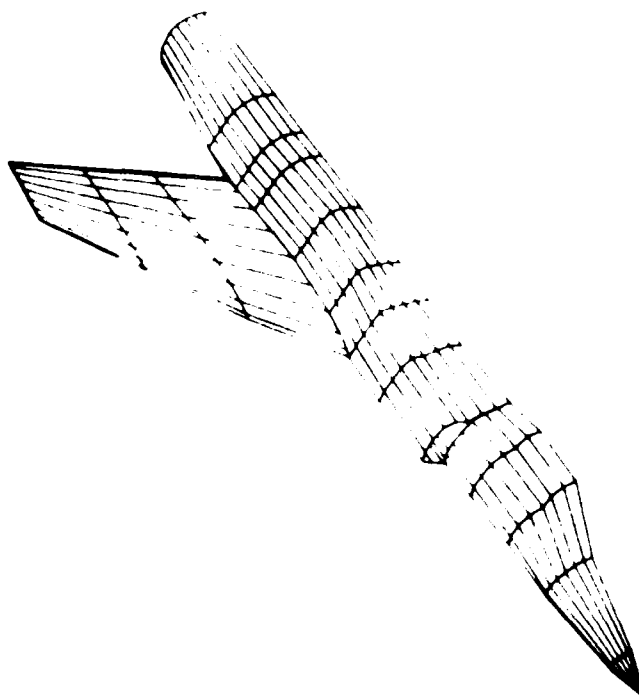
Figure 24. Arrangement of panels for the sample test case.

CASE TITLE: REPORT TEST CASE,TRANS. CALC., 2DSTRIP BL, M=0.6, ALPHAS   ALPHA = 1.30 MACH = 0.6000
PAGE TITLE: USER INPUT DATA   VISCOUS/INVISCID CYCLE NO. 0

CASE TITLE: REPORT TEST CASE,TRANS. CALC., 2DSTRIP BL, M=0.6, ALPHAS

NAMELIST "A" INPUT DATA:

IBL3D =   0   IPNTB3 =   0   IPNTGM =   0   IPNTNU =   0   KINKNO =   0
LIFT3D =   1   MAXAMG =   2   MAXCYC =   2   MLINE = 21   NLINE =   5
ALPHAI =   1.300000
AMACH =   0.600000   3.400000

NAMELIST "B" INPUT DATA:

IAUTOM =   2   IPCV   =   1   ITERAT =   1   IVNSP =   0   LIFSEC =   1
LINEAR =   0   LIST   =   0   NOFF   =   0   NSYM1 =   1   NSYM2 =   0
IXFLAG =   3   0   0   0   0   0   0   0   0   0   0
NLINE1 =   0   0   0   0   0   0   0   0   0   0   0
NLINEN =   0   0   0   0   0   0   0   0   0   0   0
NSTRIP =   4   0   0   0   0   0   0   0   0   0   0
NSORCE = 20   0   0   0   0   0   0   0   0   0   0
NMAKE =   1   0   0   0   0   0   0   0   0   0   0
BOV2   = 12.955000   ORIGNX =   0.0   ORIGNY =   0.0   ORIGNZ =   0.0
REFCMD =   8.291200   RFAREA =   95.904007

BOUNDARY LAYER INPUT DATA:

AL2D   =   0.000000   RC   =   0.70000E+07   RSTART =   0.0   VGP   =   1.125353
ETAE   =   8.000000   DETA1 =   0.015775

UPPER SURFACE DATA
NB = 70   ITR   =   2   ISMP   = 10   NTRM   =   0

LOWER SURFACE DATA
NB = 51   ITR   =   2   ISMP   =   5   NTRM   =   0

START COMPUTING ALPHA =   1.300

Figure 25. Output from the sample test case.

TUESDAY,   APR 15, 1986

CASE TITLE: REPORT TEST CASE,TRANS. CALC., 2DSTRIP BL, M=0.6, ALPHAS
PAGE TITLE: INPUT DATA

ALPHA = 1.30 MACH = 0.6000
VISCOUS/INVISCID CYCLE NO. 0

INPUT FLAGS

ICYCLE = 0
BOV2   = 12.95500
CIVAL = 0.0
HGND   = 0.0
IAUTOW = 2
IBLFIT = 1
ICONT = 1
ICONV = 1
IOUT   = 0
IPCV   = 1
ITERAT = 1
KUTTA = 1
IVNSP = 0
LIFSEC = 1
LINEAR = 0
LIST   = 0
MAXCYC = 2
MPR   = 0
NLR   = 0
NOFF   = 0
NSYM1 = 1
NSYM2 = 0
ORIGNX = 0.0
ORIGNY = 0.0
ORIGNZ = 0.0
RFAREA = 95.90401
REFCHD = 8.29120
RMACH = 0.60000

RUN MODE = 0 (0=INITIAL RUN. 1=BLOWING RUN.)

NSORCE = 20
NWAKE = 1
NSTRIP = 4
IXFLAG = 3

INPUT UNIFORM ONSET FLOWS IN DEGS AND COMPONENTS

(1) DEG -- 1.299999 COMPONENTS --   0.999743   0.0   0.022687

INPUT MACH NO. = 0.600000 BETA = 0.800000E+00

----------- # -----------

Figure 25. (Continued) Output from the sample case.

3-D VISCOUS-INVISCID INTERACTIVE PROGRAM

TUESDAY, APR 15, 1986

CASE TITLE
PAGE TITLE — REPORT TEST CASE,TRANS. CALC.,2DSTRIP BL, M=0.6; ALPHAS
PAGE TITLE — INPUT PANEL CORNER POINTS AND COMPUTED PANEL QUANTITIES

ALPHA = 1.30 MACH = 0.6000
VISCOUS/INVISCID CYCLE NO. 0

PNL NO	IV	IU	IX	E/X	XA	YA	ZA	XB DEFINING N-LINES	YB	ZB	NX NORMALS	NY	NZ	AVERAGE PROJ.DIST	MAXIMUM DIAGONAL	PROJECTED AREA
1	1	TYP=LIFT			29.52001	12.95000	5.67000	29.27000	9.33000	5.67000	0.10929	-0.00222	-0.99401	0.001278	3.624596	0.37137
2					29.24818	12.95000	5.65953	29.13795	9.33000	5.65805	0.11523	-0.00105	-0.99334	0.003709	3.653433	1.07383
3					29.03900	12.95000	5.64273	28.75801	9.33000	5.60651	0.05738	-0.00639	-0.99833	0.001543	3.725430	1.67248
4					28.71248	12.95000	5.62705	28.16208	9.33000	5.56917	0.03021	-0.00324	-0.99951	0.005184	3.847998	2.10782
5					28.30119	12.95000	5.60425	27.40961	9.33000	5.52255	0.05410	-0.00352	-0.99853	0.010833	4.010833	2.33594
6					27.84604	12.95000	5.56804	26.57628	9.33000	5.46991	0.07109	-0.01408	-0.99737	0.003351	4.187514	2.33741
7					27.39096	12.95000	5.52954	25.74344	9.33000	5.46991	0.04511	-0.00611	-0.99896	0.003680	4.343831	2.10698
8					26.98000	12.95000	5.50361	24.99162	9.33000	5.42695	0.04090	-0.00805	-0.99913	0.004027	4.449197	1.67299
9					26.65373	12.95000	5.48220	24.39452	9.33000	5.42695	-0.04511	-0.00805	-0.99652	0.000889	4.482141	1.07461
10					26.44441	12.95000	5.46784	24.01219	9.33000	5.39567	-0.07686	-0.03227	-0.94035	0.002981	4.431656	0.38034
11					26.37100	12.95000	5.48291	23.88837	9.33000	5.43812	-0.27423	0.20135	-0.85040	0.003127	4.430559	0.40875
12					26.65025	12.95000	5.51190	24.00941	9.33000	5.50783	-0.43796	0.29157	-0.99152	0.001114	4.480996	1.07802
13					26.97580	12.95000	5.53701	24.39128	9.33000	5.54743	-0.10865	0.07127	-0.99428	0.001655	4.447989	1.67683
14					27.38554	12.95000	5.56973	24.98685	9.33000	5.59786	-0.08975	0.05795	-0.99070	0.001324	4.342628	2.11475
15					27.84024	12.95000	5.61485	25.73460	9.33000	5.68774	-0.11555	0.07192	-0.99490	0.003436	4.187966	2.34150
16					28.29628	12.95000	5.66001	26.56686	9.33000	5.75087	-0.08371	0.05631	-0.99967	0.008647	4.012593	2.33662
17					28.70892	12.95000	5.68171	27.40086	9.33000	5.74160	-0.00963	-0.02370	-0.99968	0.005717	3.849562	2.11149
18					28.15419	12.95000	5.68318	28.15419	9.33000	5.71196	0.02415	-0.00741	-0.99969	0.000378	3.726239	1.67861
19					29.03690	12.95000	5.67587	28.75334	9.33000	5.69648	0.03776	0.00397	-0.99928	0.000230	3.653674	1.07835
20					29.24754	12.95000	5.66948	29.13805	9.33000	5.68037	0.04816	0.00044	-0.99884	0.000781	3.624587	0.37073
21					29.52001	12.95000	5.67000	29.27000	9.33000	5.67000	0.0	0.0	1.00000	0.002004	3.622074	0.37102
1	2				29.27000	9.33000	5.67000	29.22000	5.70000	5.67000	0.09411	-0.00115	-0.99556	0.000266	3.638230	0.59441
2					29.13795	9.33000	5.65805	29.02602	5.70000	5.65112	0.12199	-0.00319	-0.99253	0.002400	3.692335	1.71883
3					28.16208	9.33000	5.60651	28.46606	5.70000	5.58714	0.07822	-0.00162	-0.99693	0.004696	3.813978	2.67675
4					27.40961	9.33000	5.56917	27.59184	5.70000	5.50912	0.02288	0.01428	-0.99964	0.002424	3.999170	3.37360
5					26.57628	9.33000	5.55680	26.48625	5.70000	5.47897	0.01591	0.01161	-0.99981	0.010493	4.219386	3.73916
6					25.74344	9.33000	5.52255	25.26028	5.70000	5.48045	0.02767	-0.00659	-0.99960	0.014789	4.432336	3.74083
7					24.99162	9.33000	5.46991	24.03377	5.70000	5.47608	0.01409	-0.01212	-0.99982	0.007990	4.593949	3.37264
8					24.39452	9.33000	5.42695	22.92799	5.70000	5.47648	-0.00918	-0.01735	-0.99981	0.005450	4.672458	2.67814
9					24.01219	9.33000	5.39567	22.04999	5.70000	5.47933	0.00449	-0.05243	-0.99714	0.005177	4.651081	1.72121
10					23.88837	9.33000	5.43812	21.48695	5.70000	5.45894	0.05449	0.16808	-0.99714	0.003924	4.533655	0.59741
11					24.00941	9.33000	5.50783	21.29839	5.70000	5.50273	0.26231	0.16808	-0.95023	0.003785	4.530722	0.67371
12					24.39128	9.33000	5.54743	21.49162	5.70000	5.59086	-0.42567	0.31672	-0.84764	0.008763	4.646369	1.73498
13					24.98685	9.33000	5.54743	22.04639	5.70000	5.69222	-0.14757	0.12961	-0.98052	0.001625	4.672473	2.69231
14					25.73460	9.33000	5.68774	22.92105	5.70000	5.77438	0.08939	0.09817	-0.99115	0.010295	4.593665	3.39129
15					26.56686	9.33000	5.75087	24.02501	5.70000	5.85565	-0.09162	0.09467	-0.99128	0.011455	4.432856	3.74899
16					27.40086	9.33000	5.74160	25.25134	5.70000	5.89181	-0.04808	0.06244	-0.99689	0.005650	4.221378	3.74025
17					28.15419	9.33000	5.71196	26.47662	5.70000	5.85028	0.02465	0.02676	-0.99934	0.006043	4.001312	3.37981
18					28.75334	9.33000	5.69648	27.58229	5.70000	5.77690	0.05532	0.01247	-0.99839	0.005292	3.815083	2.68679
19					29.13805	9.33000	5.68037	28.46187	5.70000	5.72801	0.04349	0.00810	-0.99902	0.002849	3.692742	1.72593
20					29.27000	9.33000	5.67000	29.02650	5.70000	5.69029	0.05660	0.00256	-0.99839	0.001024	3.638208	0.59340
21					29.40248	9.33000	5.67000	29.41472	5.70000	5.67000	0.09383	-0.00073	-0.99559		3.634578	0.59385
43	3	1			29.22000	5.70000	5.67000	29.16177	1.63104	5.67000	0.07834	-0.00201	-0.99692	0.001809	4.083470	0.91498
					29.02602	5.70000	5.65112	28.90755	1.62853	5.65365	0.07834	-0.00201	-0.99692	0.001809	4.083470	0.91498

Figure 25. (Continued) Output from the sample case.

3-D VISCOUS-INVISCID INTERACTIVE PROGRAM

TUESDAY, APR 15, 1986

CASE TITLE   REPORT TEST CASE TRANS CALC., 2DSTRIP BL, M=0.6, ALPHAS
PAGE TITLE   INPUT PANEL CORNER POINTS AND COMPUTED PANEL QUANTITIES

ALPHA = 1.30   MACH = 0.6000
VISCOUS/INVISCID CYCLE NO. 0

PNL NO	IU	IV	IE X	XA	YA	ZA	XB	YB	ZB	NX	NY	NZ	AVERAGE PROJ.DIST	MAXIMUM DIAGONAL	PROJECTE AREA
44	2			28.46606	5.70000	5.58714	28.17281	1.63357	5.60051	0.09007	-0.00650	-0.99591	0.006644	4.155313	2.64594
45	3			27.59184	5.70000	5.50912	27.02955	1.68795	5.52141	0.07733	-0.01136	-0.99694	0.005085	4.262078	4.10008
46	3			26.48625	5.70000	5.47897	25.58682	1.77617	5.49062	0.02365	-0.00737	-0.99969	0.001998	4.406711	5.09187
47	5			25.26028	5.70000	5.48045	23.98625	1.83578	5.53868	-0.01761	-0.00406	-0.99984	0.010056	4.602991	5.53808
48	6			24.03377	5.70000	5.47608	22.38866	1.94199	5.61974	-0.02774	-0.01585	-0.99949	0.019194	4.732355	5.46672
49	7			22.92799	5.70000	5.47648	20.94963	2.05391	5.69694	-0.03193	-0.03350	-0.99893	0.017456	4.781501	4.82229
50	8			22.04999	5.70000	5.47933	19.80632	2.13268	5.75927	-0.05411	-0.04928	-0.99820	0.013554	4.749308	3.73834
51	9			21.48695	5.70000	5.45894	19.07140	2.17502	5.78621	-0.00766	-0.08031	-0.99674	0.012314	4.625520	2.36084
52	10			21.29839	5.70000	5.50273	18.84647	2.20004	5.87724	-0.30168	-0.11448	-0.94651	0.007721	4.404711	0.80284
53	11			21.04639	5.70000	5.59086	19.09769	2.19325	5.99694	-0.38998	-0.36394	-0.84585	0.000404	4.396436	0.93019
54	12			22.04639	5.70000	5.69222	19.81845	2.13085	6.13643	-0.17003	-0.22631	-0.95910	0.001449	4.592165	2.42994
55	13			22.02105	5.70000	5.77438	20.95973	2.03263	6.21539	-0.07081	-0.16140	-0.98434	0.009470	4.743588	3.81329
56	14			22.02501	5.70000	5.85565	22.40240	1.92678	6.24798	-0.03891	-0.12971	-0.99079	0.018784	4.793959	4.88158
57	15			25.25134	5.70000	5.89181	24.00360	1.83852	6.22560	-0.00188	-0.09538	-0.99544	0.016850	4.741836	5.48845
58	16			26.47662	5.70000	5.85028	25.60114	1.77469	6.11573	-0.05485	-0.06174	-0.99658	0.012906	4.601089	5.54991
59	17			27.58229	5.70000	5.77690	27.03862	1.68638	5.96145	-0.09048	-0.04023	-0.99509	0.013508	4.410319	5.10722
60	18			28.46187	5.70000	5.72801	28.18015	1.62168	5.82466	-0.09225	-0.02518	-0.99542	0.016240	4.265160	4.12453
61	19			29.02650	5.70000	5.69029	28.91148	1.62589	5.71483	-0.11508	-0.00926	-0.99354	0.013185	4.167491	2.66030
62	20			29.22000	5.70000	5.67000	29.16177	1.63104	5.67000	-0.14522	-0.00011	-0.98940	0.004006	4.086027	0.91352
63	21		X	29.41472	5.70000	5.67000	29.41631	1.63104	5.67000	0.0	-0.0	1.00000	0.0	4.076810	0.91398
64	1	*		29.16177	1.63104	5.67000	29.14000	0.0	6.17000	0.03304	-0.29778	-0.95406	0.003971	1.734078	0.46668
65	2	*		28.90755	1.62855	5.60365	28.84802	0.0	6.16821	0.04389	-0.31171	-0.94916	0.008309	1.926078	1.35720
66	3	*		27.02955	1.68795	5.60051	28.00394	0.0	6.15013	0.02153	-0.33633	-0.94150	0.015783	2.275011	2.17747
67	5	*		25.58682	1.77617	5.49062	26.68895	0.0	6.23597	-0.02688	-0.36258	-0.93156	0.017741	2.710762	2.90402
68	6	*		23.98625	1.83578	5.53868	25.03412	0.0	6.41274	-0.06703	-0.38749	-0.91943	0.019998	3.111118	3.39134
69	7	*		22.38866	1.94199	5.61974	23.20605	0.0	6.65753	-0.09914	-0.41166	-0.90593	0.020614	3.376588	3.62136
70	8	*		20.94963	2.05391	5.69694	21.38409	0.0	6.92859	-0.11689	-0.44096	-0.88988	0.025084	3.530232	3.52737
71	9	*		19.80632	2.13268	5.75927	19.75064	0.0	7.15018	-0.11683	-0.47512	-0.87213	0.020892	3.545797	2.99242
72	10	*		19.07140	2.17502	5.78621	18.45403	0.0	7.28252	-0.10056	-0.50794	-0.85550	0.014675	3.414163	2.01416
73	11	*		18.84647	2.20004	5.87724	17.62001	0.0	7.42204	-0.42297	-0.30845	-0.85203	0.004936	3.214189	0.64297
74	12	*		19.09769	2.19325	5.99694	17.36226	0.0	7.55301	-0.30590	-0.67700	-0.66940	0.000658	3.138953	0.88292
75	13	*		19.81845	2.13085	6.13643	17.64458	0.0	6.60223	0.07191	0.60203	0.79523	0.010760	3.358908	2.18778
76	14	*		20.95973	2.03263	6.21539	18.48807	0.0	7.55601	0.01107	0.55435	0.83221	0.011951	3.489580	3.15301
77	15	*		22.40240	1.92678	6.24798	19.80338	0.0	7.43768	0.04143	0.52233	0.85174	0.016122	3.491758	3.67073
78	16	*		24.00360	1.83852	6.22560	21.45753	0.0	7.25374	0.06493	0.48502	0.87209	0.020823	3.367968	3.74950
79	17	*		25.60114	1.77469	6.11573	23.28661	0.0	6.98579	0.10709	0.43396	0.89455	0.022546	3.131994	3.47307
80	18	*		27.03862	1.68638	5.96145	25.10378	0.0	6.69297	0.15806	0.38812	0.91034	0.015895	2.764696	2.94201
81	19	*		28.18015	1.62168	5.82466	26.73785	0.0	6.43695	0.17824	0.35316	0.92211	0.015719	2.338412	2.19527
82	20	*		28.91148	1.62589	5.71483	28.03258	0.0	6.24725	0.21157	0.31733	0.93142	0.014695	1.984590	1.35857
83	20	*		29.16177	1.63104	5.67000	28.85895	0.0	6.17000	0.0	0.29094	0.93305	0.006306	1.756554	0.46408
84	21	* X		29.41631	1.63104	5.67000	29.43172	0.0	6.17000	0.0	0.29309	0.95608	0.0	1.728189	0.46594
SEC 85	1	1		1.44000	0.0	6.16000	3.00000	0.0	6.90000	-0.42309	0.14344	0.89466	0.001006	1.726101	0.17374
86	2	1		1.44000	0.00643	6.16123	3.00000	0.19285	6.86682	-0.41087	0.45684	0.78897	0.000447	1.722223	0.17160
87	3	1		1.44000	0.01043	6.15704	3.00000	0.49166	6.61642	-0.39078	0.70527	0.59152	0.000757	1.711767	0.17041

Figure 25. (Continued) Output from the sample case.

3 D VISCOUS INVISCID INTERACTIVE PROGRAM

CASE TITLE   REPORT TEST CASE, TRANS, CALC, ZDSTRIP BL, M-0.6, ALPHAS
PAGE TITLE   INPUT PANEL CORNER POINTS AND COMPUTED PANEL QUANTITIES

ALPHA =   1.30 MACH = 0.6000
VISCOUS/INVISCID CYCLE NO.   0

PNL NO	IV	IU	ZA	YA	XA	ZA	YB	XB	ZB	NX	NY	NZ	AVERAGE PROJ.DIST	MAXIMUM DIAGONAL	PROJECTED AREA
88			1 44000	0 01034		6 15174	0 56079	3 00000	6 43560	-0 36566	0 87265	0 32368	0 000901	1.697409	0.16635
89			1 44000	0 00855		6 14952	0 56044	3 00000	6 23747	-0 33205	0 94321	-0 01005	0 000831	1.679407	0.16568
90			1 44000	0 00274		6 15037	0 49591	3 00000	6 05307	-0 29944	0 89093	0 34145	0 002733	1.658980	0.16069
91			1 44000	0 00019		6 14938	0 56010	3 00000	5 91436	-0 25990	0 68514	-0 68047	0 000666	1.639813	0.15903
92			1 44000	0 00048		6 14568	0 18800	3 00000	5 81871	-0 23695	0 48513	-0 84173	0 001491	1.617753	0.15974
93			1 44000	0		6 14000	0	3 00000	5 76000	-0 22778	0 31623	-0 92093	0 002693	1.606968	0.15882
94			3 00000	0 19285		6 90300	0 37576	6 60000	8 00000	-0 27766	0 25662	0 92577	0 009384	3.779055	1.10557
95			3 00000	0 36318		6 86682	0 67208	6 60000	7 87556	-0 23700	0 60155	0 76287	0 013172	3.766819	1.10104
96			3 00000	0 49160		6 76705	0 90969	6 60000	7 60736	-0 20313	0 77640	0 59660	0 004941	3.738248	1.10452
97			3 00000	0 56073		6 61642	1 07016	6 60000	7 28157	-0 17698	0 90856	0 37840	0 002809	3.714481	1.09220
98			3 00000	0 56044		6 43560	1 14071	6 60000	6 91110	-0 16053	0 98016	0 11624	0 011686	3.697779	1.08704
99			3 00000	0 49591		6 23747	1 03076	6 60000	6 51729	-0 13204	0 94731	-0 29183	0 003658	3.686629	1.07619
100			3 00000	0 56010		5 91436	0 75277	6 60000	6 13531	-0 09101	0 71643	-0 69169	0 000676	3.668593	1.07681
101			3 00000	0 18800		5 81871	0 39365	6 60000	5 66702	-0 06519	0 45749	-0 88682	0 003050	3.644127	1.07826
102			3 00000	0		5 76000	0	6 60000	5 58000	-0 05156	0 24272	-0 96873	0 005625	3.622647	1.08073
			6 00000			8 00000	0 51516	9 04000	9 40000	-0 45840	0 53769	0 82209	0 016216	2.897902	1.32817
							0 79554	9 04000	9 14874	-0 30618	0 76984	0 56000	0 032902	2.890693	1.23567

Figure 25. (Continued) Output from the sample case.

S D VISCOUS INVISCID INTERACTIVE PROGRAM

TUESDAY, APR 15, 1986

METHOD IEJ CASE TRANS. CALC. 2DSTRIP BL, M=0.6, ALPHAS
INPUT PANEL CORNER POINTS AND COMPUTED PANEL QUANTITIES

ALPHA = 1.30 MACH = 0.6000
VISCOUS/INVISCID CYCLE NO. 0

#		IA	DEFINING N-LINES YA	ZA	N-LINES XB	YB	ZB	NX	NY	NZ	AVERAGE PROJ.DIST	MAXIMUM DIAGONAL	PROJECTED AREA
164	5	25.89417	1.83177	7.75529	26.95972	1.67389	7.47342	0.06649	0.97928	0.19131	0.002345	3.165515	1.55137
165	6	25.88525	1.82139	7.24548	26.95723	1.67881	6.97343	0.04836	0.99881	-0.00595	0.003884	3.164968	1.55282
166	7	25.88583	1.84205	6.73567	26.95937	1.69102	6.47266	0.05053	0.99819	-0.03260	0.002017	3.172443	1.55508
167	8	25.89360	1.84257	6.22568	26.96979	1.69079	5.97178	0.04928	0.99878	0.00117	0.000152	3.180747	1.55368
170	1	26.97006	0	8.95094	28.43298	0.0	8.92383	0.03150	0.12796	0.99128	0.009598	1.553557	0.73858
171	2	26.97418	0.49796	8.90591	28.43552	0.50353	8.83938	0.04736	0.37291	0.92666	0.004812	1.557402	0.73767
172	3	26.96544	0.96514	8.72838	28.43382	0.97184	8.64061	0.05335	0.67869	0.73249	0.009107	1.564067	0.73594
173	4	26.95724	1.34274	8.40390	28.42628	1.33215	8.28244	0.05058	0.88395	0.46483	0.004036	1.581067	0.73987
174	5	26.95972	1.58263	7.96596	28.42099	1.56277	7.82708	0.03764	0.98725	0.15467	0.007003	1.602433	0.73958
175	6	26.95937	1.67389	7.47342	28.42369	1.62768	7.32153	0.03531	0.99937	0.00194	0.002899	1.608027	0.74132
176	7	26.95937	1.69102	6.97343	28.42809	1.62088	6.81054	0.04342	0.99887	-0.01918	0.001340	1.618658	0.74132
177	8	26.96979	1.69079	5.97178	28.44263	1.61640	5.78917	0.04546	0.99891	-0.01039	0.002722	1.634870	0.74231
178	1	28.43298	0	8.92383	30.76100	0.0	8.91839	0.00382	0.17222	0.98505	0.001758	2.382419	1.18172
179	2	28.43552	0.50353	8.83938	30.76100	0.49706	8.82790	0.00777	0.39969	0.91662	0.002484	2.382488	1.17569
180	3	28.43382	0.97184	8.64061	30.76102	0.95524	8.62269	0.01138	0.70797	0.70615	0.001036	2.389291	1.17767
181	4	28.42628	1.33215	8.28244	30.76102	1.30854	8.26553	0.00404	0.87428	0.48540	0.009718	2.394282	1.18474
182	5	28.42099	1.56277	7.82708	30.76102	1.57001	7.83461	-0.00642	0.99006	0.14052	0.003398	2.393654	1.18289
183	6	28.42369	1.62768	7.32153	30.76100	1.64727	7.33864	-0.00847	0.99989	-0.01250	0.000208	2.396280	1.18786
184	7	28.42380	1.62782	6.81054	30.76100	1.64137	6.32798	-0.00680	0.99997	-0.00435	0.002344	2.393211	1.18656
185	8	28.44263	1.61640	5.78917	30.76100	1.62955	5.82297	-0.00493	0.99978	-0.02050	0.000513	2.381105	1.18128
186	1	30.76100	0	8.91839	36.00000	0.0	8.89000	0.00440	0.16946	0.98553	0.002472	5.262889	2.45523
187	2	30.76100	0.49706	8.82790	35.99997	0.42667	8.82165	0.00691	0.41152	0.91137	0.000754	5.269319	2.44759
188	3	30.76102	0.95524	8.62269	35.99997	0.82006	8.64235	0.01054	0.67918	0.73390	0.011086	5.275148	2.44541
189	4	30.76102	1.30854	8.26553	35.99997	1.15188	8.36545	0.01045	0.83307	0.55307	0.010256	5.282365	2.45018
190	5	30.76102	1.57001	7.83461	35.99997	1.40774	8.01714	0.01592	0.97508	0.22131	0.017216	5.288132	2.43503
191	6	30.76100	1.64727	7.33864	35.99997	1.55620	7.60670	0.02144	0.99973	-0.00932	0.000595	5.296791	2.45830
192	7	30.76100	1.64137	6.83327	35.99998	1.53336	7.17385	0.02668	0.99882	-0.04065	0.009025	5.307860	2.45411
193	8	30.76100	1.62955	5.82297	35.99997	1.31294	6.35332	0.06171	0.97541	-0.21158	0.048875	5.320848	2.40371

SEC 5,TYP=NLIF

#		IA	YA	ZA	XB	YB	ZB	NX	NY	NZ	PROJ.DIST	DIAGONAL	AREA
194	1	13.24000	2.33368	6.08937	16.42842	2.33368	5.93854	-0.04156	0.16378	-0.98562	0.005181	3.285070	1.95443
195	2	13.24000	1.86802	5.99559	16.42966	1.75313	5.83150	-0.05030	0.07576	-0.99586	0.002861	3.273629	1.96647
196	3	13.24000	1.23555	5.95322	16.42834	1.15746	5.78050	-0.04189	0.29804	-0.95363	0.003951	3.270663	1.95509
197	4	13.24000	0.63137	5.75612	16.42856	0.59213	5.61208	-0.04803	0.11126	-0.99263	0.007266	3.258414	1.9651
			0.0	5.53106	16.42874	0.0	5.53106						
198	1	16.42842	2.33368	5.93854	18.82666	2.19727	5.85649	-0.04986	0.32227	-0.94533	0.042979	2.495832	1.50712
199	2	16.42966	1.75313	5.83150	18.83253	1.74812	5.61213	-0.08748	0.07287	-0.99350	0.003692	2.485142	1.43054
200	3	16.42834	1.15746	5.78050	18.82961	1.16044	5.57671	-0.06611	0.21870	-0.97355	0.020159	2.488068	1.41082
201	4	16.42856	0.59213	5.61208	18.83125	0.58211	5.48809	-0.05052	0.13545	-0.98950	0.000016	2.482788	1.42554
		16.42874	0.0	5.53106	18.83109	0.0	5.40837						
202	1	18.82666	2.19727	5.85649	20.88670	2.05842	5.69828	-0.05260	0.57492	-0.81652	0.029500	2.155057	0.97577
		18.83253	1.74812	5.61213	20.87991	1.73170	5.39641						

Figure 25. (Continued) Output from the sample case.

3-D VISCOUS-INVISCID INTERACTIVE PROGRAM

CASE TITLE: REPORT TEST CASE,TRANS. CALC., 2DSTRIP BL, M=0.6, ALPHAS
PAGE TITLE: INPUT PANEL CORNER POINTS AND COMPUTED PANEL QUANTITIES

ALPHA =   1.30 MACH = 0.600
VISCOUS/INVISCID CYCLE NO

PNL. NO.	IV	IU	E X	XA	YA	ZA	XB	YB	ZB	NX	NY	NZ	AVERAGE PROJ DIST	MAXIMUM DIAGONAL	PROJECTED AREA
203	2			18.82961	1.16044	5.57671	20.87648	1.15297	5.37175	-0.10178	0.05172	-0.99356	0.002551	2.142354	1.2017?
204	3			18.83125	0.58211	5.48809	20.88133	0.57510	5.33481	-0.08623	0.10709	-0.99058	0.012838	2.147238	1.1955?
205	4			18.83109	0.0	5.40837	20.87863	0.0	5.28024	-0.06786	0.11517	0.99103	0.005988	2.138645	1.1961?
206	1			20.88670	2.05842	5.69828	23.87218	1.84097	5.54329	0.02409	0.50225	0.84490	0.048341	3.039751	1.2184?
207	2			20.87991	1.73170	5.39641	23.85594	1.46304	5.43510	0.01990	0.01300	0.88972	0.008531	3.072762	1.5495?
208	3			20.87648	1.15297	5.37175	23.85582	0.96787	5.44572	0.04577	0.86515	0.99682	0.037354	3.053928	1.5455?
209	4			20.87863	0.57510	5.28024	23.84995	0.48296	5.55211	0.07140	0.11818	0.99842	0.007054	3.027284	1.5864?
210	1			23.87218	1.84097	5.54329	26.95326	1.69297	5.52020	0.01966	0.10326	0.99446	0.034123	3.107005	1.8560?
211	2			23.85594	1.46304	5.43510	26.94032	1.40435	5.55860	0.05373	0.12344	0.99098	0.025300	3.135065	1.9075?
212	3			23.85582	0.96787	5.44572	26.93628	0.92895	5.66865	0.85420	0.11586	0.99178	0.024083	3.125156	1.9555?
213	4			23.84995	0.48296	5.55211	26.93353	0.47460	5.67155	0.85956	0.14188	0.98910	0.061319	3.125757	1.9026?
214	1			26.95326	1.69297	5.52020	28.43810	1.62904	5.62337	0.05714	0.89934	0.99398	0.005634	3.317960	0.925?
215	2			26.94032	1.40435	5.55860	28.42143	1.32829	5.63921	0.05028	0.25016	0.98900	0.008165	3.301738	0.758?
216	3			26.93628	0.92895	5.66865	28.41695	0.88051	5.77571	0.05714	0.04630	0.99726	0.012196	3.354078	0.63?
217	4			26.93349	0.47460	5.60617	28.41734	0.45097	5.73098	0.03603	0.14842	0.98810	0.002911	3.357029	0.62?
218	1			28.43810	1.62904	5.62337	30.77306	1.62954	5.82408	0.07717	0.09943	0.99697	0.000933	3.378035	0.755?
219	2			28.42143	1.32829	5.63921	30.77306	1.28273	5.80082	0.85394	0.25570	0.96525	0.009743	3.413580	0.815?
220	3			28.41695	0.88051	5.77571	30.77307	0.85044	5.89722	0.03780	0.18562	0.98180	0.017911	3.396266	0.844?
221	4			28.41734	0.45097	5.65738	30.77306	0.43325	5.78187	0.02567	0.15565	0.98762	0.001306	3.399284	
222	1			30.77306	1.62954	5.82408	35.99997	1.31292	6.35329	0.08801	0.50241	0.86013	0.017459	5.260428	
223	2			30.77306	1.28273	5.80082	35.99997	1.07926	6.03748	0.01893	0.17143	0.98501	0.002557	5.253882	2.23??
224	3			30.77307	0.85044	5.89722	35.99997	0.75934	6.01017	0.01325	0.29326	0.95533	0.000681	5.231007	1.1680?
225	4			30.77306	0.43325	5.71667	36.00000	0.0	6.12000	0.01795	0.15258	0.98013	0.000661	5.247340	2.1601?

Figure 25. (Continued) Output from the sample ...

3-D VISCOUS-INVISCID INTERACTIVE PROGRAM

TUESDAY   APR 15 1986

CASE TITLE: REPORT TEST CASE,TRANS. CALC., 2DSTRIP BL, M=0.6, ALPHAS
PAGE TITLE: INTEGRATED PRESSURES

ALPHA   1.30 MACH   0.600
VISCOUS INVISCID CYCLE NO c

|<---- BASED UPON INPUT VALUES OF AREF,BOV2,CREF ---->|

TYPE	SEC	NV	CL	CD	CSF	CPITCH	CROLL	CYAW	ETA	SECTCL	SECTCD	ASTRIP	CIRCULTN
LIFT	1	1	0.0045	-0.0003	0.0006	-0.0155	-0.0026	-0.0014	0.8463	0.0286	-0.0018	15.0991	-0.0062
		2	0.0226	-0.0007	0.0020	-0.0700	-0.0075	-0.0042	0.5712	0.0858	-0.0028	24.1998	-0.0175
		3	0.0512	-0.0001	0.0064	-0.1443	-0.0185	-0.0113	0.2759	0.1383	-0.0002	35.5155	-0.0322
SECT. TOT:			0.0784	-0.0011	0.0090	-0.2297	-0.0284	-0.0170					
NLIF	2	1	-0.0008	0.0010	-0.0016	0.0010	0.0005	0.0003					
		2	-0.0029	0.0009	-0.0024	0.0026	0.0014	0.0010					
SECT. TOT:			-0.0037	0.0018	-0.0040	0.0035	0.0019	0.0013					
NLIF	3	1	-0.0019	-0.0000	0.0051	0.0019	-0.0048	-0.0032					
		2	0.0037	-0.0005	0.0092	-0.0051	-0.0112	-0.0074					
		3	0.0023	-0.0000	0.0042	-0.0034	-0.0061	-0.0040					
SECT. TOT:			0.0041	-0.0005	0.0184	-0.0067	-0.0222	-0.0147					
NLIF	4	1	0.0028	0.0001	0.0034	-0.0050	-0.0060	-0.0039					
		2	0.0019	0.0000	0.0011	-0.0041	-0.0023	-0.0015					
		3	0.0027	0.0007	0.0076	-0.0060	-0.0178	-0.0115					
		4	0.0064	0.0009	0.0131	-0.0166	-0.0350	-0.0227					
		5	0.0042	-0.0007	0.0083	-0.0125	-0.0251	-0.0163					
		6	-0.0004	-0.0000	-0.0007	0.0012	0.0024	0.0016					
		7	-0.0011	-0.0000	-0.0037	0.0039	0.0133	0.0086					
		8	-0.0013	-0.0001	-0.0031	0.0050	0.0125	0.0081					
SECT. TOT:			0.0153	0.0023	0.0259	-0.0340	-0.0580	-0.0377					
NLIF	5	1	-0.0008	-0.0001	0.0001	0.0014	-0.0002	-0.0002					
		2	0.0011	-0.0001	-0.0001	-0.0023	0.0002	0.0002					
		3	-0.0003	-0.0000	-0.0003	0.0007	0.0009	0.0001					
		4	-0.0015	-0.0000	-0.0003	0.0041	0.0009	-0.0006					
		5	0.0024	-0.0000	0.0000	0.0073	0.0000	-0.0000					
		6	0.0006	-0.0000	0.0000	-0.0019	-0.0001	-0.0001					
		7	0.0030	-0.0001	-0.0007	-0.0107	-0.0000	-0.0000					
		8	0.0024	-0.0000	-0.0007	-0.0096	-0.0029	-0.0019					
SECT. TOT:			0.0021	0.0000	-0.0011	-0.0110	0.0038	0.0025					
CONFIG.TOT:			0.0962	0.0026	0.0483	-0.2779	0.0058	0.0657					

Figure 25. (Continued) Output from the sample case.

3-D VISCOUS-INVISCID INTERACTIVE PROGRAM

ALPHA = 1.30 MACH = 0.6000
VISCOUS/INVISCID CYCLE NO. ?

CASE TITLE: REPORT TEST CASE,TRANS. CALC., 2DSTRIP BL, M=0.6, ALPHAS
PAGE TITLE: INPUT DATA

INPUT FLAGS

ICYCLE =   2
BOV2   =   12.95500
CIVAL   =   0.0
MGND   =   0.0
IAUTOM =   2
IBLFIT =   1
ICONT   =   1
ICONV   =   1
IOUT   =   0
IPCV   =   1
ITERAT =   1
KUTTA   =   2
IVNSP   =   3
LIFSEC =   1
LINEAR =   0
LIST   =   0
MAXCYC =   2
MPR   =   0
NLR   =   0
NOFF   =   0
NSYM1   =   1
NSYM2   =   0
ORIGNX =   0.0
ORIGNY =   0.0
ORIGNZ =   0.0
RFAREA =   95.90401
REFCHD =   8.29120
RMACH   =   0.60000

RUN MODE = 1   (0=INITIAL RUN. 1=BLOWING RUN.)

NSORCE = 20
NWAKE = 1
NSTRIP = 4
IXFLAG = 3

OFF - BODY KUTA CONDITION HAS BEEN SELECTED...
        PRINTED CP DISTRIBUTION AND FORCE CALCULATION
        WILL USE OFF - BODY PRESSURES

INPUT UNIFORM ONSET FLOWS IN DEGS AND COMPONENTS

(1) DEG --   1.299999 COMPONENTS --   0.999743   0.0   0.022687

INPUT MACH NO. =   0.600000 BETA = 0.800000E+00

Figure 25. (Continued) Output from the sample case.

TUESDAY,   APR 15, 1986

3-D VISCOUS-INVISCID INTERACTIVE PROGRAM

CASE TITLE: REPORT TEST CASE, TRANS. CALC., 2DSTRIP BL, M=0.6, ALPHAS
PAGE TITLE: FUNDAMENTAL FLOW SOLUTION

ALPHA = 1.30   MACH = 0.6000
VISCOUS/INVISCID CYCLE NO. 2

***** WARNING ***** PRINTED CP, VX, VY, VZ AND FORCES ARE COMPUTED AT OFF - BODY POINTS

PNL NO.	SEC NO.	SEC TYPE	IV	IU	CONTROL POINTS X	CONTROL POINTS Y	CONTROL POINTS Z	INCOMPRESSIBLE POTENTIAL FL SOLUTN VX	VY	VZ	VT	CPVISC	VISCOUS FLOW SOLUTION DELS	M	CF
1	1	LIFT	1	1	29.24013	10.96359	5.66436	0.93231	-0.01307	0.08559	0.93632	0.12468	0.01364	1.44747	0.00215
2				2	29.03622	10.96347	5.64078	0.98662	-0.01499	0.10140	0.99193	0.01610	0.01122	1.40443	0.00254
3				3	28.64761	10.96357	5.60907	1.02211	-0.01426	0.05038	1.02345	-0.04725	0.00901	1.37516	0.00296
4				4	28.11116	10.96349	5.58675	1.01983	-0.01113	0.02401	1.02018	-0.04061	0.00763	1.37522	0.00314
5				5	27.48058	10.96350	5.52079	1.01973	-0.01228	0.04799	1.02094	-0.04215	0.00627	1.38920	0.00326
6				6	26.81805	10.96352	5.52064	1.03064	-0.01718	0.06576	1.03287	-0.06643	0.00467	1.40574	0.00350
7				7	26.18784	10.96351	5.48367	1.04009	-0.01847	0.03926	1.04099	-0.08304	0.00308	1.43536	0.00392
8				8	25.65141	10.96352	5.46120	1.02644	-0.00792	0.03486	1.02706	-0.05459	0.00160	1.56275	0.00413
9				9	25.26169	10.96329	5.44005	1.07117	-0.03579	0.07396	1.07432	-0.15203	0.00118	2.65748	0.00141
10				10	25.06764	10.97600	5.44348	1.10662	-0.04894	-0.32796	1.15523	-0.32460	0.00056	2.40618	0.00590
11				11	25.05743	10.96301	5.48399	0.77459	0.17063	0.38051	0.87971	0.23075	0.00046	2.46123	0.00507
12				12	25.25879	10.96352	5.52620	1.02922	-0.02358	0.11381	1.03135	-0.14583	0.00086	2.43471	0.00267
13				13	25.64748	10.96352	5.56395	1.03308	0.00116	0.08888	1.03966	0.08031	0.00154	1.50915	0.00128
14				14	26.18195	10.96356	5.62001	1.07420	-0.01810	0.11678	1.07788	0.15949	0.00342	1.41828	0.00416
15				15	26.81053	10.96352	5.68236	1.07533	-0.02718	0.08719	1.07571	0.15494	0.00503	1.40258	0.00382
16				16	27.47318	10.96349	5.71222	1.03977	-0.02277	0.00927	1.04034	-0.08171	0.00687	1.40091	0.00308
17				17	28.10471	10.96350	5.70677	1.01909	-0.01909	-0.02585	1.01960	-0.03944	0.00865	1.40261	0.00285
18				18	28.64288	10.96350	5.69308	0.99370	-0.01648	-0.03353	0.99440	0.01118	0.01035	1.42634	0.00248
19				19	29.03436	10.96348	5.68132	0.95605	-0.01389	-0.03472	0.95670	0.12377	0.01385	1.47251	0.00205
20				20	29.24001	10.96351	5.67272	0.91564	-0.01339	-0.07040	0.91844	0.15867	0.02141	1.44938	0.00192
22	1	LIFT	2	1	29.16090	7.39987	5.66218	0.96203	-0.01540	0.10577	0.96795	0.06342	0.01746	1.40458	0.00224
23				2	28.84059	7.39991	5.62529	1.01934	-0.01629	0.07057	1.02191	-0.04413	0.01333	1.36412	0.00267
24				3	28.23080	7.39988	5.56673	1.05561	-0.01010	0.01658	1.03580	-0.07240	0.01075	1.35239	0.00292
25				4	27.38876	7.39995	5.52653	1.03201	-0.00625	-0.00969	1.03207	-0.06479	0.00877	1.35971	0.00307
26				5	26.39757	7.39989	5.50779	1.02821	-0.00451	0.02158	1.02845	0.05741	0.00675	1.37464	0.00325
27				6	25.35545	7.39992	5.48668	1.01886	0.00109	0.00754	1.01889	0.03800	0.00473	1.40066	0.00353
28				7	24.36435	7.39990	5.46707	1.00530	0.01013	-0.00161	1.00535	-0.01072	0.00266	1.45147	0.00410
29				8	23.52112	7.39990	5.45788	1.03720	-0.00732	0.05109	1.03849	-0.07790	0.00136	2.36798	0.00194
30				9	22.90884	7.40013	5.44205	1.00541	-0.01494	-0.27981	1.04373	0.08866	0.00082	2.48810	0.00259
31				10	22.58910	7.39812	5.45092	0.86744	0.13831	0.39963	0.94709	0.10397	0.00061	2.51505	0.00348
32				11	22.58403	7.39007	5.51242	1.06614	-0.02158	0.15716	1.07788	-0.15948	0.00111	2.46504	0.00193
33				12	22.90768	7.40009	5.58819	1.06370	-0.02201	0.09246	1.06794	-0.13873	0.00161	1.68904	0.00320
34				13	23.51645	7.39992	5.65806	1.07619	-0.02539	0.09736	1.08088	0.16577	0.00570	1.41164	0.00381
35				14	24.35703	7.39988	5.73437	1.10116	-0.03913	0.05167	1.10306	-0.21255	0.00823	1.38025	0.00334
36				15	25.34647	7.39989	5.80141	1.08644	-0.04081	-0.02645	1.08753	-0.17974	0.01117	1.37638	0.00299
37				16	26.38838	7.39992	5.81260	1.04551	-0.03223	-0.05783	1.04760	-0.09662	0.01394	1.38115	0.00273
38				17	27.37976	7.39987	5.77294	1.02087	-0.02363	-0.04470	1.02212	-0.04455	0.01786	1.38313	0.00256
39				18	28.22421	7.39993	5.72987	0.99281	-0.01870	-0.05043	0.99426	0.01144	0.02341	1.41612	0.00216
40				19	28.83855	7.39991	5.69944	0.99944	-0.01499	-0.06952	0.91909	0.15745	0.02719	1.49192	0.00159
41				20	29.16106	3.57454	5.67782	0.91634	-0.00560	0.05300	0.91909	0.18781	0.02183	1.45170	0.00180
43	1	LIFT	3	1	29.07686	3.57524	5.66122	0.90135	-0.01021	0.07431	0.95299	0.09044	0.02183	1.40367	0.00213
44				2	28.63852	3.59075	5.62328	0.95113	-0.01397	0.06878	0.95409	0.04495	0.01639	1.36383	0.00254
45				3	27.80554	3.62799	5.55483	1.00331	-0.01597	0.01731	1.00576	0.01155	0.01256	1.34654	0.00281
46				4	26.65736	3.66661	5.50029	1.05838	-0.01597	0.03865	1.03865	-0.07823	0.00989	1.34876	0.00302
47				5	25.30577	3.70989	5.49795	1.03428	-0.01472	-0.02421	1.03467	-0.07010	0.00742	1.36786	0.00320
48				6	23.88484	3.70989	5.53098	1.01736	-0.01250	-0.03422	1.01801	-0.03623	0.00742	1.36786	0.00320
49				7	22.53481	3.76683	5.57135	1.00265	-0.00704	-0.03848	1.00341	-0.00683	0.00475	1.40352	0.00354

Figure 25. (Continued) Output from the sample case.

TUESDAY, APR 15, 1986

3-D VISCOUS-INVISCID INTERACTIVE PROGRAM

ALPHA = 1.30 MACH = 0.6000

CASE TITLE: REPORT TEST CASE.TRANS. CALC., 2DSTRIP BL, M=0.6, ALPHAS
PAGE TITLE: FUNDAMENTAL FLOW SOLUTION

VISCOUS/INVISCID CYCLE NO. ?

****** WARNING ****** PRINTED CP, VX, VY, VZ AND FORCES ARE COMPUTED AT OFF - BODY POINTS

PNL. NO.	SEC. NO.	SEC. TYPE	IV	IU	X	Y	Z	VX	VY	VZ	VT	CPVISC	DELS	M	CF
50	1	LIFT	3	8	21.38661	3.81661	5.60855	0.99272	-0.00028	-0.03998	0.99352	0.01293	0.00203	1.56006	0.00360
51				9	20.55191	3.84817	5.62768	1.00214	-0.00469	-0.01359	1.00224	-0.00449	0.00131	2.44320	0.00174
52				10	20.12907	3.87635	5.66301	0.83159	0.09117	-0.27961	0.88207	-0.22642	0.00068	2.49230	0.00337
53				11	20.12923	3.86983	5.75069	0.95051	0.07616	0.41043	1.03814	-0.07719	0.00089	2.42182	0.00257
54				12	20.56233	3.85267	5.86353	1.08542	-0.04040	0.19328	1.10323	-0.21291	0.00153	2.48262	0.00130
55				13	21.38992	3.81062	5.96442	1.10391	-0.06462	0.08515	1.10908	-0.22533	0.00220	1.49197	0.00388
56				14	22.53728	3.75731	6.03259	1.10148	-0.06255	0.04788	1.10429	-0.21517	0.00501	1.40145	0.00306
57				15	23.88872	3.70660	6.06332	1.10401	-0.06082	0.00550	1.10570	-0.21814	0.00790	1.36897	0.00306
58				16	25.30960	3.66691	6.02750	1.08764	-0.05335	-0.05668	1.09042	-0.18582	0.01118	1.36281	0.00279
59				17	26.65891	3.62719	5.93108	1.04836	-0.03743	-0.09349	1.05319	-0.10816	0.01507	1.34786	0.00257
60				18	27.80655	3.58724	5.82587	1.01444	-0.02249	-0.09333	1.01897	-0.03817	0.01918	1.37711	0.00237
61				19	28.64058	3.57153	5.74079	0.97141	-0.01339	-0.10459	0.97712	-0.04542	0.02515	1.41573	0.00196
62				20	29.07799	3.57391	5.68655	0.89678	-0.00625	-0.11344	0.90395	-0.18590	0.03385	1.50455	0.00139
85	2	NLIF	1	1	2.46411	0.06440	5.63511	0.75468	0.07703	0.38173	0.84923	0.28587	0.0	0.0	0.0
86				2	2.47168	-0.18659	6.59474	0.77080	0.22390	0.31014	0.86050	0.26566	0.0	0.0	0.0
87				3	2.47205	0.28618	6.51136	0.79471	0.31750	0.19068	0.87677	0.23612	0.0	0.0	0.0
88				4	2.46727	0.35007	6.39909	0.82226	0.35025	0.05226	0.89527	0.20205	0.0	0.0	0.0
89				5	2.47436	0.37490	6.27388	0.85603	0.31877	-0.07974	0.91693	0.16153	0.0	0.0	0.0
90				6	2.47711	0.35302	6.14681	0.88443	0.24658	-0.17317	0.93435	0.12844	0.0	0.0	0.0
91				7	2.47280	0.28379	6.03986	0.91063	0.14755	-0.21602	0.94746	0.10325	0.0	0.0	0.0
92				8	2.47440	0.18161	5.96121	0.92291	0.08655	-0.22223	0.95322	0.09211	0.0	0.0	0.0
93				9	2.47641	0.06238	5.90800	0.92732	0.04277	-0.22565	0.95534	0.08800	0.0	0.0	0.0
94	2	NLIF	2	1	5.00345	0.14725	7.47020	0.89886	0.08386	0.25269	0.93746	0.12248	0.0	0.0	0.0
95				2	5.00385	0.41482	7.33160	0.92507	0.17022	0.15698	0.95361	0.09137	0.0	0.0	0.0
96				3	5.00407	0.62980	7.11092	0.94500	0.18820	0.07900	0.96679	0.06569	0.0	0.0	0.0
97				4	5.01137	0.78530	6.84464	0.95977	0.18308	0.01148	0.97714	0.04538	0.0	0.0	0.0
98				5	5.00465	0.86400	6.54678	0.97014	0.16587	-0.04871	0.98543	0.02900	0.0	0.0	0.0
99				6	5.00488	0.83868	6.24607	0.98382	0.10714	-0.10447	0.99514	0.00970	0.0	0.0	0.0
100				7	5.00902	0.68681	5.98742	0.99554	0.03233	-0.10223	1.00129	-0.00259	0.0	0.0	0.0
101				8	5.00489	0.44066	5.80510	0.99954	0.00351	-0.07620	1.00245	-0.00490	0.0	0.0	0.0
102				9	5.00645	0.15131	5.69692	1.00081	-0.00223	-0.05834	1.00251	-0.00503	0.0	0.0	0.0
103	3	NLIF	1	1	7.89182	0.22528	8.64750	0.82161	0.22572	0.39664	0.93985	0.11790	0.0	0.0	0.0
104				2	7.88930	0.59265	8.35452	0.98438	0.33180	0.08057	1.04191	-0.08492	0.0	0.0	0.0
105				3	7.89877	0.77934	7.92960	1.04804	0.08741	-0.04195	1.05251	-0.10674	0.0	0.0	0.0
106				4	7.89551	0.97142	7.50561	1.00056	0.17571	0.06801	1.01815	-0.03650	0.0	0.0	0.0
107				5	7.89360	1.19285	7.08127	1.02065	0.17370	-0.04643	1.03636	-0.07355	0.0	0.0	0.0
108				6	7.89500	1.23320	6.60854	1.03699	-0.06773	-0.10944	1.04494	-0.09115	0.0	0.0	0.0
109				7	7.89226	1.05357	6.16956	1.03518	-0.02399	-0.06834	1.03771	-0.07632	0.0	0.0	0.0
110				8	7.89304	0.69748	5.84617	1.02804	-0.03618	-0.01388	1.02877	-0.05806	0.0	0.0	0.0
111				9	7.89288	0.24317	5.67151	1.02366	-0.01818	0.01985	1.02402	-0.04840	0.0	0.0	0.0
112	3	NLIF	2	1	10.26125	0.26061	9.29051	1.07871	-0.02324	0.02212	1.07919	-0.16222	0.0	0.0	0.0
113				2	10.25645	0.63987	8.90867	1.07430	-0.04798	0.07313	1.07786	-0.15943	0.0	0.0	0.0
114				3	10.24283	0.85733	8.40572	1.06318	0.03595	0.11801	1.07032	-0.14368	0.0	0.0	0.0
115				4	10.26551	1.13351	7.94864	1.03754	0.10870	-0.10739	1.04853	-0.09853	0.0	0.0	0.0
116				5	10.26760	1.36949	7.43462	1.03834	0.08569	-0.00160	1.04187	-0.08484	0.0	0.0	0.0
117				6	10.26759	1.41179	6.85602	1.03155	0.03951	-0.01427	1.03241	-0.06548	0.0	0.0	0.0
118				7	10.26149	1.24667	6.30984	1.02184	0.03644	-0.02743	1.02286	-0.04604	0.0	0.0	0.0

Figure 25. (Continued) Output from the sample case.

TUESDAY, APR 15, 1986

3-D VISCOUS-INVISCID INTERACTIVE PROGRAM

CASE TITLE: REPORT TEST CASE,TRANS. CALC., 2DSTRIP BL, M=0.6, ALPHAS
PAGE TITLE: FUNDAMENTAL FLOW SOLUTION

ALPHA = 1.30 MACH = 0.6000
VISCOUS/INVISCID CYCLE NO 2

***** WARNING ***** PRINTED CP, VX, VY, VZ AND FORCES ARE COMPUTED AT OFF - BODY POINTS

PNL. NO.	SEC NO.	SEC TYPE	IV	IU	X	Y	Z	VX	VY	VZ	VT	CPVISC	DELS	M	CF
119	3	NLIF	2	8	10.26603	0.84292	5.91563	1.01702	-0.00011	-0.02802	1.01740	-0.03499	0.0	0.0	0.0
120				9	10.26438	0.29268	5.72676	1.01421	-0.00976	0.00525	1.01427	-0.02868	0.0	0.0	0.0
121	3	NLIF	3	1	12.34360	0.24696	9.16012	1.01049	-0.14054	-0.10332	1.02543	-0.05127	0.0	0.0	0.0
122				2	12.35182	0.66708	8.81478	1.04388	-0.10325	0.07386	1.05157	-0.10480	0.0	0.0	0.0
123				3	12.36334	1.06277	8.43107	1.04331	-0.02604	-0.10303	1.04871	-0.09890	0.0	0.0	0.0
124				4	12.35467	1.38806	7.97498	1.03911	0.04294	0.07992	1.04306	-0.08728	0.0	0.0	0.0
125				5	12.35265	1.51473	7.39872	1.03449	0.04922	-0.04605	1.03669	-0.07422	0.0	0.0	0.0
126				6	12.35251	1.49562	6.80041	1.02226	0.05510	0.03178	1.02423	-0.04884	0.0	0.0	0.0
127				7	12.35432	1.30585	6.24793	1.00809	0.04920	0.00862	1.00933	-0.01871	0.0	0.0	0.0
128				8	12.35233	0.87543	5.88525	0.99928	0.02364	-0.01897	0.99974	-0.00050	0.0	0.0	0.0
129				9	12.35274	0.29784	5.73324	0.99587	0.00502	-0.01280	0.99596	-0.00806	0.0	0.0	0.0
130	4	NLIF	1	1	14.83243	0.85290	8.96744	1.01332	-0.03786	-0.01951	1.01422	-0.02857	0.0	0.0	0.0
131				2	14.81987	1.38545	8.75072	1.01778	-0.02637	0.04250	1.01841	-0.03703	0.0	0.0	0.0
132				3	14.82926	1.94886	8.44981	1.01881	0.01155	0.05396	1.01927	-0.03878	0.0	0.0	0.0
133				4	14.81589	2.44425	8.25629	1.01509	0.04459	0.03807	1.02049	-0.04125	0.0	0.0	0.0
134				5	14.83490	2.64464	8.03695	1.00206	-0.00398	-0.05892	1.01681	-0.03379	0.0	0.0	0.0
135				6	14.81558	2.65907	7.51805	1.00185	-0.10824	0.00814	1.00792	-0.01587	0.0	0.0	0.0
136				7	14.81826	2.53438	6.88611	1.01401	-0.10566	0.08836	1.01127	-0.02262	0.0	0.0	0.0
137				8	14.81548	2.30328	6.29290	1.01046	0.01554	0.16673	1.02774	-0.05597	0.0	0.0	0.0
138	4	NLIF	2	1	17.62799	0.89480	8.90782	1.01609	-0.01046	-0.01159	1.01620	-0.03258	0.0	0.0	0.0
139				2	17.62973	1.45180	8.78426	1.01640	0.03112	0.00143	1.01688	-0.03394	0.0	0.0	0.0
140				3	17.61188	1.99848	8.56722	1.01595	-0.00679	0.04446	1.01694	-0.03407	0.0	0.0	0.0
141				4	17.63661	2.32518	8.36462	1.01395	0.02477	0.02356	1.01452	-0.02918	0.0	0.0	0.0
142				5	17.62924	2.37434	7.99501	1.00682	-0.05185	-0.00936	1.00820	-0.01643	0.0	0.0	0.0
143				6	17.62631	2.36945	7.39805	0.99670	0.08586	0.03758	1.00110	-0.00220	0.0	0.0	0.0
144				7	17.63345	2.31426	6.78852	0.98847	0.09352	0.09261	0.99719	-0.00560	0.0	0.0	0.0
145				8	17.63456	2.16673	6.19088	0.98939	0.04386	0.19010	0.99844	-0.01692	0.0	0.0	0.0
146	4	NLIF	3	1	19.84778	0.28660	8.90368	1.02450	-0.00772	0.00007	1.02452	-0.04943	0.0	0.0	0.0
147				2	19.84860	0.85210	8.80477	1.02681	0.01447	0.01380	1.02700	-0.05446	0.0	0.0	0.0
148				3	19.85272	1.40577	8.66814	1.03018	0.00341	0.03359	1.03074	-0.06207	0.0	0.0	0.0
149				4	19.85573	1.91566	8.46865	1.03566	0.02156	-0.00359	1.03589	-0.07259	0.0	0.0	0.0
150				5	19.84579	2.15694	8.04858	1.02490	-0.10692	0.00329	1.03047	-0.06153	0.0	0.0	0.0
151				6	19.84290	2.16018	7.47127	1.02741	-0.11163	0.07018	1.03584	-0.07248	0.0	0.0	0.0
152				7	19.83890	2.14716	6.89521	1.03749	-0.10755	0.13700	1.05200	-0.10569	0.0	0.0	0.0
153				8	19.83937	2.12780	6.31944	1.10913	-0.09247	0.22279	1.13506	-0.28096	0.0	0.0	0.0
154	4	NLIF	4	1	22.38484	0.26312	8.94598	1.04788	0.00365	0.02033	1.04808	-0.09760	0.0	0.0	0.0
155				2	22.38852	0.78501	8.88060	1.04862	0.01918	0.02368	1.04907	-0.05963	0.0	0.0	0.0
156				3	22.38708	1.29275	8.75813	1.05153	0.04001	-0.00354	1.05230	-0.10630	0.0	0.0	0.0
157				4	22.39178	1.71345	8.50278	1.04941	-0.02684	-0.07748	1.05261	-0.10694	0.0	0.0	0.0
158				5	22.38063	1.91412	8.06254	1.05108	-0.09434	-0.01369	1.05539	-0.11269	0.0	0.0	0.0
159				6	22.37453	1.93714	7.53778	1.06434	-0.07500	0.01928	1.06715	-0.13708	0.0	0.0	0.0
160				7	22.36932	1.93539	7.01049	1.07669	-0.07225	0.02459	1.07939	-0.16264	0.0	0.0	0.0
161				8	22.37270	1.93994	6.48318	1.10738	-0.06949	0.10274	1.11430	-0.23644	0.0	0.0	0.0
162	4	NLIF	5	1	25.43065	0.75176	8.95608	1.03454	0.01043	-0.02387	1.03486	-0.07049	0.0	0.0	0.0
163				2	25.43256	0.74674	8.87438	1.03418	0.02101	-0.05039	1.03562	-0.07203	0.0	0.0	0.0
164				3	25.43010	1.19996	8.67944	1.03129	-0.01214	-0.09134	1.03540	-0.07159	0.0	0.0	0.0
165				4	25.42825	1.53300	8.32792	1.03249	-0.06128	-0.07411	1.03695	-0.07477	0.0	0.0	0.0

Figure 25. (Continued) Output from the sample case.

TUESDAY,   APR 15, 1986

3-D VISCOUS-INVISCID INTERACTIVE PROGRAM

CASE TITLE: REPORT TEST CASE,TRANS. CALC., 2DSTRIP BL, M=0.6, ALPHAS
PAGE TITLE: FUNDAMENTAL FLOW SOLUTION

ALPHA = 1.30 MACH = 0.6000
VISCOUS/INVISCID CYCLE NO. 2

****** WARNING ****** PRINTED CP, VX, VY, VZ AND FORCES ARE COMPUTED AT OFF - BODY POINTS

PNL. NO.	SEC. NO.	SEC. TYPE	IV	IU	X	Y	Z	VX	VY	VZ	VT	CPVISC	DELS	M	CF
166	4	NLIF	5	5	25.42151	1.70469	7.86266	1.03962	-0.06153	-0.04600	1.04245	-0.08603	0.0	0	0.0
167				6	25.41881	1.75172	7.36230	1.04612	-0.05009	-0.04612	1.04822	-0.09788	0.0	0	0.0
168				7	25.41711	1.75855	6.85720	1.05115	-0.05059	-0.05659	1.05389	-0.10959	0.0	0	0.0
169				8	25.42238	1.76684	6.35180	1.03797	-0.05059	0.02418	1.03948	-0.07994	0.0	0	0.0
170	4	NLIF	6	1	27.70573	0.25036	8.90493	0.99409	0.00540	-0.03690	0.99479	0.01040	0.0	0	0.0
171				2	27.70613	0.73465	8.77844	0.99400	0.00236	-0.05632	0.99305	0.01386	0.0	0	0.0
172				3	27.70192	1.15299	8.51363	0.98821	-0.01439	-0.06350	0.99036	0.01922	0.0	0	0.0
173				4	27.69508	1.45510	8.11951	0.98601	-0.02706	-0.06094	0.98826	0.02357	0.0	0	0.0
174				5	27.69247	1.61170	7.64675	0.98503	-0.02921	-0.05920	0.98724	0.02541	0.0	0	0.0
175				6	27.69366	1.65022	7.14436	0.98444	-0.03510	-0.06313	0.98708	0.02572	0.0	0	0.0
176				7	27.69446	1.65454	6.63872	0.98637	-0.04194	-0.06506	0.98940	0.02113	0.0	0	0.0
177				8	27.70216	1.65640	6.13291	0.99925	-0.04588	-0.03929	1.00107	-0.00214	0.0	0	0.0
178	4	NLIF	7	1	29.59558	0.25010	8.87738	0.98785	0.00911	-0.00911	0.98790	0.02409	0.0	0	0.0
179				2	29.59525	0.73196	8.73264	0.98705	-0.00711	0.01605	0.98720	0.02548	0.0	0	0.0
180				3	29.59332	1.14206	8.45273	0.98534	-0.00386	-0.02437	0.98565	0.02856	0.0	0	0.0
181				4	29.58984	1.44342	8.05233	0.98261	0.00697	-0.02531	0.98297	0.03388	0.0	0	0.0
182				5	29.58868	1.60191	7.58049	0.97873	0.01081	-0.03563	0.97944	0.04084	0.0	0	0.0
183				6	29.59019	1.63428	7.07597	0.97395	0.00783	-0.04399	0.97497	0.04965	0.0	0	0.0
184				7	29.59125	1.63222	6.56790	0.96798	0.00686	-0.04924	0.96926	0.06086	0.0	0	0.0
185				8	29.59599	1.62816	6.06016	0.96016	0.00350	-0.06822	0.96348	0.07218	0.0	0	0.0
186	4	NLIF	8	1	33.31235	0.23139	8.86471	0.99270	-0.00184	-0.00929	0.99275	0.01446	0.0	0	0.0
187				2	33.31532	0.67604	8.72855	0.99251	-0.00325	-0.01355	0.99261	0.01475	0.0	0	0.0
188				3	33.31471	1.06076	8.47324	0.99208	-0.00092	-0.01968	0.99227	0.01541	0.0	0	0.0
189				4	33.31329	1.36159	8.11887	0.99159	-0.00071	-0.02439	0.99189	0.01618	0.0	0	0.0
190				5	33.31270	1.54207	7.69636	0.99085	-0.00976	-0.03303	0.99145	0.01705	0.0	0	0.0
191				6	33.31296	1.59096	7.23419	0.98980	-0.02157	-0.03272	0.99058	0.01879	0.0	0	0.0
192				7	33.31207	1.57947	6.76468	0.98902	-0.02776	-0.03493	0.99003	0.01986	0.0	0	0.0
193				8	33.30974	1.52285	6.30544	0.98450	-0.06499	-0.01540	0.98676	0.02635	0.0	0	0.0
194	5	NLIF	1	1	14.81527	2.11342	5.96469	1.00894	-0.12577	-0.02604	1.01708	-0.03434	0.0	0	0.0
195				2	14.81896	1.50402	5.89102	1.00106	-0.05295	-0.05104	1.00375	-0.00752	0.0	0	0.0
196				3	14.81444	0.90450	5.77646	0.99856	0.04162	-0.03541	1.00005	-0.00011	0.0	0	0.0
197				4	14.81868	0.30595	5.65057	0.99545	-0.01609	-0.05097	0.99688	-0.00623	0.0	0	0.0
198	5	NLIF	2	1	17.59962	2.00868	5.81144	0.99139	0.18477	0.00601	1.00847	-0.01699	0.0	0	0.0
199				2	17.62697	1.45485	5.70048	0.97745	0.07718	0.08565	0.98423	0.03137	0.0	0	0.0
200				3	17.62782	0.87312	5.61447	0.98096	0.03946	-0.06274	0.98375	0.03232	0.0	0	0.0
201				4	17.62646	0.29358	5.51007	0.98284	0.01370	0.05315	0.98437	0.03109	0.0	0	0.0
202	5	NLIF	3	1	19.83246	1.93489	5.64308	0.98520	0.04634	-0.01727	0.98801	0.02388	0.0	0	0.0
203				2	19.85184	1.44836	5.48953	0.99082	0.01755	-0.06274	0.99733	0.00531	0.0	0	0.0
204				3	19.85269	0.86769	5.44299	1.00256	0.00839	-0.08983	1.00673	-0.01348	0.0	0	0.0
205				4	19.85269	0.28941	5.37808	1.01070	-0.04276	-0.07250	1.01333	-0.02677	0.0	0	0.0
206	5	NLIF	4	1	22.34166	1.77620	5.51893	0.96990	-0.03363	-0.00205	0.97085	-0.05774	0.0	0	0.0
207				2	22.32808	1.33181	5.41150	1.01904	-0.02886	0.01518	1.01971	-0.03966	0.0	0	0.0
208				3	22.32729	0.79658	5.42419	1.02086	-0.01835	0.04388	1.02221	-0.04472	0.0	0	0.0
209				4	22.32355	0.26516	5.40892	1.01996	-0.03048	0.06628	1.02228	-0.04487	0.0	0	0.0
210	5	NLIF	5	1	25.32568	1.60299	5.51299	1.03458	-0.02373	0.01250	1.03511	-0.07099	0.0	0	0.0
211				2	25.39319	1.19102	5.52680	1.01902	-0.02373	0.05330	1.02068	-0.04164	0.0	0	0.0
212				3	25.37105	0.71381	5.58322	1.01594	-0.00179	0.05088	1.01721	-0.03462	0.0	0	0.0

Column group headers: |<---- CONTROL POINTS ---->| (X, Y, Z); |<INCOMPRESSIBLE POTENTIAL FL SOLUTN>| (VX, VY, VZ, VT); |<--- CPVISC; VISCOUS FLOW SOLUTION ---->| (DELS, M, CF)

Figure 25. (Continued) Output from the sample case.

TUESDAY,   APR 15, 1986

3-D VISCOUS-INVISCID INTERACTIVE PROGRAM

CASE TITLE: REPORT TEST CASE,TRANS. CALC., 2DSTRIP BL, M=0.6, ALPHAS
PAGE TITLE: FUNDAMENTAL FLOW SOLUTION

ALPHA = 1.30 MACH = 0.6000
VISCOUS/INVISCID CYCLE NO. 2

****** WARNING ****** PRINTED CP, VX, VY, VZ AND FORCES ARE COMPUTED AT OFF - BODY POINTS

PNL. NO.	SEC. NO.	SEC. TYPE	IV	IU	CONTROL POINTS X	Y	Z	INCOMPRESSIBLE POTENTIAL FL SOLUTN VX	VY	VZ	VT	CPVISC	VISCOUS FLOW SOLUTION DELS	M	CF
213	5	NLIF 5		4	25.38698	0.23939	5.57731	1.01413	-0.00103	0.03567	1.01476	-0.02965	0.0	0.0	0.0
214	5	NLIF 6		1	27.69252	1.51353	5.58560	0.98902	0.03070	0.04963	0.99074	0.01846	0.0	0.0	0.0
215				2	27.67360	1.13571	5.66022	0.98591	0.02010	0.04173	0.98700	0.02589	0.0	0.0	0.0
216				3	27.66954	0.68392	5.71137	0.98876	0.00774	0.05273	0.99019	0.01955	0.0	0.0	0.0
217				4	27.66939	0.23143	5.66630	0.99183	0.00289	0.03418	0.99243	0.01511	0.0	0.0	0.0
218	5	NLIF 7		1	29.62930	1.46696	5.72402	0.95142	-0.05193	0.06995	0.95540	0.08789	0.0	0.0	0.0
219				2	29.58521	1.08563	5.77759	0.96061	0.01215	0.04671	0.96183	0.07540	0.0	0.0	0.0
220				3	29.59535	0.65382	5.79646	0.96842	0.00182	0.03352	0.96900	0.06136	0.0	0.0	0.0
221				4	29.58678	0.22110	5.72153	0.97199	0.00262	0.01941	0.97219	0.05511	0.0	0.0	0.0
222	5	NLIF 8		1	33.45131	1.32301	6.00874	0.97882	-0.03100	0.07828	0.98244	0.03492	0.0	0.0	0.0
223				2	33.32368	0.99475	5.88553	0.98698	0.03491	0.02059	0.98781	0.02428	0.0	0.0	0.0
224				3	33.34593	0.60794	5.79339	0.98681	0.02723	-0.00987	0.98723	0.02542	0.0	0.0	0.0
225				4	33.33748	0.20518	5.70091	0.98630	0.01035	-0.02095	0.98658	0.02671	0.0	0.0	0.0

Figure 25. (Continued) Output from the sample case.

TUESDAY,   APR 15, 1986

3-D VISCOUS-INVISCID INTERACTIVE PROGRAM

CASE TITLE: REPORT TEST CASE,TRANS. CALC., 2DSTRIP BL, M=0.6, ALPHAS
PAGE TITLE: INTEGRATED PRESSURES

ALPHA = 1.30 MACH = 0.6800
VISCOUS/INVISCID CYCLE NO. 2

|<---- BASED UPON INPUT VALUES OF AREF,BOV2,CREF ---->|

***** WARNING ***** PRINTED CP, VX, VY, VZ AND FORCES ARE COMPUTED AT OFF - BODY POINTS

| TYPE	SEC	NV	CL	CD	CSF	CPITCH	CROLL	CYAW	ETA	SECTCL	SECTCD	ASTRIP	CIRCULTN
LIFT	1	1	0.0039	-0.0002	0.0005	-0.0135	-0.0022	-0.0013	0.8463	0.0246	-0.0015	15.0991	-0.0058
		2	0.0207	-0.0006	0.0019	-0.0637	-0.0070	-0.0040	0.5712	0.0820	-0.0025	24.1940	-0.0165
		3	0.0484	-0.0001	0.0062	-0.1354	-0.0178	-0.0109	0.2759	0.1306	-0.0003	35.5155	-0.0310
SECT. TOT:			0.0729	-0.0010	0.0086	-0.2126	-0.0271	-0.0162					
NLIF	2	1	-0.0008	0.0010	-0.0016	0.0010	0.0005	0.0003					
		2	-0.0029	0.0009	-0.0024	0.0026	0.0015	0.0010					
SECT. TOT:			-0.0037	0.0018	-0.0040	0.0035	0.0019	0.0013					
NLIF	3	1	-0.0019	-0.0000	0.0051	0.0019	-0.0048	-0.0032					
		2	0.0037	-0.0005	0.0091	-0.0051	-0.0111	-0.0074					
		3	0.0023	-0.0000	0.0041	-0.0034	-0.0061	-0.0040					
SECT. TOT:			0.0041	-0.0005	0.0183	-0.0066	-0.0220	-0.0146					
NLIF	4	1	0.0027	0.0001	0.0033	-0.0048	-0.0058	-0.0038					
		2	0.0018	0.0000	0.0010	-0.0039	-0.0020	-0.0013					
		3	0.0026	0.0007	0.0073	-0.0057	-0.0171	-0.0111					
		4	0.0062	-0.0009	0.0128	-0.0161	-0.0341	-0.0221					
		5	0.0041	0.0007	0.0080	-0.0121	-0.0244	-0.0158					
		6	-0.0004	-0.0008	-0.0008	-0.0013	-0.0028	-0.0018					
		7	-0.0011	-0.0000	-0.0035	0.0039	0.0126	0.0081					
		8	-0.0012	-0.0001	-0.0029	0.0046	0.0115	0.0074					
SECT. TOT:			0.0148	0.0022	0.0251	-0.0330	-0.0564	-0.0367					
NLIF	5	1	-0.0007	-0.0000	0.0001	0.0013	-0.0002	-0.0001					
		2	-0.0012	-0.0001	-0.0001	0.0024	0.0003	0.0002					
		3	-0.0002	-0.0000	-0.0001	0.0005	0.0002	0.0001					
		4	-0.0015	-0.0000	-0.0003	0.0041	0.0009	0.0006					
		5	-0.0024	-0.0000	0.0000	0.0074	0.0000	0.0000					
		6	-0.0005	-0.0001	-0.0000	0.0017	-0.0001	-0.0001					
		7	0.0027	-0.0001	-0.0000	-0.0099	-0.0000	-0.0008					
		8	0.0022	-0.0000	-0.0007	-0.0089	0.0027	0.0017					
SECT. TOT:			0.0018	0.0000	-0.0011	-0.0096	0.0037	0.0024					
CONFIG.TOT:			0.0899	0.0026	0.0469	-0.2583	0.0040	0.0639					

Figure 25.   (Concluded) Output from the sample case.
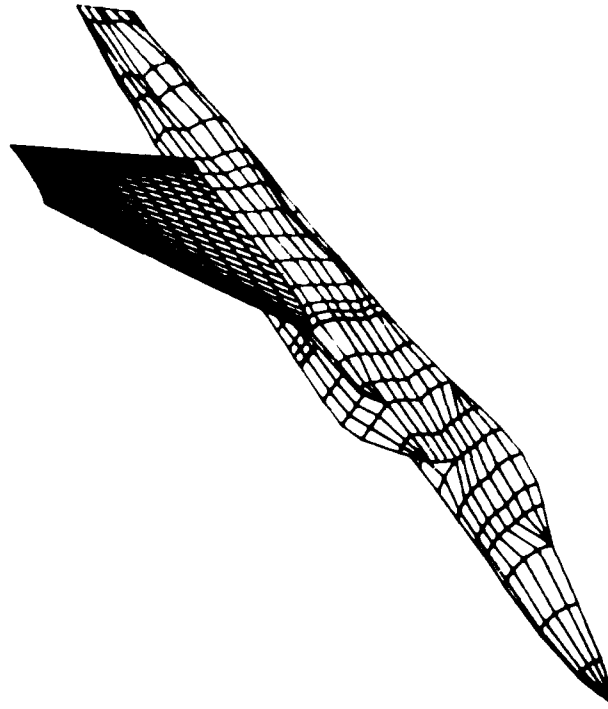
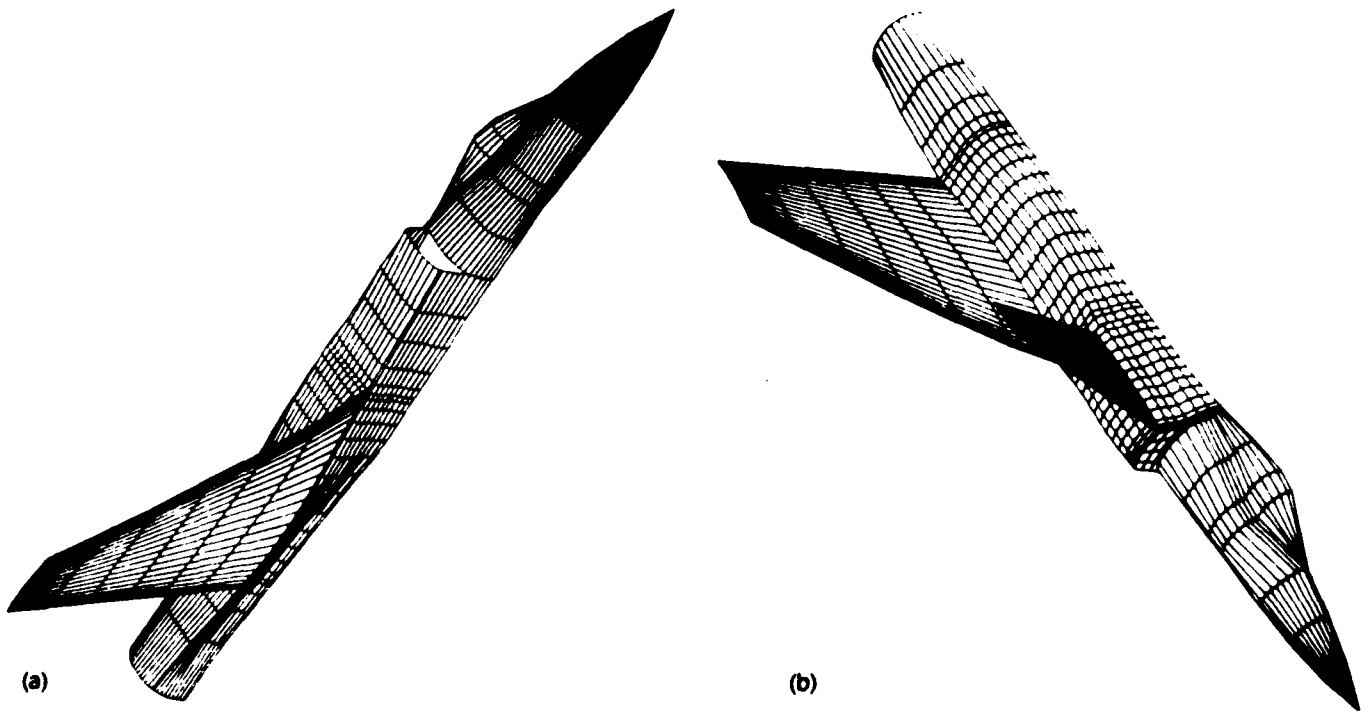Figure 26. Panel arrangement for test case 1.

(a)

(b)

Figure 27. Panel arrangement for test case 2, (a) without canard, (b) with canard.
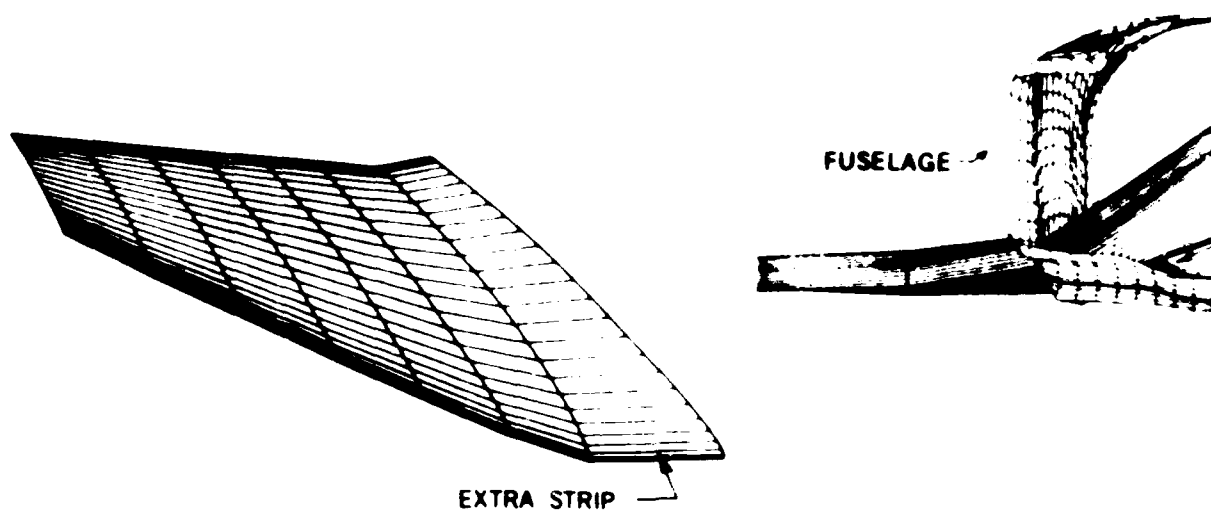
EXTRA STRIP

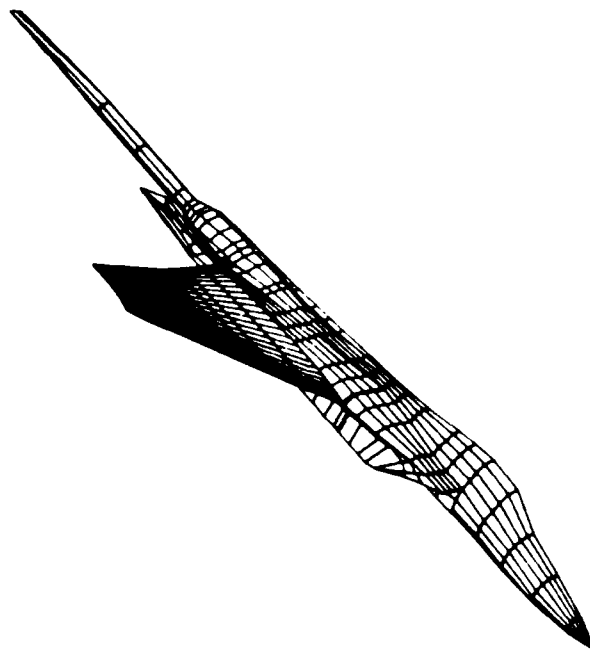Figure 28. Panel arrangement of the wing for test case 2.

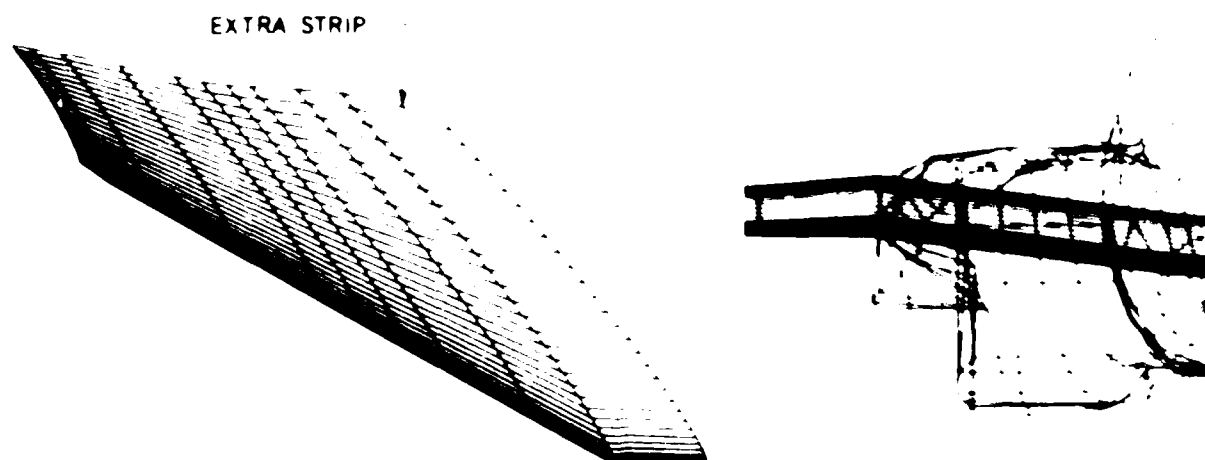FUSELAGE

Figure 29. Panel arrangement for test case 3.

EXTRA STRIP

Figure 30. Panel arrangement of the wing for test case 3.

EMD

6 – 8

D